The Frequency of Occurrence of Circumnuclear Starbursts in Seyfert Galaxies - A Challenge for the Unified Scheme?

T.P.R. van der Laan, BSc.
Supervisors: Dr. E. Schinnerer & Prof. Dr. P.D. Barthel

June 26, 2008

Contents

1 Introduction

In about 1 in a 100 galaxies we find an active galactic nucleus (AGN). These nuclei have energetic phenomena which cannot be related to stellar activity. The current paradigm for the AGN phenomenon is a hot accretion disk surrounding a central super-massive black hole. Energy is generated by gravitational infall of material which is heated to high temperatures in a dissipative accretion disk.
A general division is made between AGN on the basis of their luminosity. Lower-luminosity AGN, with M_B > -21.5 + 5log(h_0)[1] for the nucleus are called Seyfert galaxies. Higher-luminosity AGN are called quasars. In a Seyfert galaxy the host galaxy is clearly detectable. AGN are further divided into types based on the apperance of their optical emission line spectrum [Pet97].
The unifying theorem states that orientation, obscuration and radiation anisotropy are important factors in the classification of the various types of AGN [Ant93]. Seyfert galaxies type 1 and type 2 are, in this scheme, physically the same, but viewed from different perspectives. In type 1 Seyferts broad line emission from hydrogen recombination is observed, while in type 2 Seyferts these broad lines are lacking. It is thought that our line of sight to these broad emission lines in these galaxies is blocked by a dust torus.
However, it has been claimed that type 2 Seyfert have younger starbursts. Heckman et al. [Hea95] claim that the featureless continuum seen in Seyfert 2 galaxies can not be in total attributed to reradiation of the nuclear radiation by dust, but should in part be from a young stellar population. Ohsuga & Umemura [OU99] have proposed a theoretical model that would give a basis for this difference in stellar populations between the two Seyfert types. It says that at the point where the radiative force and the gravitational force of the system (black hole, starburst, bulge and disk) are in equilibrium a stable dust torus can exist. The radiative strength of the starburst has a dependence on time, because of stellar evolution and the occurrence of supernova. The stability of this torus would decrease with the age of the starburst. This model implies that type 2 Seyferts host younger starbursts then their type 1 counterparts.
Using the infrared (R=1500) spectra of 21 Seyfert galaxies obtained with the 10m Keck telescope, Schinnerer and collaborators have attempted to shed light on this issue. The observations were done on 4 nights in 2001 and consist of H and K band long slit spectra covering the nucleus as well as the circumnuclear regions of the selected galaxies. My MSc research, as reported here, consisted of the final stages of the data reduction of this project, as well as the first analysis of the results. I hope to answer the following questions.

- Are nuclear powerful starbursts present in Seyfert type 1 galaxies?
- Is there a difference in circumnuclear stellar populations between type 1 and type 2 Seyfert galaxies?
- What are the typical ages of the stellar populations in Seyfert galaxies?

Previous studies looking for the age of the circumnuclear stellar populations have always had problems with small number statistics. Oliva et al. [OOM99] find powerful starbursts in 5 out of 13 of their type 2 Seyfert galaxies (H and K band longslit spectroscopy). Ivanov et al. [IR00] find no strong starbursts in the majority of their 16 Seyfert 2 galaxies (based on the CO band head in the K band). Davies et al. [DMST$^+$07] find evidence for recent starbursts in the last 10-300 Myr, but no difference between AGN types (H and K band integral field unit spectroscopy). Our sample is the largest compiled to date. Our starting hypothesis will be that the starbursts have the same age. In §2 background theory related to this research will be explained. In §3 we will briefly outline our dataset and its reduction. §4 will give our final spectra and their important features. §5 will analyze our results with the Starburst99 models. Finally in §6 we will summarize our results and give recommendations for further study.

[1] h_0 is the Hubble parameter which we set to 0.70

2 Basics

Using long slit near infrared spectra to get the age of the stellar population, we search for a difference in the stellar population in the nuclear and circumnuclear region for type 1 and type 2 Seyfert galaxies. We observe in the near-infrared to minimize the contribution of dust and the AGN to the stellar light. The process which leads to the age determination will be explained in this section.

2.1 Seyfert Galaxies within the unification model

Seyfert galaxies are a part of the class 'Active Galaxies'. These are galaxies which show energetic phenomena in their nuclei which cannot be related to stars. A general division is made between quasars and Seyferts on the basis of their nuclear luminosity related to the galaxy luminosity. Seyfert galaxies are lower-luminosity AGNs, with $M_B > -21.5 + 5log(h_0)$ for the active nucleus. This means that the host galaxy, which has a similar luminosity, is also visible.
The unification model speaks of a tiny, central source of photoionizing photons. This source is surrounded by a region called the Broad Line Region (BLR) and a dust torus at a radius of 1-2pc, farther out is a secondary gas and dust torus which has been developed for Seyfert galaxies. This torus is at a radius of 50 to 100 pc from the nucleus. In a cone outwards from the nucleus and the torus is the Narrow Line Region (NLR), at a distance of 50 to several kpc from the nucleus. The type of a Seyfert galaxy is determined by the line of sight from the observer to the nucleus. If we can observe the nucleus directly it is a type 1, when we see the nucleus through the secondary torus it is a type 2 (see also Figure 1). Type 1 Seyferts show permitted emission lines with a broad component, Δv(FWHM) of $\gtrsim 10^4$ km/s. These lines are thought to originate close to the central source. There the gravitational potential can Doppler-broaden the lines to these high velocities. Type 2 Seyferts do not show these broad emission lines in their direct spectra, but only narrow lines. The classification into types is continuous with intermediate classes. These are called type 1.9, 1.8 or 1.5, based on the detection of a weak broad component in Hα, Hα and Hβ or a broad component comparable to the narrow component. [Pet97]

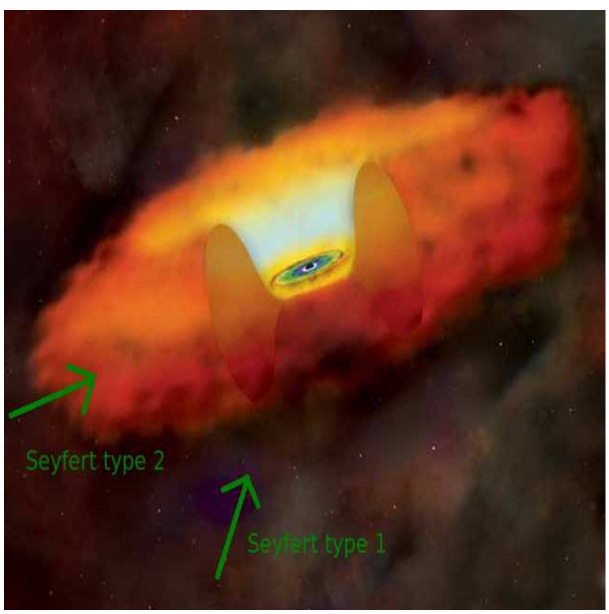

Figure 1: Shown here are the two types of Seyfert galaxies as explained by the unification model. It can be seen here that the viewing angle, parallel or perpendicular to the dust torus determines whether we see a type 1 or type 2 Seyfert. Figure adapted from: http://researchnews.osu.edu/archive/blackholenew.jpg

2.2 Giant and Supergiant Stars

Sometimes the presence of HII regions is interpreted as indicating the presence of young stars. However hydrogen can also be ionized by shocks or an AGN. This makes HII regions unreliable probes to detect stellar populations in Seyfert galaxies. We will use absorption lines which can be directly attributed to stars.

In the infrared the stellar radiation is dominated by the red stars; specifically the red giants and supergiants. The red supergiants are massive stars ($10 - 20\mathrm{M}_{\odot}$) that are burning helium in their cores. Because of their masses these are relatively young stars ($\gtrsim 10^6$ years). The giants are intermediate mass stars which have exhausted the hydrogen in their cores and have gone on with shell hydrogen burning. This leads to an expansion of the star and also their distinct red color.

The difference between red giants and supergiants is in the first place the mass, and therefore age, of the star. Only stars heavier than 10 solar masses can become supergiants. These stars are massive enough to continue nuclear fusion beyond helium.

Supergiants are a probe for relatively young stellar populations; the main sequence time of the stars is short and their evolution as supergiants is also rapid. Supergiants end their lives as supernova type II. Typically all this happens in 10 to 50 Myr. Giants take longer to evolve and thus are a probe for intermediate age stellar populations (100Myr- 500Myr). So now we need a infrared probe that can differentiate between the supergiants and giants.

2.3 Stellar features in the Near-Infrared spectral range

The stellar spectra in the near-infrared show a wealth of absorption features. We follow the selected absorption lines as proposed by [OMO93] and [FS00]; the SiI 1.5892μm line, the CO(6-3) 1.6187μm vibrational line and the $\Delta\nu = 2$ CO vibrational band, especially the CO(2-0) 2.2935μm line. We have excluded the Brγ emission line at 2.166μm, because of the probable AGN origin of the line in our galaxies. The Brγ line is in non-active galaxies a good indicator of young stellar populations (smaller than a few 10^6 years), since it indicates the presence of shortlived hot O stars from the main sequence. However in active galaxies it is also generated by the high energy photons from the nucleus. We will return to Brγ briefly when we qualitatively discuss the off-nuclear spectra.

The absorption lines of SiI, CO(6-3) and CO(2-0) are well visible in most stellar spectra and have good established variations with stellar temperature and surface gravity. It is well established that the equivalent widths of the absorption lines are bigger at younger ages, i.e. when the light is dominated by supergiants. This is also well shown in the K band spectra of giants and supergiants by [FS00] and Figure 3. This makes the equivalent widths of these absorption lines good infrared probes.

2.4 Correcting for Continuum radiation from the AGN and dust

The luminosity of the AGN in the galaxy is of the same order as the luminosity of the rest of the system.[Pet97] Light from warm dust can also be present. It is therefore expected that our spectra (including the nucleus) will contain large amounts of continuum radiation from the AGN itself, and not only the stellar populations. This dilutes our measured equivalent widths (EW). We can correct for this with observed equivalent widths from a stellar library of giants and supergiants ([OMO93] [Iea04] [DBJ96] [MEHS99] [KH86] [FS00] [WH])

[OOKM95] propose $\log(EW_{1.62}/EW_{1.59})$[2] as a dilution-free temperature indicator. This is based on two observations. First we find that $EW_{1.59}$ is flat as a function of temperature, while $EW_{1.62}$ evolves very strongly with temperature (Figure 2). Second the amount of dilution around $EW_{1.59}$ and $EW_{1.62}$ will be equal, because the two lines have a small wavelength difference. That makes the ratio dilution independent, while its value is temperature dependent. In a $\log(EW_{1.62}/EW_{1.59})$ vs. $EW_{1.62}$ plot (Figure 4, top), our galaxies will fall in or below the area covered by the stellar measurements. The H band dilution can be determined by taking the ratio between the location of the area and our measurement. The two blue lines seen in Figure 4 give the borders of the area in which our measurements are expected to fall. We will set our dilution corrected assumption of the

[2] $EW_{1.59}$: equivalent width of SiI, $EW_{1.62}$: equivalent width of CO(6-3) and $EW_{2.29}$: equivalent width of CO(2-0), see also table 3.

equivalent width to the middle of the vertical borders, where the horizontal position is calculated from the dilution-free parameter $\log(EW_{1.62}/EW_{1.59})$. A caveat here is that if our value already falls within the area, the dilution is set to zero.
Once the dilution corrected value of $EW_{1.62}$ has been determined, we can also constrain the dilution in the K band. This is done by the relation between the value of $EW_{1.62}$ and $EW_{2.29}$, also determined by the stellar library (Figure 4, bottom). The dilution corrected values are determined in the same manner as described for the H band.

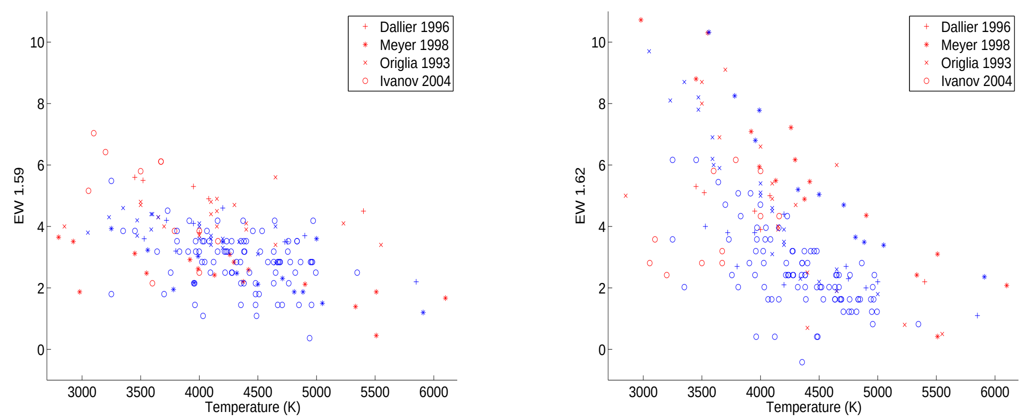

Figure 2: Red points are the supergiant stars, the blue points are the giant stars. We see that $EW_{1.59}$ has almost no dependence on temperature, while $EW_{1.62}$ does.

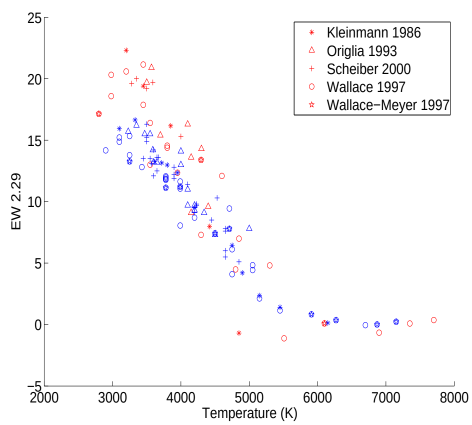

Figure 3: Red points are the supergiant stars, the blue points are the giant stars. The relation between $EW_{2.29}$ and temperature. A clear difference between giants and supergiants can be seen, where supergiants have higher equivalent widths at the lowest temperatures.

2.5 Errors from the continuum correction

The errors in the H band, $EW_{1.59}$ and $EW_{1.62}$, can be much better restrained then in the K band. This has two causes; the stellar library is bigger in the H band and in the K band the errors from our H band calculations propagate.
Looking at Figure 4 we see that especially the datapoints of the Ivanov library fall below the trend given by the other libraries' data points. This effect cannot be explained by extraction effects

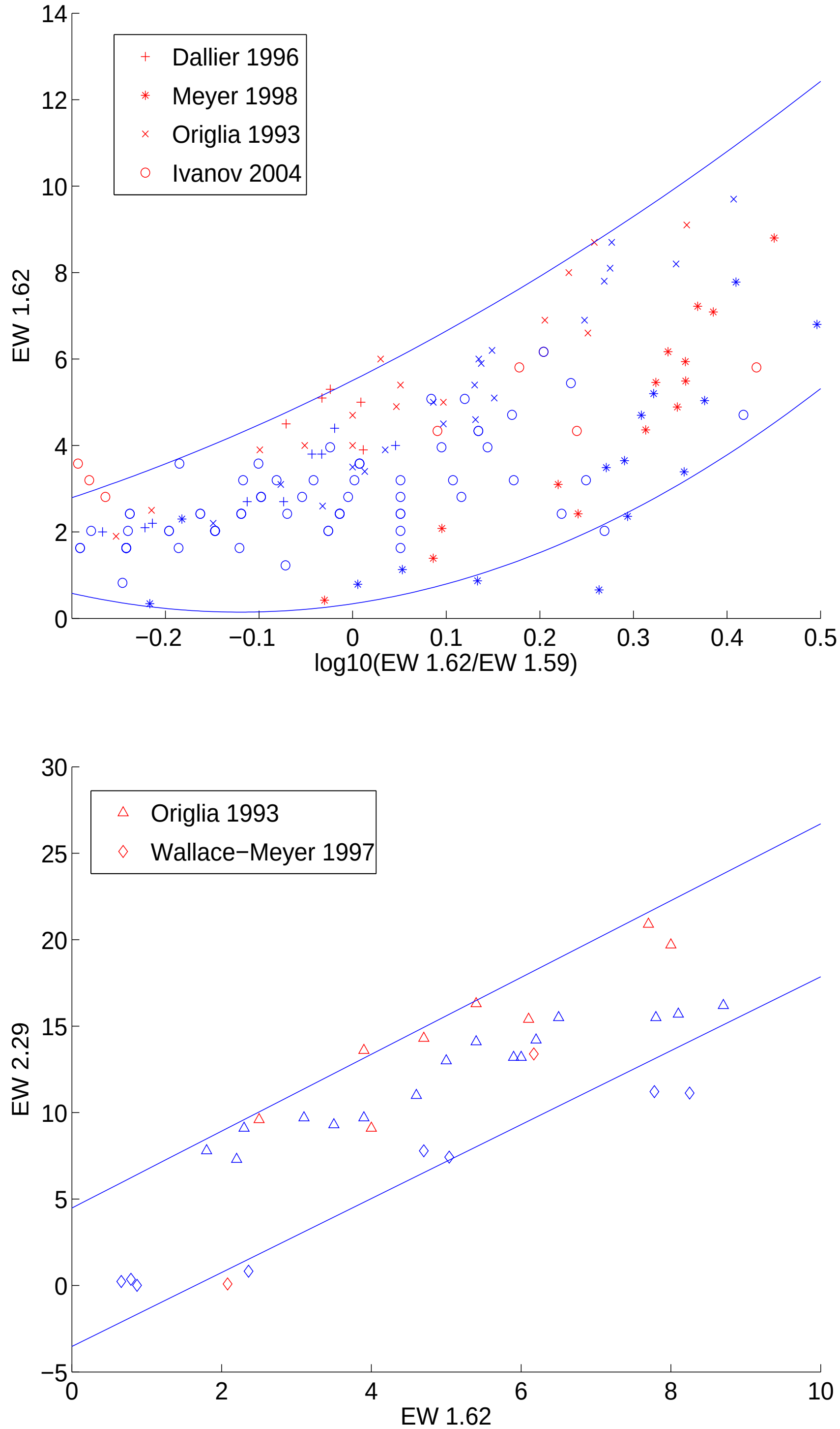

Figure 4: Red points are the supergiants, the blue points are the giants. In the top panel we see the relation between the CO(6-3)/SiI equivalent width ratio and the equivalent width of CO(6-3). The area covered by the two blue lines indicates the region in which we expect our measured equivalent width of CO(6-3) to fall, given that it is not diluted. In case of dilution it will fall under this area. The bottom panel gives the relation between the equivalent widths of CO(6-3) and CO(2-0). As in the top panel we expect our measured equivalent width of CO(2-0) to fall within the area covered by the two blue lines. In the case of dilution the value will fall below the covered area.

or metallicity. Both parameters are the same or very similar in all stellar libraries used for this correction. The error induced here dominate the errors from other reduction steps. We will now give an estimate for this error.
Figure 4 (top) contains 192 points (= 4σ spread). We define a 1σ error for $EW_{1.62}$ as

$$\sigma(EW_{1.62}) = \frac{Bound_{top} - Bound_{bottom}}{4}$$

The 1σ error of $EW_{1.59}$ is calculated from this. We know:

$$\begin{aligned} \sigma^2(EW_{1.59}) &= (\frac{dEW_{1.59}}{dEW_{1.62}})^2 * \sigma^2(EW_{1.62}) \\ EW_{1.59} &= \frac{EW_{1.62}}{10^x}, x = log10(\frac{EW_{1.62}}{EW_{1.59}}) \\ \sigma(EW_{1.59}) = \frac{EW_{1.59}}{EW_{1.62}} * \sigma^2(EW_{1.62}) &= \frac{EW_{1.59}}{EW_{1.62}} \end{aligned} \quad (1)$$

Finally we derive an error estimate for $EW_{2.29}$ from Figure 4 (bottom) in a manner similar to our error estimation of $EW_{1.62}$. Due to our lower number of points, we have a 2σ spread. The error from $EW_{1.62}$ does not add significantly to this.

$$\sigma(EW_{2.29}) = \frac{Bound_{top} - Bound_{bottom}}{2}$$

As can be seen from section 4.1, the general size of the errors related to the dilution correction will be of the order: $EW_{1.59} \approx 1$Å, $EW_{1.62} \approx 1.5$Å and $EW_{2.29} \approx 4.2$Å.

2.6 The effect of Earth's atmosphere in the Near-Infrared

When observing from the ground in the infrared, one has to correct for the influence of the atmosphere. The atmosphere has a wealth of emission and absorption lines, mainly due to carbon dioxide and water vapor. These lines are so numerous, they overlap and influence the complete waveband (Figure 5). Large parts of the infrared sky are invisible to us from the ground. A few windows are open, but these still suffer from non uniform transmission. This transmission is also variable over time. Further it depends on airmass; the longer the pathlength through the atmosphere the bigger its influence. The best observations are made from dry sites where the total water column is smallest. Mauna Kea, Hawaii, is such a site.
Every spectrum observed in the infrared can be seen as a product of the Earth's atmospheric spectrum and the 'real' spectrum of the object we wish to observe. We can correct for this effect by observing astronomical objects with a known spectrum. As long as the observation has been done around the same time and at a similar airmass (and at the same telescope/geographical location).

2.7 Statistics

After we have derived ages for the stellar population from our circumnuclear spectra, we wish to compare the age of the type 1 Seyferts against those of the type 2 Seyferts. We are dealing with two independent samples which we cannot assume to be normally distributed (Gaussian distribution). This forces us to use the Mann-Whitney test (also known as the Wilcoxon rank sum test). This method performs a test on the null hypothesis that data in the two groups are independent samples from identical continuous distributions with equal medians, against the alternative that they do not have equal medians.

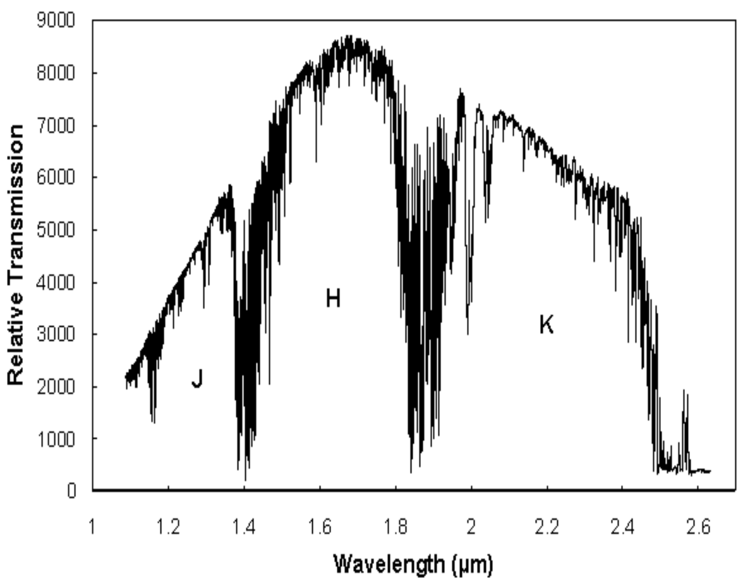

Figure 5: Shown is a general image of the transmission of the atmosphere in the near-infrared. J, H and K stand for the names for the filters available in this wavelength range. Figure taken from: http://www.cfht.hawaii.edu/Instruments/Detectors/IR/Redeye/Manual/Images/fig4-1.gif

3 The Data

3.1 Selection and Observation

The Seyfert sample selection was based on the Hβ and [OIII] λ 5007Å line emission from the Whittle [Whi92] and the Ho [HFS97] samples. The selection criteria fulfill F(Hβ) $> 10^{-14}$ erg s^{-1} cm^{-2} and F([OIII])$> 10^{-13}$ erg s^{-1} cm^{-2}. This way the brightest Seyfert galaxies will be selected.
This selection was made to avoid biases toward or against AGNs with circumnuclear starbursts. Hβ (and [OIII]) can both be excited by the AGN as well as young stars. The absolute flux limit was made to introduce no bias regarding the mass of the accreting black hole.
To allow for high spatial resolution observations the velocity range was restricted to < 5000 km/s. This is sufficiently small to avoid dilution of the nuclear light by circumnuclear starburst rings which have typical diameters of 500 to 1500 pc[Mea96] as well as the diameter for the starformation ring (diameter 200pc) proposed by [OU99].
The data were taken with the Keck NIRSPEC camera on 4 nights in 2001. The observing strategy was to observe first the sky and than the object in H than K band, or vice-versa. Around this time also selected G2V stars were observed for the atmospheric correction.
Observations were made in the H (1.5 - 1.7 μm) and K band (2.0 - 2.5 μm) (see also Figure 5). These were long-slit spectral observations with a slit length of 0.772" by 42" and an angular pixel scale of 0.144"/pixel. The final reduced 2D data consists of a 101 pixels wide spectrum. The typical integration times for the Seyfert galaxy observations are 0.5 hr. The typical seeing at Mauna Kea of 0.7" gives us a spatial resolution of <250 pc for the entire sample. The declination limit at Keck is at -70 deg. From Table 1 we can thus see that our objects are all well above that.

Seyfert	type	RA	Dec	redshift	seeing	observed night
Mrk 1066	2	02h59m58.6s	+36d49m14s	0.012025	0.65	Nov1
Mrk 1	2	01h16m07.2s	+33d05m22s	0.015946	0.70	nov2
Mrk 3	2	06h15m36.3s	+71d02m15s	0.013509	0.70	nov2
NGC 1320	2	03h24m48.7s	-03d02m32s	0.008883	0.70	nov2
NGC 1667	2	04h48m37.1s	-06d19m12s	0.015167	0.65	mar2
NGC 2110	2	05h52m11.4s	-07d27m22s	0.007789	0.65	nov1
NGC 2273	2	06h50m08.6s	+60d50m45s	0.006138	0.90	mar1
NGC 262	2	00h48m47.1s	+31d57m25s	0.015034	0.70	nov2
NGC 2685	2	08h55m34.7s	+58d44m04s	0.002945	0.65	nov1
NGC 2992	2	09h45m42.0s	-14d19m35s	0.007710	0.90	mar1
NGC 3081	2	09h59m29.5s	-22d49m35s	0.007976	0.65	mar2
NGC 3185	2	10h17m38.6s	+21d41m18s	0.004060	0.70	nov2
NGC 3516	1.5	11h06m47.5s	+72d34m07s	0.008836	0.65	mar2
NGC 4051	1.2	12h03m09.6s	+44d31m53s	0.002336	0.90	mar1
NGC 4151	1.5	12h10m32.6s	+39d24m21s	0.003319	0.90	mar1
NGC 4253	1.5	12h18m26.5s	+29d48m46s	0.012929	0.65	mar2
NGC 4388	2	12h25m46.7s	+12d39m44s	0.008419	0.65	mar2
NGC 5273	1.5	13h42m08.3s	+35d39m15s	0.003549	0.90	mar1
NGC 5506	1.9	14h13m14.8s	-03d12m27s	0.006181	0.65	mar2
NGC 7450	1.5	23h00m47.8s	-12d55m07s	0.010624	0.65	nov1
NGC 931	1.5	02h28m14.5s	+31d18m42s	0.016652	0.65	nov1

Table 1: Main information about the datasets selected for this research. The columns are the name of the target, its Seyfert type, its position in RA and Dec, its redshift, seeing and the observation night in 2001.

3.2 Reduction of the Data

The data was almost fully reduced. The observed Seyfert galaxies and corresponding calibrator stars were already flat-fielded, bad pixel corrected, wavelength calibrated and distortion corrected. For this project we now needed to correct for the atmosphere, obtain the relevant spectra, extract the equivalent widths and dilution correct them. All software codes related to the first steps of the calibration can be found in Appendix A.
Directly before or after the observations of the Seyfert galaxy another spectra were taken of a star at a close angular distance. This ensured that the spectrum of the atmosphere can to a first order approximation be assumed to be the same for both the star and the galaxy. The atmospheric spectrum has a dependence on airmass, geographical location and time. All these effects are minimized by this procedure.
The stars were selected on their spectral type. To get a somewhat similar spectrum between the star and galaxy G2V stars were chosen.[3] These stars are fairly common and are fairly featureless in the H and K band. This ensures that the spectral lines from the atmosphere are easily identified and do not result in artificial features in the atmospheric (and thus galaxy) spectra. The spectra of these types of stars have also been included in several spectral libraries with great accuracy. This gives us the possibility to extract the atmospheric spectrum, which we can then apply to the Seyfert galaxies data. From the Meyer library (H band, [MEHS99]) we have selected the star HR4374 (G2V), from the Wallace library (K band, [WH]) we selected the star HR483 (G1.5V). Both spectra are presented in Figure 6. Both spectra had been normalized to one. As both spectra were rectified we multiplied them both with a Planck curve with a temperature of 5830K. This is a general estimate for the temperature of G2V stars.

Before we can extract the atmospheric spectrum a few details had to be corrected for first. The spectra have to be aligned to the same wavelength grid (see table 2). This is the wavelength grid of our NIRSPEC spectra, because we want to leave the observed spectra untouched as much as possible. The library spectra were therefore interpolated to that wavelength grid with the MATLAB function INTERPOL (setting 'nearest'). The observed stellar spectra also showed small shifts in wavelength (max 0.002 μm) with respect to each other and were interpolated with the same routine, while keeping the number of datapoints intact. The routine makes sure the errors introduced here are small. At most the wavelength error is half a stepsize.

From the observed stellar spectra the inner spatial pixels were selected and summed to gain a good signal-to-noise. After that a simple division between the observed stars and the library stars is enough to obtain the atmospheric spectrum.

Spectral band	starting point	stepsize	number of points
H	1.4920 μm	2.86e-4 μm	1024
K	1.9760 μm	4.27e-4 μm	1024

Table 2: The standard wavelength grids used for the remainder of this research.

Several of the atmospheric spectra showed small artificial features due to an imperfect match between the library and observed star. These features had to be removed and were replaced by simple interpolation lines at those wavelengths (fig. 7 and fig. 8). Although not all spectra showed these features, the decision was made to treat all spectra with this routine to maintain an even set. The artificial features occur at 1.58 (twice), 2.11 and 2.37 μm. The features were identified by comparing the library star, the observed star and the atmospheric correction. Features not present in the observed star, but who were seen in the library star were flagged. These features lead to the peaks we see in the atmospheric spectra.
Great care was taken around the two artificial features around 1.58 μm. This is in the range of one of the absorption features we hope to use; the SiI line. To reduce the risk of influencing the Seyfert spectra, the artificial features were removed very shallowly. This leads to a somewhat incomplete removal at times, but the worst of the artifact is still removed. The location of the artificial features are: 1.575-1.577μm, 1.588-1.589μm, 2.105-2.110μm and 2.380-2.385μm. As can be seen from table 3 the interpolation is inside the wavelength range of our SiI feature.

[3]G2V = Luminosity type G, subdivision 2, spectral type V (dwarf star)

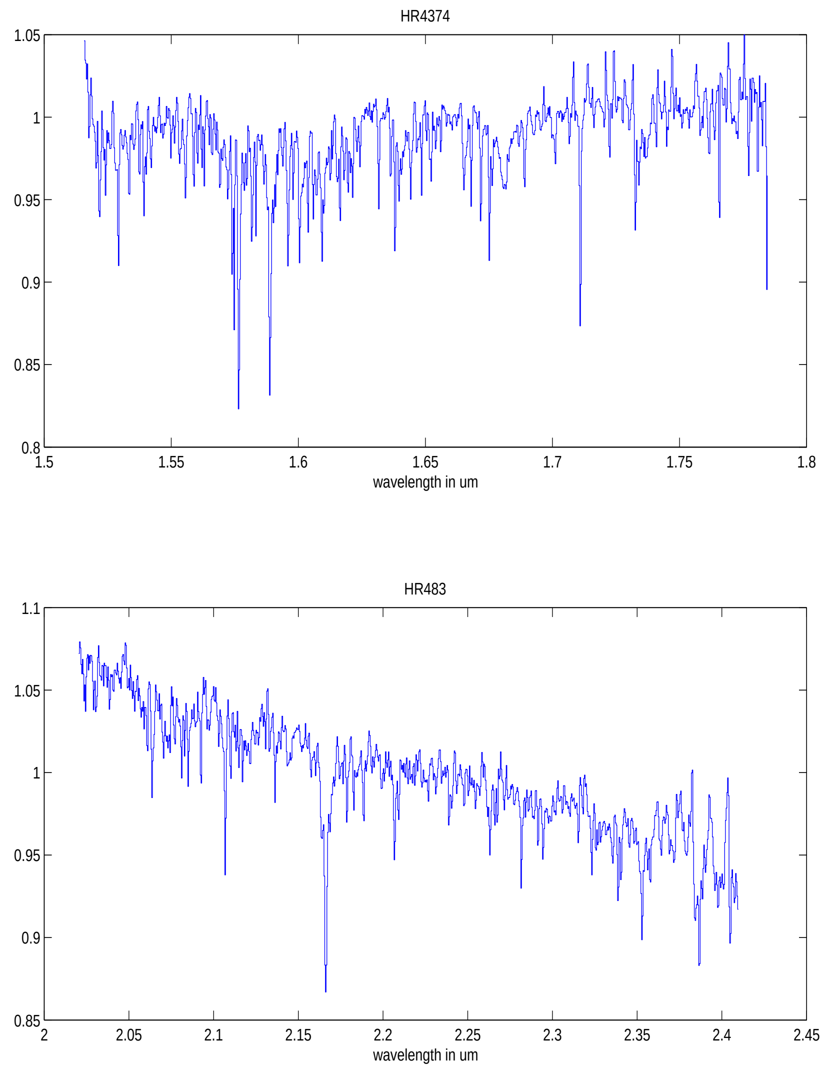

Figure 6: The standard stars HR4374 ([MEHS99]) and HR483 ([WH]), interpolated to the common wavelength grid as given in 2, but not yet multiplied by their corresponding Planck curves (T_{eff} = 5830K.

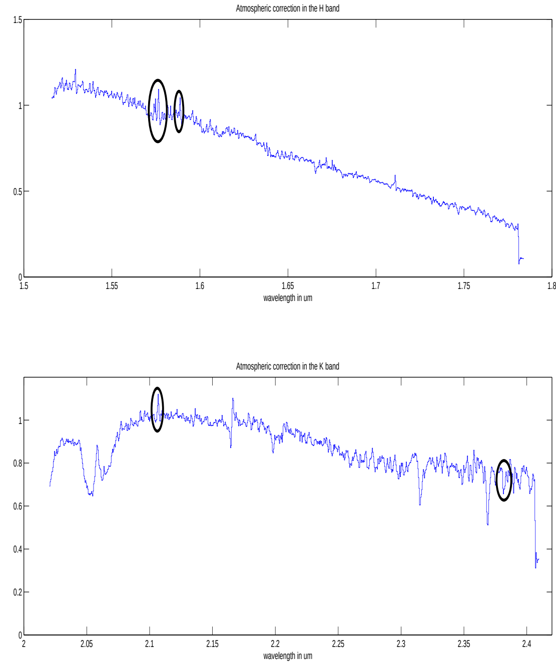

Figure 7: Two of the atmospheric spectra. The circles indicate the four artificial features which were identified (see text for details).

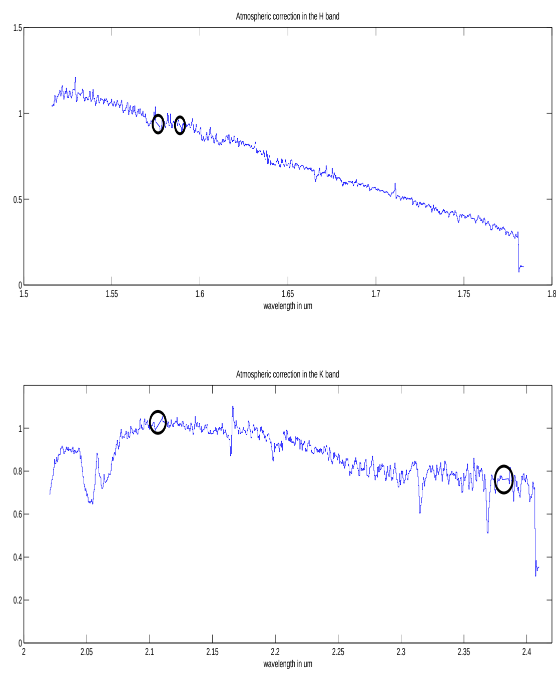

Figure 8: Two of the atmospheric spectra. The circles now indicate the interpolation applied for these parts of the spectra to remove the artificial features. In increasing wavelength the regions of interpolation are: 1.575-1.577μm, 1.588-1.589μm, 2.105-2.110μm and 2.380-2.385μm.

The behavior of the atmosphere can be very well seen in fig 8. The H band shows a few small features and a slant, which has to be corrected for. The K band shows more prominent features, particularly the wide double absorption band around 2.05 μm.
The reduced Seyfert spectra were finally obtained by dividing each observation with their individual atmospheric corrections.

3.3 Defining Nuclear and Circumnuclear positions

We wish to look at circumnuclear starbursts, therefore we define three bands of equal spatial (radial) size for all galaxies (see Figure 9). These are a 250pc inner-nuclear band (i.e. circle), a 500pc nuclear band and a circumnuclear 665pc band (i.e. 'ring'), where the inner 250pc have been removed. These bands are chosen with both the signal-to-noise and the seeing in mind. The largest seeing limited radius we see in table 4 is 208pc. We defined our first band outside this radius. A second band was defined to enable us to detect any possible gradients in the equivalent widths between the inner-nuclear band and the circumnuclear band. The circumnuclear band deserves some special attention. It is made up of light from both sides of the circumnuclear position, a 665pc radius without the inner-nuclear band. The equivalent widths we extract here may be influenced by rotation of the galaxy. We therefore analyze these spectra in two parts; the 'left' and 'right' side.
The 665pc outer radius has been chosen based on the noise level of our data. From the closest galaxy in our sample (Mkr 1) we then use the inner 75 columns of the total 101. This is the maximal width at which we still have good signal-to-noise for this galaxy, without including border effects at the ends of our slit.
The signal-to-noise given in tables 4 and 5 has been computed with the procedure given by [FS00]. It is taken as the inverse of the standard deviation about the mean flux after division by a straight line fitted over the range 2.242-2.256 μm. This region is a 'line-free' part of the spectrum. Although officially this only gives a signal-to-noise for the K band spectra, to first order we assume that the H band spectra have a similar value.

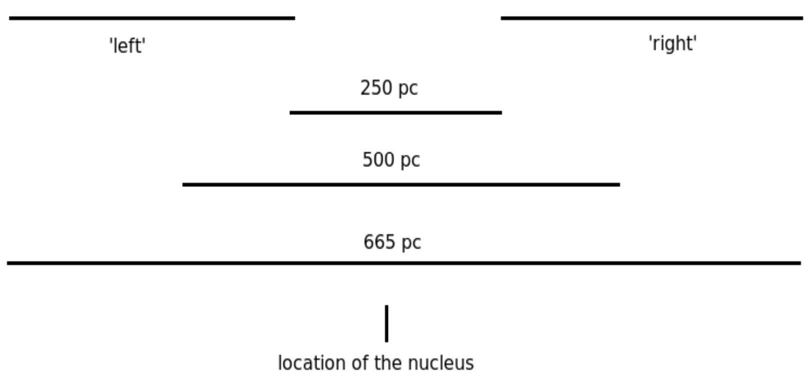

Figure 9: This is a schematic representation of the location of the extracted spectra.

3.4 Extracting Equivalent Widths

We have used the [OMO93] definitions for the determination of the continuum and integration limits of the absorption features. The computer codes for this section can be found in appendix B. The equivalent width, as a measure of the strength of absorption features, is defined as

$$EW_\lambda = \int_{\lambda_1}^{\lambda_2} (1 - f_\lambda) d\lambda,$$

where f_λ is the spectrum normalized to a flat continuum as determined by the continuum points in table 3. These points are used to fit a first, or in the case of ^{12}CO (2-0) a zeroth, order slope to the spectrum. λ_1 and λ_2 are the integration limits also given in table 3. $d\lambda$ is given in Angstroms. The equivalent widths extracted in this way still suffer from dilution by non-stellar (continuum) radiation. This is corrected for with the method described in section 2.4.

Feature (μm)	Symbol	Continuum points[4] (μm)	Integration limits (μm)
SiI 1.5892	$EW_{1.59}$	1.5850,1.5930	1.5870-1.5910
^{12}CO (6-3) 1.6187	$EW_{1.62}$	1.6160,1.6270	1.6175-1.6220
^{12}CO (2-0) 2.2935	$EW_{2.29}$	2.2900	2.2924-2.2977

Table 3: The continuum points and intervals for the absorption features SiI, CO(6-3) and CO(2-0) as defined by [OMO93]

[4]Central wavelength of the 0.002-0.003 μm wide intervals used to fit the normalizing continuum

			250 pc			500 pc			665 pc			
Name	seeing (pc)	pixel size (pc)	(pixel)	(pc)	S/N	(pixel)	(pc)	S/N	(pixel)	(pc)	S/N (left)	S/N (right)
Mrk 1066	147	32.6	8	261	25	15	489	24	20	652	20	23
Mrk 1	208	42.9	6	257	23	12	514	25	16	686	24	22
Mrk 3	187	38.5	6	231	47	13	501	47	17	655	49	46
NGC 1320	116	23.9	10	239	85	21	501	80	28	669	47	57
NGC 1667	194	43.0	6	258	59	12	517	57	15	646	44	35
NGC 2110	103	23.0	11	253	69	22	505	65	29	666	33	50
NGC 2273	112	17.9	14	251	84	28	502	84	37	664	52	72
NGC 262	195	40.1	6	240	96	12	481	96	17	681	94	40
NGC 2685	43	9.6	26	249	69	52	497	59	70	670	16	17
NGC 2992	158	25.3	10	253	95	20	507	92	26	659	68	75
NGC 3081	118	26.1	10	261	34	19	496	34	25	653	33	34
NGC 3185	71	14.7	17	249	60	34	498	57	45	660	34	28
NGC 3516	117	26.0	10	260	130	19	493	129	26	675	69	83
NGC 4051	55	8.9	28	248	74	56	497	73	75	665	22	15
NGC 4151	74	11.9	21	249	92	42	498	91	56	665	54	51
NGC 4253	179	39.7	6	238	69	13	516	68	17	675	41	50
NGC 4388	123	27.3	9	246	44	18	491	38	24	655	34	13
NGC 5273	76	12.2	20	244	66	41	501	65	54	660	33	38
NGC 5506	91	20.2	12	242	93	25	504	95	33	666	66	70
NGC 7450	122	27.1	9	244	43	18	488	44	25	677	27	34
NGC 931	205	45.4	6	273	77	11	500	79	15	682	71	63

Table 4: The seeing for each Seyfert galaxy, as given in table 1, has been converted into a physical scale, as is the width of a single pixel. Furthermore the number of spatial pixels needed for the diameters of 250pc, 500pc and 665pc have been included. The signal-to-noise of each spectrum has been included. There are two S/Ns for the 665pc, since that circumnuclear band was analyzed in two parts, the ‘left’ and ‘right’ sides. (see section 3.3)

Name	seeing (pc)	pixel size (pc)	170 pc (pixel)	170 pc (pc)	170 pc S/N	550 pc (pixel)	550 pc (pc)	S/N (whole)	S/N (left)	S/N (right)
NGC 2110	103	23.0	7	161	70	24	551	65	41	56
NGC 2273	112	17.9	9	161	86	31	556	84	61	76
NGC 3081	118	26.1	7	183	34	21	548	34	32	34
NGC 4051	55	8.9	19	168	74	62	550	72	45	38
NGC 4151	74	11.9	14	166	93	46	546	90	66	59
NGC 4388	123	27.3	6	164	46	20	546	37	37	18
NGC 5273	76	12.2	14	171	66	45	550	65	55	46

Table 5: A small subsection containing 3 Seyfert 1 and 4 Seyfert 2 is shown here. For this set new spectral bands were defined, with a smaller nuclear band, i.e. below the 100pc radius limit of [OU99]. Included are the number of pixels for the diameters 170pc and 550pc. The circumnuclear band in this sample is defined by a 550-170pc extracted 'ring'. As in table 4 the signal-to-noise is given for the extracted spectra. (see section 3.3)

4 Resulting NIR spectra

After the steps described in the last section, we now have our dilution corrected equivalent widths for SiI, CO(6-3) and CO(2-0). The next 4 tables contain the results for the total sample (Tables 6, 7, 8 and 9). The results for our smaller selection, which was chosen for higher spatial resulution, is given in Tables 10, 11, 12 and 13.
The tables in this section give, for each Seyfert galaxy, the dilution corrected values of SiI, CO(6-3) and CO(2-0) with the error due to the uncertainty in the continuum correction (see section 2.5). The final two columns of each table give the dilution factor of the spectra around 1.6μm (H) and 2.3 μm (K). These values should not be extrapolated to the entire H and K band.
In section 4.2 we will discuss qualitatively the results we find here for the total sample. The smaller sample will be discussed in section 4.3.

4.1 Tables

Name	$EW_{1.59}$	$\sigma(EW_{1.59})$	$EW_{1.62}$	$\sigma(EW_{1.62})$	$EW_{2.29}$	$\sigma(EW_{2.29})$	dilution H	dilution K
Mrk 1066	2.96	0.83	6.06	1.70	13.69	4.26	0.46	0.33
Mrk 1	2.95	0.82	6.16	1.09	13.90	4.26	0.29	0.32
Mrk 3	2.67	0.44	10.73	1.76	23.88	4.46	0.70	0.78
NGC 1320	2.97	0.91	5.41	1.66	12.27	4.23	0.40	0.60
NGC 1667	2.96	0.86	5.80	1.69	13.13	4.25	0.27	0.21
NGC 2110	2.97	1.05	4.43	1.56	10.13	4.19	0.30	0.68
NGC 2273	2.97	0.89	5.56	1.67	12.61	4.24	0.30	0.15
NGC 262	2.78	0.54	9.16	1.78	20.44	4.39	0.74	0.75
NGC 2685	4.28	1.23	4.79	1.38	12.69	4.21	0	0[5]
NGC 2992	2.94	1.24	3.24	1.37	7.53	4.14	0.50	0.71
NGC 3081	2.98	1.03	4.55	1.58	10.41	4.20	0.07	0.70
NGC 3185	2.98	1.02	4.65	1.59	12.61	4.20	0.09	0
NGC 3516	2.95	1.20	3.49	1.42	8.08	4.15	0.34	0.63
NGC 4051	2.98	1.01	4.71	1.60	10.75	4.20	0.48	0.67
NGC 4151	2.86	0.63	8.09	1.77	18.11	4.34	0.67	0.90
NGC 4253[6]	-	-	-	-	-	-	-	-
NGC 4388	2.98	1.01	4.71	1.60	10.75	4.20	0.16	0.68
NGC 5273	2.97	1.06	4.34	1.55	10.80	4.19	0.09	0
NGC 5506[7]	-	-	-	-	-	-	-	-
NGC 7450	2.95	0.81	6.24	1.71	14.08	4.27	0.59	0.46
NGC 931	2.97	1.11	4.02	1.51	9.23	4.17	0.78	0.88

Table 6: Results for the 250pc nuclear spectra. Given are the continuum corrected equivalent widths for $EW_{1.59}$, $EW_{1.62}$ and $EW_{2.29}$. The companion number is the error resulting from the correction. The last two columns give the fraction of non-stellar light as calculated from the correction. NGC 5506 was overexposed in its nucleus, and NGC 4253 is completely dominated by its nucleus.

[4]A dilution value of 0 means that the equivalent width extracted from the spectrum was already within the area covered by the stellar libraries (see section 2.4 and Figure 2).
[5]The active nucleus completely dominated the spectrum in NGC 4253.
[7]NGC 5506 was overexposed at the central spatial pixels.

Name	$EW_{1.59}$	$\sigma(EW_{1.59})$	$EW_{1.62}$	$\sigma(EW_{1.62})$	$EW_{2.29}$	$\sigma(EW_{2.29})$	dilution H	dilution K
Mrk 1066	2.96	0.85	5.94	1.70	13.42	4.25	0.43	0.23
Mrk 1	2.96	0.84	5.96	1.70	13.47	4.25	0.29	0.25
Mrk 3	2.75	0.50	9.67	1.77	21.57	4.41	0.67	0.73
NGC 1320	2.98	0.98	4.91	1.62	11.17	4.21	0.33	0.48
NGC 1667	2.97	0.88	5.66	1.68	12.81	4.24	0.28	0.17
NGC 2110	2.97	1.06	4.36	1.56	9.98	4.19	0.24	0.59
NGC 2273	2.97	0.89	5.61	1.68	12.71	4.24	0.30	0.12
NGC 262	2.81	0.57	8.83	1.78	19.73	4.38	0.70	0.74
NGC 2685	4.29	1.24	4.78	1.38	12.16	4.20	0	0
NGC 2992	2.94	1.21	3.40	1.40	7.90	4.15	0.46	0.64
NGC 3081	2.97	1.06	4.35	1.55	9.95	4.19	0.03	0.62
NGC 3185	2.98	1.01	4.70	1.60	12.37	4.20	0.12	0
NGC 3516	2.95	1.20	3.49	1.42	8.09	4.15	0.27	0.54
NGC 4051	2.98	1.03	4.59	1.58	10.48	4.20	0.42	0.64
NGC 4151	2.90	0.69	7.36	1.76	16.53	4.31	0.60	0.86
NGC 4253	2.50	0.33	12.83	1.70	28.45	4.54	0.91	0.98
NGC 4388	2.98	0.99	4.82	1.61	10.99	4.21	0.17	0.60
NGC 5273	2.97	1.08	4.25	1.54	11.09	4.18	0.07	0
NGC 5506	-	-	-	-	-	-	-	-
NGC 7450	2.94	0.79	6.44	1.72	14.52	4.27	0.59	0.44
NGC 931	2.96	1.15	3.78	1.47	8.72	4.16	0.72	0.84

Table 7: The results for 500pc nuclear spectra. NGC 5506 is still overexposed in the center. Further as table 6.

Name	$EW_{1.59}$	$\sigma(EW_{1.59})$	$EW_{1.62}$	$\sigma(EW_{1.62})$	$EW_{2.29}$	$\sigma(EW_{2.29})$	dilution H	dilution K
Mrk 1066	2.96	0.85	5.92	1.70	13.39	4.25	0.48	0.06
Mrk 1	2.98	0.98	4.91	1.62	13.44	4.21	0.24	0
Mrk 3	2.88	0.66	7.69	1.76	17.24	4.33	0.55	0.56
NGC 1320	2.95	1.17	3.65	1.45	10.23	4.16	0.03	0
NGC 1667	2.96	0.85	5.87	1.69	13.28	4.25	0.39	0.15
NGC 2110	2.98	0.96	5.06	1.63	11.51	4.22	0.30	0.20
NGC 2273	2.94	0.78	6.48	1.72	14.60	4.28	0.43	0.20
NGC 262	2.90	0.70	7.27	1.75	16.33	4.31	0.51	0.52
NGC 2685	3.91	1.17	4.90	1.46	11.16	4.21	0	0.09
NGC 2992	2.96	1.13	3.89	1.49	8.96	4.17	0.30	0.36
NGC 3081	3.52	1.19	4.26	1.44	9.77	4.18	0	0.47
NGC 3185	2.97	0.93	5.26	1.65	12.13	4.23	0.30	0
NGC 3516	2.96	1.13	3.90	1.49	9.28	4.17	0.14	0
NGC 4051	3.75	1.30	3.66	1.27	10.93	4.16	0	0
NGC 4151	2.97	0.94	5.23	1.65	11.89	4.22	0.18	0.16
NGC 4253	2.98	0.98	4.90	1.62	11.15	4.21	0.64	0.76
NGC 4388	2.98	0.98	4.89	1.62	11.15	4.21	0.15	0.08
NGC 5273	3.15	1.12	4.22	1.50	13.08	4.18	0	0
NGC 5506	2.16	0.19	17.09	1.50	37.74	4.72	0.84	0.89
NGC 7450	2.96	0.83	6.04	1.70	13.65	4.26	0.54	0.20
NGC 931	2.95	1.18	3.59	1.44	8.30	4.15	0.27	0.49

Table 8: The results for the left part of the 665pc - 250pc circumnuclear ring. Further as table 6.

Name	$EW_{1.59}$	$\sigma(EW_{1.59})$	$EW_{1.62}$	$\sigma(EW_{1.62})$	$EW_{2.29}$	$\sigma(EW_{2.29})$	dilution H	dilution K
Mrk 1066	2.98	0.99	4.82	1.61	14.07	4.21	0.13	0
Mrk 1	2.98	0.98	4.89	1.61	11.13	4.21	0.30	0.03
Mrk 3	2.75	0.51	9.65	1.78	21.52	4.41	0.67	0.64
NGC 1320	2.98	0.99	4.87	1.61	11.10	4.21	0.35	0.17
NGC 1667	2.98	1.00	4.74	1.60	11.25	4.20	0.16	0
NGC 2110	3.31	1.17	4.13	1.46	9.48	4.18	0	0.12
NGC 2273	2.97	0.97	5.00	1.63	12.61	4.21	0.09	0
NGC 262	2.30	0.74	6.84	1.74	15.39	4.29	0.57	0.55
NGC 2685	4.58	1.27	4.76	1.32	10.86	4.20	0	0.18
NGC 2992	2.95	1.19	3.56	1.43	8.24	4.15	0.24	0.38
NGC 3081	2.97	1.09	4.14	1.53	9.51	4.18	0.04	0.44
NGC 3185	2.97	1.08	4.25	1.54	11.89	4.18	0.03	0
NGC 3516	3.40	1.20	4.03	1.42	9.71	4.17	0	0
NGC 4051	2.97	1.07	4.33	1.55	11.58	4.19	0.09	0
NGC 4151	2.97	0.90	5.53	1.67	12.54	4.24	0.24	0.25
NGC 4253	2.96	0.84	6.01	1.70	13.59	4.26	0.7	0.83
NGC 4388	2.98	1.04	4.53	1.58	10.36	4.19	0.14	0.24
NGC 5273	2.97	1.07	4.29	1.55	11.87	4.18	0.01	0
NGC 5506	-	-	-	-	-	-	-	-
NGC 7450	2.70	0.47	10.23	1.77	22.79	4.43	0.73	0.54
NGC 931	2.91	1.35	2.44	1.13	5.79	4.11	0.32	0.25

Table 9: The results for the right side of the 665pc - 250pc circumnuclear ring. Further as table 6.

Name	$EW_{1.59}$	$\sigma(EW_{1.59})$	$EW_{1.62}$	$\sigma(EW_{1.62})$	$EW_{2.29}$	$\sigma(EW_{2.29})$	dilution H	dilution K
NGC 2110	2.97	1.07	4.32	1.55	9.90	4.19	0.31	0.74
NGC 2273	2.97	0.90	5.47	1.66	12.40	4.23	0.30	0.16
NGC 3081	2.98	1.01	4.68	1.59	10.69	4.20	0.09	0.74
NGC 4051	2.98	0.98	4.95	1.62	11.28	4.21	0.52	0.72
NGC 4151	2.81	0.56	8.84	1.78	19.75	4.38	0.72	0.92
NGC 4388	2.98	1.00	4.75	1.60	10.83	4.20	0.20	0.75
NGC 5273	2.97	1.06	4.36	1.56	10.58	4.19	0.10	0

Table 10: The results for the 170pc subsample. Further as table 6.

Name	$EW_{1.59}$	$\sigma(EW_{1.59})$	$EW_{1.62}$	$\sigma(EW_{1.62})$	$EW_{2.29}$	$\sigma(EW_{2.29})$	dilution H	dilution K
NGC 2110	2.97	1.07	4.32	1.55	9.90	4.19	0.24	0.58
NGC 2273	2.97	0.89	5.61	1.68	12.71	4.24	0.29	0.12
NGC 3081	2.97	1.07	4.31	1.55	9.90	4.19	0.02	0.61
NGC 4051	2.98	1.03	4.58	1.58	10.46	4.20	0.44	0.64
NGC 4151	2.90	0.69	7.35	1.76	16.50	4.31	0.60	0.86
NGC 4388	2.98	1.00	4.77	1.60	10.88	4.20	0.17	0.58
NGC 5273	2.97	1.08	4.26	1.54	11.09	4.18	0.06	0

Table 11: The results for the 550pc subsample. Further as table 6.

Name	$EW_{1.59}$	$\sigma(EW_{1.59})$	$EW_{1.62}$	$\sigma(EW_{1.62})$	$EW_{2.29}$	$\sigma(EW_{2.29})$	dilution H	dilution K
NGC 2110	2.98	0.94	5.16	1.64	11.74	4.22	0.35	0.28
NGC 2273	2.94	0.78	6.47	1.72	14.58	4.28	0.42	0.20
NGC 3081	3.34	1.15	4.26	1.47	9.77	4.18	0	0.45
NGC 4051	3.15	1.27	3.31	1.33	10.30	4.14	0	0
NGC 4151	2.97	0.90	5.50	1.67	12.47	4.24	0.25	0.29
NGC 4388	2.98	0.99	4.82	1.61	10.99	4.21	0.10	0.20
NGC 5273	3.18	1.11	4.36	1.52	12.82	4.19	0	0

Table 12: The results of the left off nucleus subsample. Further as table 6.

Name	$EW_{1.59}$	$\sigma(EW_{1.59})$	$EW_{1.62}$	$\sigma(EW_{1.62})$	$EW_{2.29}$	$\sigma(EW_{2.29})$	dilution H	dilution K
NGC 2110	3.05	1.14	3.99	1.49	9.18	4.17	0	0.45
NGC 2273	2.97	0.94	5.22	1.65	12.19	4.22	0.16	0
NGC 3081	3.00	1.10	4.17	1.53	9.57	4.18	0	0.45
NGC 4051	2.97	1.06	4.40	1.56	10.07	4.19	0.07	0.01
NGC 4151	2.96	0.86	5.84	1.69	13.21	4.25	0.30	0.35
NGC 4388	2.98	1.00	4.77	1.60	10.89	4.20	0.19	0.34
NGC 5273	2.97	1.10	4.08	1.52	11.17	4.17	0.07	0

Table 13: The results of the right off nucleus subsample. Further as table 6.

4.2 Discussion of the results of our total sample

When we look at the results for the 250pc nuclear (Table 6), 500pc nuclear (Table 7), left off-nuclear (Table 8) and right off-nuclear (Table 9) spectra, a few things are noticeable. First almost all the equivalent widths of the SiI line $EW_{1.59}$ are close to 3. The equivalent widths of the CO(6-3) line have a little more scatter; most values are between 4 and 6 with some outliers to both sides. As we will see from Figure 14, these general values for the equivalent widths are consistent with almost all ages. The biggest spread in values is for the equivalent widths of CO(2-0), values between 8 and over 20 are recorded. The errors associated with the equivalent widths are of the order 33% of the value.

There are a few outliers we will now take a closer look at. For some Seyfert galaxies the observed equivalent widths of SiI are significantly higher than 3. This is seen in NGC 2685 in all 4 tables and NGC 3081 and NGC 4051 in the left off-nuclear results (Table 8), while NGC 2685 and NGC 3516 show the same in the right off-nuclear results (Table 9). Further we note that the other equivalent widths of these galaxies do not show higher than average values.

NGC 262 shows very high values of $EW_{1.62}$ and $EW_{2.29}$ in all tables, while NGC 4151 only does so at both nuclear results (Tables 6 and 7, maybe a nuclear starburst?). NGC 7450 shows extreme values of $EW_{1.62}$ and $EW_{2.29}$ in the right off-nuclear results (Table 9).

These high values of equivalent widths are found in galaxies for which we have also calculated a high dilution factor. This could indicate that we are dealing with some form of overcorrection, but this is not a one-to-one relation. We also find low and intermediate values of the equivalent widths in galaxies with high dilution.

4.2.1 Short inspection of Brγ in our sample.

When we are looking at the Brγ (λ = 2.166 μm) line in our spectra we must always remember that at least at the nuclear positions the emission will be at least dominated by the AGN and very likely not come from young stars. However, several spectra (Appendix C) do show Brγ in their circumnuclear spectra.

For instance Mrk 1066, Mrk 1, Mrk 3, NGC 2110 (weak line), NGC 2273 (weak line), NGC 2992,

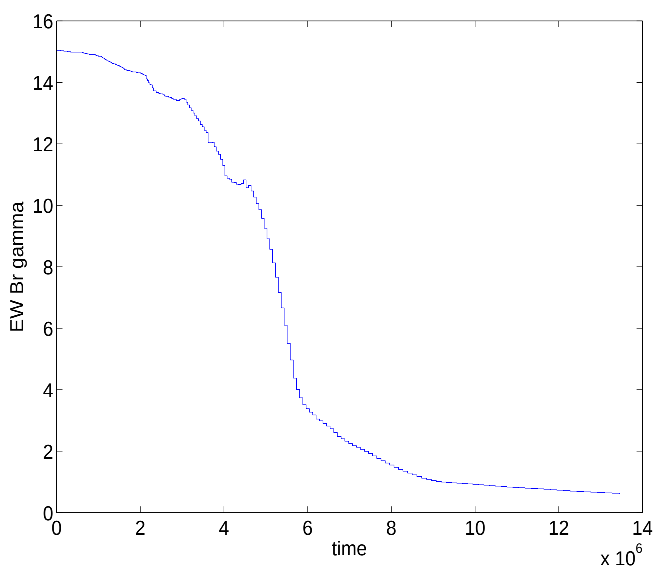

Figure 10: As can be seen from this figure Brγ is a tracer of young stellar population. This is modelled data for the equivalent width expected from a 1 Myr starburst population using Starburst99.

NGC 3081, NGC 3185 (only in the circumnuclear spectrum), NGC 4253, NGC4388, NGC 5506 (circumnuclear spectrum only) and maybe a very broad, but low intensity, line in NGC 931.

The most interesting one is NGC 3185, where we can be certain of the stellar origin of the line, since nothing is detected from the AGN. If we look at the results for the circumnuclear spectra (Tables 8 and 9) we do not see any particular values for the stellar equivalent widths of NGC 3185. They fall within the average regions, which we found to be consisted with most ages. We speculate that there is a very young stellar population (starburst less then a few million years ago), while the infrared spectrum is still being dominated by an older stellar population. The same may be true for NGC 5506, but there the nuclear spectra are unreliable since they were overexposed.

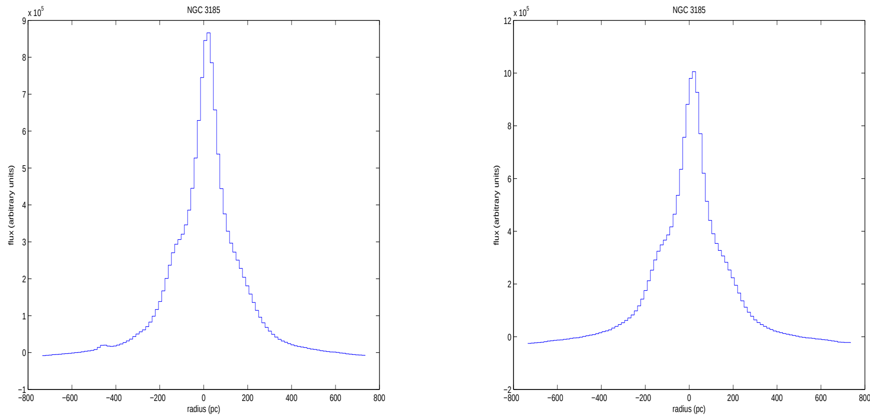

Figure 11: Shown is the lightcurve for the H and K bands of Seyfert galaxy NGC 3185. Note the distinct bump at the left side of the curve at the radius of 200pc.

4.2.2 Light profiles

We also examined the light profiles as a function of radius for our galaxies. We did this primarily to find the position of the slit edges. There are a few galaxies that deserve extra attention at this point.
Most light is dominated by the nucleus and therefore all light profiles show a declining flux to the outer edges. However a few galaxies show slight bumps in this falling curve (i.e. Figure 11). These are the Seyferts Mrk 1066, NGC 2273, NGC 2992, NGC 3185 and NGC 4388. This is a quick visual inspection and is in no way complete, but it is interesting to note that all these galaxies are also named in our inspection of Brγ. The calibrator stars for these galaxies do not show such a feature, making it very unlikely that this is an artifact from the NIRSPEC instrument.
A last note should be added about NGC 4151. The maximum flux (in the nucleus) is in almost all galaxies twice as high in the K band, as it is in the H band. The exception is NGC 4151, here the flux is almost four times as high in the K band. Maybe this is related to the higher values of $EW_{1.62}$ and $EW_{2.29}$ we found for this galaxy.

4.3 Discussion of the results of our smaller sample

A similar analysis can also be made for the subsample with higher spatial resolution. NGC 3081 again shows a high value of $EW_{1.59}$ in the left off-nucleus sample. This means that it likely originate at a radius between 85 and 250 pc from the nucleus (the overlap in radii between the two spectra). NGC 4051 does not show a very high $EW_{1.59}$ value in the left off-nucleus sample, indicating that those values are from further out in the galaxy.
NGC 4151 shows its high values of $EW_{1.62}$ and $EW_{2.29}$ also in the nuclear spectra of this subsample, constraining the origin of these equivalent widths to within a radius of 85 pc around the nucleus.

5 Analysis

5.1 Description of Starburst99

Starburst99 ([Lea99], [VL05]) is a so called evolutionary population synthesis model. This class of models is made by starting with a synthetic Hertzsprung-Russell diagram (HRD) made from theoretical stellar tracks and an assumed initial mass function (IMF). This HRD is then merged with observable parameters of single stars. These can either be theoretically derived or from observations. The Starburst99 code saw first light in 1987 as a simple code to calculate ionizing fluxes for individual O stars. From there it has been expanded to handle a single stellar population and provide several parameters including absorption and emission line equivalent widths in addition to the ionizing flux. Origlia et al.[Oea99] have added equivalent widths modelled from individual stars [OMO93] for SiI, CO(6-3) and CO(2-0).

The input for Starburst99 allow for many parameters to be set. The first important one is the choice between continuous or instantaneous starburst. We chose the latter, since we expect the starformation inside the dust ring to be an short-lived event. Other important parameters are the assumed IMF, the stellar tracks used and the computing time step (setting the time resolution). [Lea99]

From the four options for stellar tracks we have used the Padova tracks with thermally pulsing AGB stars as the stellar tracks of our choice following a discussion by [OO00]. All calculations were done with a 1000 logarithmically distributed timesteps between 10^4 years and $5*10^9$ years.

As can be seen from Figure 12, there is little difference between a simple Salpeter ($\alpha = 2.35$, 0.1 - 100 $M_\odot$) and a standard Kroupa IMF ($\alpha = 1.3$, 0.1 - 0.5 $M_\odot$, $\alpha = 2.3$, 0.5 - 100 $M_\odot$).

However there is a significant difference if we vary the metallicity of the stellar tracks. The higher

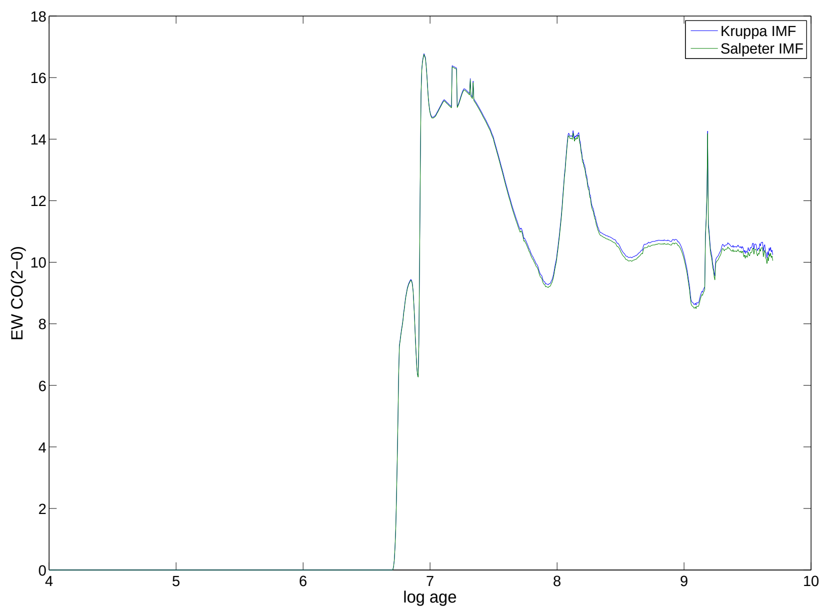

Figure 12: Shown here are the EW CO(2-0) for two IMF, Salpeter and Kroupa.

the metallicity, the higher the overall equivalent widths (fig. 13). From [Oea99] we know that the models fail at subsolar metallicities. Supersolar metallicities are also unlikely, as the material for starformation in the nuclear starburst rings has very likely been transported in from farther out in the disk. Also our continuum corrections are obtained from mostly solar metallicity models, which makes it erroneous to use a metallicity different from solar here. Lastly we know that our Seyfert galaxies are all of similar Hubble type (Sa or Sb), so we assume a similar metallicity.

Further we have investigated the influence of changing the value of the microturbulence ξ on the

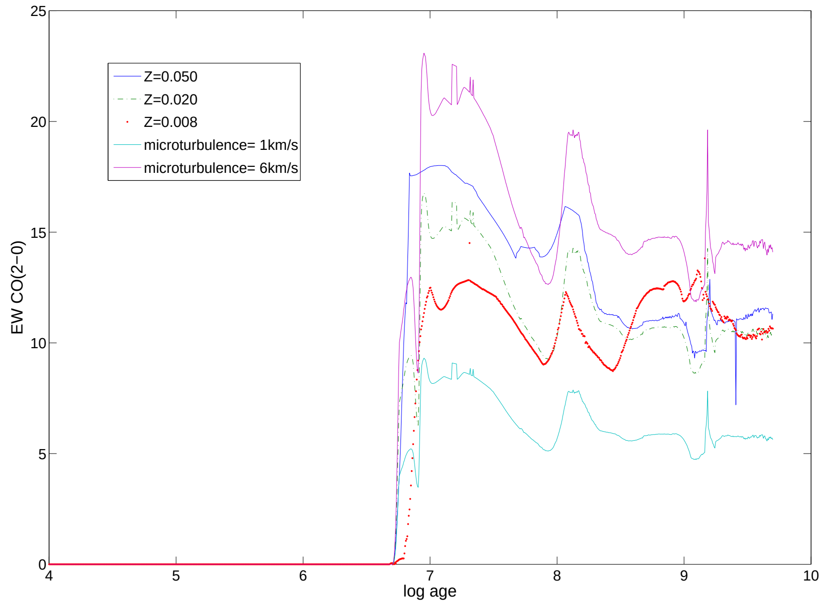

Figure 13: The output of Starburst99 for $EW_{2.29}$ for different metallicities and microturbulences. Similar results are obtained for $EW_{1.59}$ and $EW_{1.62}$. blue line: Z=0.050 (super-solar), ξ = 3km/s; dot-dashed line: Z=0.020 (solar), ξ = 3km/s; red dot line: Z=0.008 (sub-solar), ξ = 3km/s; light blue line: Z=0.020, ξ = 1km/s and pink line: Z=0.020, ξ = 6km/s.

equivalent widths. Microturbulence is the chaotic flow of gas in the atmosphere of stars. It is a poorly understood phenomenon that cannot be theorized or modeled very well.[SC05] The empirical models for the equivalent widths as given by [Oea99] are valid for microturbulence values between 1 km/s and 6 km/s. As we see from Figure 13, the higher the microturbulence, the higher the equivalent widths. At this time the best anyone can say about microturbulance is that it is of order a few km/s. We therefore set it to ξ = 3 km/s.

So finally the parameters for our model are: 1 Myr burst time of a stellar population with a mass of $10^6 M_\odot$, Kroupa IMF, Padova solar metallicity tracks with thermally pulsing AGB stars included, microturbulence 3km/s and out to ages of 5 Gyr. While there is some degeneracy in the model, we are for the largest part interested in the difference between Seyfert type 1 and type 2 galaxies and thus relative differences. Errors in the model only affect the absolute age estimate.

As can be seen from Figure 14 all three equivalent widths appear after several Myr, when the first supergiants appear. The absorption features are strongest there and then fall off. At a 100 Myr there is another bump, this is due to stars evolving along the AGB. At that moment the star experiences a convective episode where the outer convective zone penetrates inwards, a *dredge up*. Due to this episode the mixing increases the equivalent widths of the molecular species.

5.2 Analysis of the full sample with Starburst99

As can be seen from Figure 15 and Appendix C our method is at most times not constrained enough to differentiate between supergiants and giants. Most values we found can be equally well fitted with a supergiant population and an AGB population or equally ages around 10 Myr or 200 Myr, respectively. In most cases we cannot even rule out old (> 1 Gyr) populations.

However a few spectra do show definite signs of a younger population. These are characterized by low equivalent widths of CO(6-3) and CO(2-0) (table 14 and Figure 16). Although as can been seen even that is not a very firm conclusion. Under 'young' population we will mean signs of Brγ in the circumnuclear spectra and/or low equivalent widths of CO(6-3) and CO(2-0) detected in the spectra.

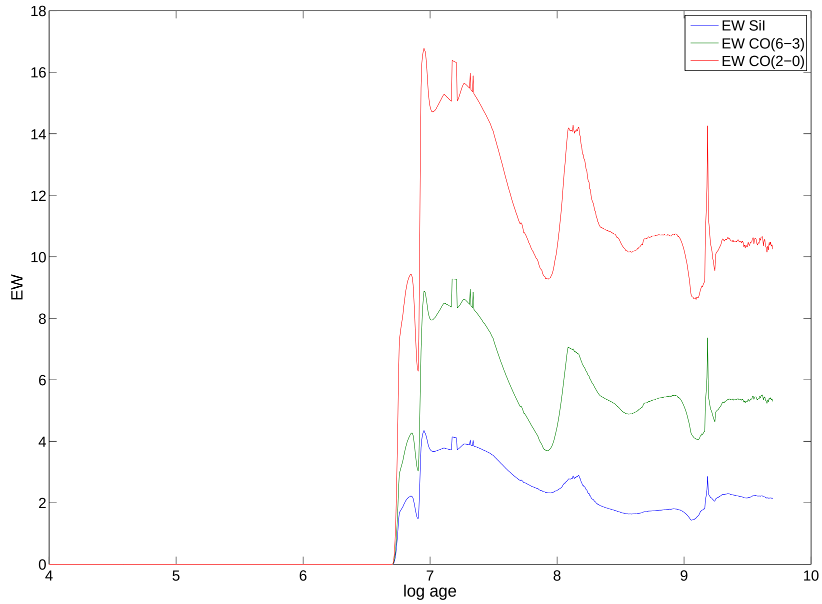

Figure 14: Shown here are the equivalent widths as a function of the age of the stellar population for the three absorption lines we use: SiI, CO(6-3) and CO(2-0).

Our results suffer from large errors, which make firm conclusions about the individual sources impossible. We can however still answer the questions posed at the beginning of this report.

Do we see a powerful starburst in Seyfert 1 host galaxies?

- NGC 3516: no Brγ detected, possible 2-6 Myr old starburst (Starburst99).
- NGC 4051: no signs of a young population, age cannot be further constrained.
- NGC 4151: no Brγ detected, large values of $EW_{2.29}$ in the nucleus; possibly a supergiant population.
- NGC 4253: Brγ emission in the circumnuclear spectra.
- NGC 5273: no signs of a young population, age cannot be further constrained.
- NGC 5506 (type 1.9 Seyfert): shows Brγ emission in the circumnuclear spectra.
- NGC 7450: no Brγ detected, large values of $EW_{2.29}$ in the right circumnuclear spectrum; possibly a supergiant population. An old population can be excluded.
- NGC 931: Brγ emission in the circumnuclear spectra and possible 2-6 Myr old starburst (Starburst99).

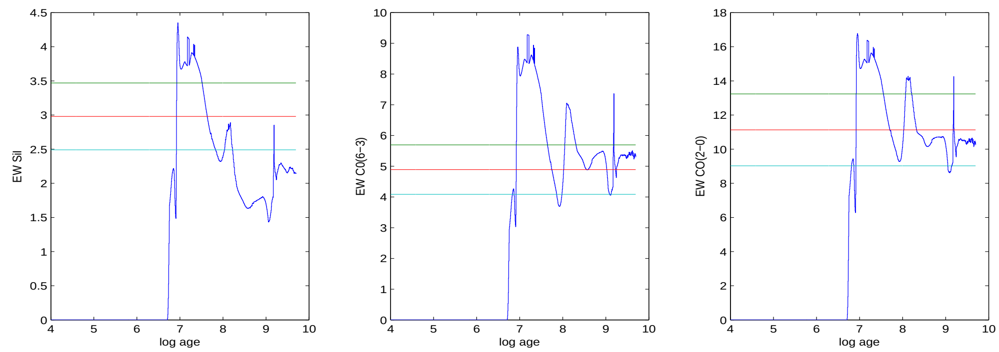

Figure 15: An example of the results obtained with Starburst99, the other results can be found in Appendix C. These are the results for the 'right' circumnuclear spectrum of Mrk 1. The blue line is the theoretical value of SiI, CO(6-3) and CO(2-0) (top to bottom), while the red line (horizontal) is the value we found as given in section 4.1 and the green and light blue line are the 0.5*σ upper and lower boundaries for this value as a function of age for a delta burst.

So there are signs of recent starformation (age < 10 Myr) for the nuclear and circumnuclear regions in 5 out of 8 of our Seyfert 1 galaxies.

Is there a difference in stellar populations between Seyfert type 1 and Seyfert type 2 galaxies?
If we look at the off-nuclear spectra, we found several with 'young' populations (table 14). Giving these the values of 1 and the others the value of 2, we computed a Mann-Whitney test. We have 5 of the 8 Seyfert type 1 and 8 out of 13 Seyfert type 2 with a 'young' population.
We test under the hypothesis that the two are from the same age population at the 5% level of significance. We find a probability of 100%; we cannot find a difference in age.
Finally when we looked at the lightcurves, we found several with 'bumps' which we assume to be compact stellar populations. These are all Seyfert 2, but since Seyfert 1 cores are generally brighter this could likely be just an artifact.

What are the typical ages of the stellar populations in Seyfert galaxies?
This is the one question we cannot really answer. We have seen evidence for recent starformation in several Seyfert galaxies, but for most we cannot determine the age to any useful accuracy.

5.3 Description of the Spectral Fitting Method GANDALF

GANDALF[8] is a direct fitting method that can distinguish between stellar continuum and nebular emission. Originally it was planned to also use this method to find the ages of the stellar populations in our sample. Due to time-issues this has not been done. Given the large errors in our current method, this is unfortunate. GANDALF has two great advantages over evolutionary population synthesis models.
First it uses the whole observed spectrum to fit a superposition of stellar templates. This makes it more stable against dust or emission lines filling up the stellar features. Second it takes an integral approach to the determination of the non-stellar continuum.
GANDALF is an extension of the PPXF software developed by Cappellari & Emsellem [CE04]. This software fits the superposition of stellar templates but cannot handle emission lines, which have to be masked. As was shown in [Sea06] this introduces biases to the fit. GANDALF has overcome this problem.
It works as follows. The stellar templates are convolved with a stellar line of sight velocity distri-

[8]GANDALF was developed by the SAURON team and is available from the SAURON website (ww.strw.leidenuniv.nl/sauron). See also Sarzi et al.[Sea06] for details.

Name	type	250pc	500pc	left	right
Mrk 1066	2			γ	γ
Mrk 1	2			γ	γ
Mrk 3	2			γ	γ
NGC 1320	2				
NGC 1667	2				
NGC 2110	2			γ	γ
NGC 2273	2			γ	γ
NGC 262	2				
NGC 2685	2				
NGC 2992	2	✓	✓	✓, γ	✓, γ
NGC 3081	2			γ	γ
NGC 3185	2			γ	γ
NGC 3516	1.5	✓	✓	✓	✓
NGC 4051	1.2				
NGC 4151	1.5				
NGC 4253	1.5			γ	γ
NGC 4388	2			γ	γ
NGC 5273	1.5				
NGC 5506	1.9				
NGC 7450	1.5				
NGC 931	1.5	✓	✓	✓, γ	✓, γ

Table 14: Each check marks where we found evidence for a relatively young population with ages between 1Myr and 5Myr. γ means we found Brγ in the circumnuclear spectra, this indicates populations younger than 10 Myr.

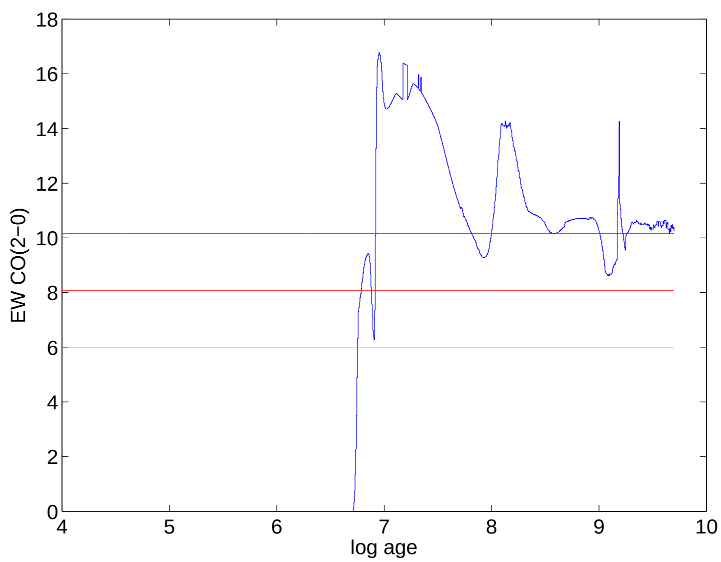

Figure 16: Value for NGC 2992 250pc nuclear spectrum.

bution (LOSVD) and the emission lines with a Gaussian LOSVD. A usermade file is input with the location and name of the emission lines present in the spectra. The emission lines can be set to be modelled independent of each other, in specific ratios or ignored. Then iteratively an optimum is searched for which fits the stellar continuum and emission lines best.
The output gives the velocities and velocity dispersions in the spectrum and the optimum combination of stellar templates and strengths of the emission lines.

6 Summary

The unifying scheme states that Seyfert type 1 and type 2 galaxies are intrinsically the same galaxies, but viewed under different angles. This scheme is disputed by Ohsuga & Umemura [OU99], who claim a fundamental difference in age of the circumnuclear stellar population for low-luminosity AGN. Seyfert type 2 galaxies have a circumnuclear stellar population of younger age according to their model.
Using the infrared spectra of 21 nearby Seyfert galaxies selected for high spatial resolution, Schinnerer and collaborators have attempted to shed light on this issue. In the infrared the stellar light is dominated by red giants and supergiants. Three stellar absorption lines, present in these stars, have been used to estimate the ages of the stellar population.
For this project we needed to correct for the atmosphere, obtain the relevant spectra, extract the equivalent widths and dilution correct them. We have defined three spatial bands, consisting of a 250pc inner-nuclear band (i.e. circle), a 500pc nuclear band and a 665pc band without the inner 250pc (i.e. 'ring'). The errors in the extracted equivalent widths are of order 33%.
We have compared our equivalent widths against models obtained from Starburst99, an evolutionary population synthesis model. Our input to the model was a 10^6 $M_\odot$ starburst of 1 Myr burst time, with Kroupa IMF, Padova solar metallicity tracks with thermally pulsing AGB stars included, microturbulance at 3 km/s and results out to ages of 5 Gyr. We defined evidence for 'young' populations as finding Brγ line emission in the circumnuclear spectra and/or low equivalent widths of CO(6-3) and CO(2-0) in the spectra.
Our results indicate that there is no difference in starformation between Seyfert type 1 and Seyfert type 2 galaxies. We found evidence for young populations in 5 out of 8 type 1 Seyfert galaxies and 8 out of 13 type 2 Seyferts. For most galaxies in our sample the equivalent widths can be equally well fitted with a supergiant and a giant population, not even stellar populations older than 1Gyr can be excluded for most galaxies. A final interesting feature we found was the bump in the light profile of NGC 3185, which might be related to the Brγ emission from this region, indicating a compact, very young stellar population.

6.1 Recommendations for further study

This research has been limited by time. As already briefly touched upon in section 5.3, GANDALF is a superior method to use in the determination of the stellar populations. We have not had the time to do this.
Further we would like to inform the reader that while we have only used the spectral data here, the total dataset collected is much bigger. It also incorporates J, H and K images of all sources. The original proposal for these observations hold even more nearby Seyfert galaxies. The chance to extend our sample to incorporate these would give further statistical strength to our conclusions.
Lastly, just before the final version of this report was made a new line-strength index was proposed for the CO(2-0) line by [MQea] which may lead to better constrains on our measurement of CO(2-0). At the moment the errors for the equivalent width of this line are too large to give good boundaries on the stellar ages. This is in part due to the wide spread we find in the stellar libraries.

6.2 Acknowledgements

I would like to thank Eva Schinnerer and her collaborators (E. Colbert, L. Armus, N.Z. Scoville and T.M. Heckman) for providing this interesting and exciting dataset. Also the enlightening talks I have had with Eva and her invitation to the conference on nuclear starclusters are greatly appreciated.

References

[Ant93] R. Antonucci. Unified models for active galactic nuclei and Quasars. *Ann. Rev. A&A*, (31):473–521, 1993.

[CE04] M Cappellari and E Emsellem. Parametric recovery of Line-of-Sight Velocity Distributionfrom Absorption-Line Spectra of Galaxies via Penalized Likelyhood. *PASP*, (116):138–147, 2004.

[DBJ96] R. Dallier, C. Boisson, and M. Joly. A library of H band stellar spectra for stellar population analysis purposes. *A&A Sup.S*, 1996.

[DMST+07] R.I. Davies, F. Mueller Sánchez, L.J. Tacconi, E.K.S. Hicks, and S. Friedrich. A Close Look at Star Formation around Active Galactic Nuclei. *ApJ*, (671):1388:1412, 2007.

[FS00] N.M. Förster-Schreiber. Moderate-resolution near-infrared spectroscopy of cool stars: A new K-band library. *ApJ*, 120:2089–2100, 2000.

[Hea95] T. Heckman et al. The Nature of the Ultraviolet Continuum in Type 2 Seyfert Galaxies. *ApJ*, (452):549–564, 1995.

[HFS97] L.C. Ho, A.V. Filippenko, and W.L.W. Sargent. A search for 'dwarf' seyfert nuclei III. *ApJS*, (112):315–390, 1997.

[Iea04] W. Ivanov et al. A medium-resolution near-infrared spectral library of late-type stars. I. *ApJS*, 2004.

[IR00] V. Ivanov and G. et al. Rieke. Testing the agn-starburst connection in seyfert galaxies. *ApJ*, 545:190–204, 2000.

[KH86] S.G. Kleinmann and D.N.B. Hall. Spectra of late-type standard stars in the region 2.0-2.5 μm. *ApJS*, 1986.

[Lea99] C. Leitherer et al. Starburst99: synthesis models for galaxies with active star formation. *ApJS*, 123:3–40, 1999.

[Mea96] D. Maoz et al. HST ultraviolet images of five circumnuclear star-forming rings. *AJ*, 111(6):2248, 1996.

[MEHS99] M.R. Meyer, S. Edwards, K.H. Hinkle, and S.E. Strom. Near-Infrared Classification Spectroscopy: H-band spectra of fundamental MK standards. *ApJ*, 508:397, 1999.

[MQea] E. Mármol-Queraltó et al. A New Stellar Library in the region of the CO index at 2.3μm. arXiv:0806.0581v1.

[Oea99] L. Origlia et al. Evolutionary synthesis modeling of red supergiant features in the near-infrared. *ApJ*, 514:96–108, 1999.

[OMO93] L. Origlia, A.F.M. Moorwood, and E. Oliva. The 1.5-1.7 micrometer spectrum of cool stars: line identifications, indices for spectral classification and the stellar content of the seyfert galaxy NGC 1068. *A&A*, 280:536–550, 1993.

[OO00] L. Origlia and E. Oliva. Is the [CO] index an age indicator for starforming galaxies? *A&A*, 2000.

[OOKM95] E. Oliva, L. Origlia, J.K. Kotilainen, and A.F.M. Moorwood. Red supergiants as starburst tracers in galactic nuclei. *A&A*, 301:55–67, 1995.

[OOM99] E. Oliva, L. Origlia, and R. Maiolino. Starbursts in active galaxy nuclei: observational constraints from ir stellar absorption lines. *A&A*, 350:9–16, 1999.

[OU99] K. Ohsuga and M. Umemura. Formation of large-scale obscuring wall and active galactic nucleus evolution regulated by circumnuclear starbursts. *ApJ*, 521:L13–L16, 1999.

[Pet97] B.M. Peterson. *An Introduction to Active Galatic Nuclei*. Cambridge University Press, 1997.

[SC05] M. Salaris and S. Cassisi. *Evolution of Stars and Stellar Populations*. John Wiley & Sons, Ltd., 2005.

[Sea06] M. Sarzi et al. The SAURON project -V: Integral-field emission-line kinematics of 48 elliptical and lenticular galaxies. *MNRAS*, (366):1151–1200, 2006.

[VL05] A. Vázquez and C. Leitherer. Optimization of starburst99 for intermediate-age and old stellar populations. *ApJ*, 621:695–717, 2005.

[WH] L Wallace and K. Hinkle. Medium-resolution spectra of normal stars in the K band.

[Whi92] M. Whittle. Virial and jet-induced velocities in seyfert galaxies. I. a compilation of narrow line region and host galaxy properties. *ApJS*, 79:49–75, 1992.

A Computercodes for the Atmospheric correction

Atmos.m

Atmos.m is the MATLAB code that I used to interpolate the observed star spectra to the common wavelength grid, as given in table 2. This code works on one spectrum in one band at a time.

```
Obsster=fitsread('Obsstars/sterHN931.fits');       reading in the spectrum
[C,I]=max(Obsster(500,:));                         finding the flux center
Obsster=Obsster(:,I-5:I+5);                        extracting the inner 11 columns
ObssterM=mean(Obsster,2);                          averaging the inner 11 columns

begval=load('Obsstars/beginmark2val.dat');         the exact beginstep of the spectrum
stepval=load('Obsstars/step2val.dat');             the exact wavestep of the spectrum

i=21;
for k=1:1024
    oudarr(k)=begval(i)+ (k-1)*stepval(i);    constructing the old wavelength grid
end
for k=1:1024
    newarr(k)=1.4920+ (k-1)*2.86e-4;               constructing the new wavelength grid
end

newspec=interp1(oudarr,ObssterM,newarr,'nearest'); the interpolation routine

plot(newarr,newspec)
hold all
plot(oudarr,ObssterM)

matr=[newarr',newspec'];
save('sterHN931bij48.dat','matr','-ascii')
```

Stand2.m

Stand2.m is the MATLAB code I wrote to get the library spectra to the same format as my stellar spectra. It rescale the wavelength grid to μm and then interpolates the spectrum to the common wavelength grid.

```
standK=load('Libstars/hr483K.dat');                 reading in the library star
standK=standK(:,1:2);
standK(:,1)=1e4./standK(:,1);                       rescaling the wavelength grid

for k=1:1024
    newarr(k)=1.9760+ (k-1)*4.27e-4;
end

newspec=interp1(standK(:,1),standK(:,2),newarr,'nearest');  interpolating
plot(newarr,newspec)
hold all
plot(standK(:,1),standK(:,2))

matr=[newarr',newspec'];
save('standKadept2.dat','matr','-ascii')

% H band
standH=load('Libstars/hr4374H.dat');
standH(:,1)=1e4./standH(:,1);
```

```
for k=1:1024
    newarr(k)=1.4920+ (k-1)*2.86e-4;
end

newspec=interp1(standH(:,1),standH(:,2),newarr,'nearest');
figure(2)
plot(newarr,newspec)
hold all
plot(standH(:,1),standH(:,2))

matr=[newarr',newspec'];
save('standHadept2.dat','matr','-ascii')
```

Makeatmosnew.pro

Originally I started this project programming in IDL. However due to my better understanding of the MATLAB language, I switched. This is the only program I had completed by that time. Therefor it is still in IDL code.

```
; final step in determining the atmospheric correction for the NIRSPEC
; spectra using the observations of the standard stars
; uses the previously determined standard star spectra in H and K

;;;;;;;;;;;;;;;;;;;;;;;;;;;;;;;;;;;;;;;;;;;;;;;;;;;;;;;;;;;;;;;;;;;;;;;;;;;;;;;;
;;
;;
PRO atmos
; read in the standard star spectra (.dat files)
  file='standHadept.dat'
;  file='standKadept.dat'
  rdfloat, file, wave, flux, COLUMNS = [1,2]
; wave is given in um, flux in erg/cm^2/s/A
; get the observed star spectra
  sterren=sindgen(21)
  print, size(sterren)
  sterren(0)='MK1066'
  sterren(1)='MK1'
  sterren(2)='MK3'
  sterren(3)='N1320'
  sterren(4)='N1667'
  sterren(5)='N2110'
  sterren(6)='N2273'
  sterren(7)='N262'
  sterren(8)='N2685'
  sterren(9)='N2992'
  sterren(10)='N3081'
  sterren(11)='N3185'
  sterren(12)='N3516'
  sterren(13)='N4051'
  sterren(14)='N4151'
  sterren(15)='N4253'
  sterren(16)='N4388'
  sterren(17)='N5273'
  sterren(18)='N5506'
  sterren(19)='N7450'
  sterren(20)='N931bij48'
```

```
  sx=size(sterren)
  n=sx(1)

  for i=0,n-1 do begin
      file='sterH'+sterren(i)+'.dat'
      rdfloat, file, wave2, flux2, COLUMNS = [1,2]
; get black body spectrum
     temp = 5830                ;the typical temp of a G2V star

     factor=10^4        ;conversion of um to angstroms
     wave3=factor*wave ;planck expects angstroms!
     bbflux = planck(wave3,temp)
     newspec=flux*bbflux

     atmos=flux2/newspec
     help,atmos

     sx=size(atmos)
     nx=sx(1)
     print,nx
     zup=atmos(nx/4)
     atmos=atmos*(1/zup)                 all spectra were normalized on their nx/4 pixel
     outfile='atmosHMatlab'+sterren(i)+'.dat'
     print,outfile

     openw, 1, outfile
     for w=0,nx-1 do begin
         printf, 1, wave(w), atmos(w)
         format='(2(g14.8))'
     endfor
     close, 1
 endfor
end
```

Atmossmooth.m

I removed four peaks from the atmosphere spectra. I wrote a MATLAB function code for this, which works individually on all spectra and bands.

```
function suc6=atmossmooth(band,nm)
name=['Atmos/atmos',band,'Matlab',nm,'.dat'];
atmos = load(name);

if band=='H'
    % first piek                        the positions are given in pixelnumbers
    rc=((atmos(298,2)-atmos(291,2))/(2.86e-4*(298-291)));
    for i=291:298
        atmos(i,2)=atmos(291,2)+rc*2.86e-4*(i-291);
    end
    % second piek
    rc=((atmos(341,2)-atmos(337,2))/(2.86e-4*(341-337)));
    for i=337:341
        atmos(i,2)=atmos(337,2)+rc*2.86e-4*(i-337);
    end
    suc6=1;
else
```

```
    fprintf('The H band was not specified \n')
end

if band=='K'
    % first piek
    rc=((atmos(314,2)-atmos(304,2))/(4.27e-4*(314-304)));
    for i=304:314
        atmos(i,2)=atmos(304,2)+rc*4.27e-4*(i-304);
    end
    % second piek
    rc=((atmos(959,2)-atmos(948,2))/(4.27e-4*(959-948)));
    for i=948:959
        atmos(i,2)=atmos(948,2)+rc*4.27e-4*(i-948);
    end
    suc6=2;
else
    fprintf('The K band was not specified \n')
end

name=['Atmos/atmossm',band,nm,'.dat'];
save(name,'atmos','-ascii')
```

Extrgalspec2.m

In this program I divide my galactic spectra through my final set of atmospheric spectra. This is done for the complete 101 column wide galactic spectrum.

```
function [suc6,radius] = extrgalspec2(band,nme,num)

%read in galaxy spectrum
name=['Galaxies/gal',band,'/',nme,band,'.fits'];
gal = fitsread(name);
name=['Galaxies/gal',band,'/startvalue',band,'val.dat'];
start = load(name);
name=['Galaxies/gal',band,'/stepsize',band,'val.dat'];
step = load(name);

%specifying wavelength grids
for k=1:1024
    oudarr(k)=start(num)+ (k-1)*step(num);
    if band=='K'
    newarr(k)=1.9760+ (k-1)*4.27e-4;
    end
    if band=='H'
        newarr(k)=1.4920+ (k-1)*2.86e-4;
    end
end

%interpolate to new wavelength grid
for k=1:101
newspec(:,k)=interp1(oudarr,gal(:,k),newarr,'nearest');
end

%load atmos
name=['Atmos/atmossm',band,nme,'.dat'];
atmos = load(name);
```

```
%divide out atmosphere
for z=1:101
newgal(:,z)=newspec(:,z)./atmos(:,2);
end

%saving definitive galspec
matr=[newarr',newgal];
name=['Galaxies/gal',band,'/cleangalspec120208',nme,band,'.dat'];
save(name,'matr','-ascii')
```

B Computercodes for determining the Equivalent Widths

SiIdetEW.m

This is the code for determining the equivalent width of SiI. Near identical programs are available for CO (2-0) and CO (6-3).

```
 function EW = SiIdetEW(nm,num)

% SiI feature
% continuum points & integration limits
conSiI = [1.5850 1.5930];
intSiI = [1.5870 1.5910];
zed= [0.012025, 0.015946, 0.013509, 0.008883, 0.015167, 0.007789,
 0.006138, 0.015034, 0.002945, 0.007710, 0.007976, 0.004060,
 0.008836, 0.002336, 0.003319, 0.012929, 0.008419, 0.003549,
 0.006181, 0.010624, 0.016652]';

% the different spectra locations from which to choose
%name=['Galaxies/SEYFERTS/',nm,'H250pc.dat'];
%name=['Galaxies/SEYFERTS/',nm,'H300pc.dat'];
%name=['Galaxies/SEYFERTS/',nm,'H500pc.dat'];
%name=['Galaxies/SEYFERTS/',nm,'H665pc.dat'];
%name=['Galaxies/SEYFERTS/',nm,'H665pcsec.dat']; %circumnuclear
%name=['Galaxies/SEYFERTS/',nm,'H170pc.dat'];
name=['Galaxies/SEYFERTS/',nm,'H550pc.dat'];
%name=['Galaxies/SEYFERTS/',nm,'Hsmall.dat']; %circumnuclear

% if a circumnuclear band is choosen, analyse in two parts!!
% change 2:d into 2:round(d/2) or round(d/2):d
Sey=load(name);
d=size(Sey,2);
gem=nansum(Sey(:,2:d),2); %change if circumnuclear!!!
Sey=[Sey(:,1) gem];
Sey=[Sey(:,1)-zed(num)*1.5892,Sey(:,2)]; %temp!!! z*Lambda_o

% determine values of points of the continuum

num2=length(conSiI);
for i=1:num2
    index=round((conSiI(i)-Sey(1,1))/2.86e-4);
    punt(i)=mean(Sey(index-4:index+4,2));
    conpunten(i)=Sey(index,1);
end

% determine the linear fit points across the integration range

p=polyfit(conSiI,punt,1);
inval=intSiI(1):2.86e-4:intSiI(2);
valcon=polyval(p,inval);

% determine the Equivalent Width
som=0;

ind=round((intSiI(1)-Sey(1,1))/2.86e-4);
for i=1:length(valcon)
    som=som+2.86e-4*((valcon(i)-Sey(ind+i,2))/valcon(i));
```

```
end
EW=som*1e4;
```

EWbounds2.m

This is the program to determine the dilution of our spectra and correct for it in our equivalent widths.

```
 function bounds= EWbounds2(EWSi,EWCOH,EWCOK)

% begin with the H band (Origlia 1993)
x=log10(EWCOH/EWSi);

%bounds
y1=6*x^2+10.84*x+5.504;
y2=13.45*x^2+3.229*x+0.3387;

valCOH=y2 + 0.50*(y1-y2);
valSiI=valCOH/10^(x);
if valCOH <= EWCOH
    valCOH=EWCOH;
    valSiI=EWSi;
end
if valSiI <= EWSi
    valCOH=EWCOH;
    valSiI=EWSi;
end
%computer induced error
sigma1=(y1-y2)/4;
sigma2=(valSiI/valCOH)*sigma1;

% now go to the K band
x=valCOH;
y1=2.222*x+4.483;
y2=2.1378*x-3.524;

valCOK=y2 + 0.50*(y1-y2);
if valCOK <=EWCOK
    valCOK=EWCOK;
end
sigma3=(y1-y2)/2;

bounds=[valSiI sigma2 valCOH sigma1 valCOK sigma3 1-(EWCOH/valCOH) 1-(EWCOK/valCOK)];
```

C Spectra and Starburst99 results of the Seyfert Sample

Mrk 1066

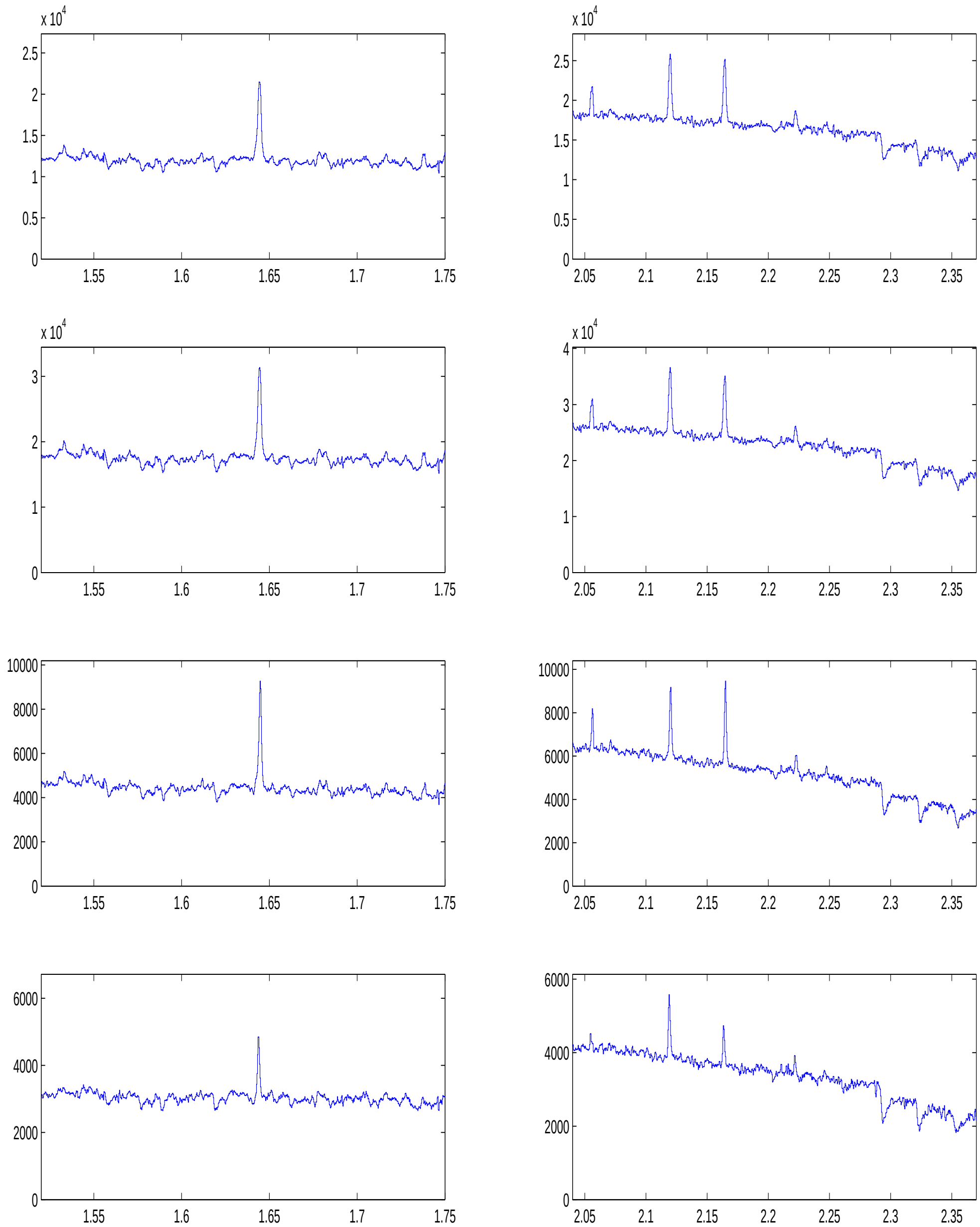

Figure 17: Shown here are the spectra of Mrk 1066. The left column is the H band, the right column the K band spectra. From top to bottom are seen: 250pc nuclear, 500pc nuclear, 665-250pc circumnuclear 'left', 665-250pc circumnuclear 'right'.

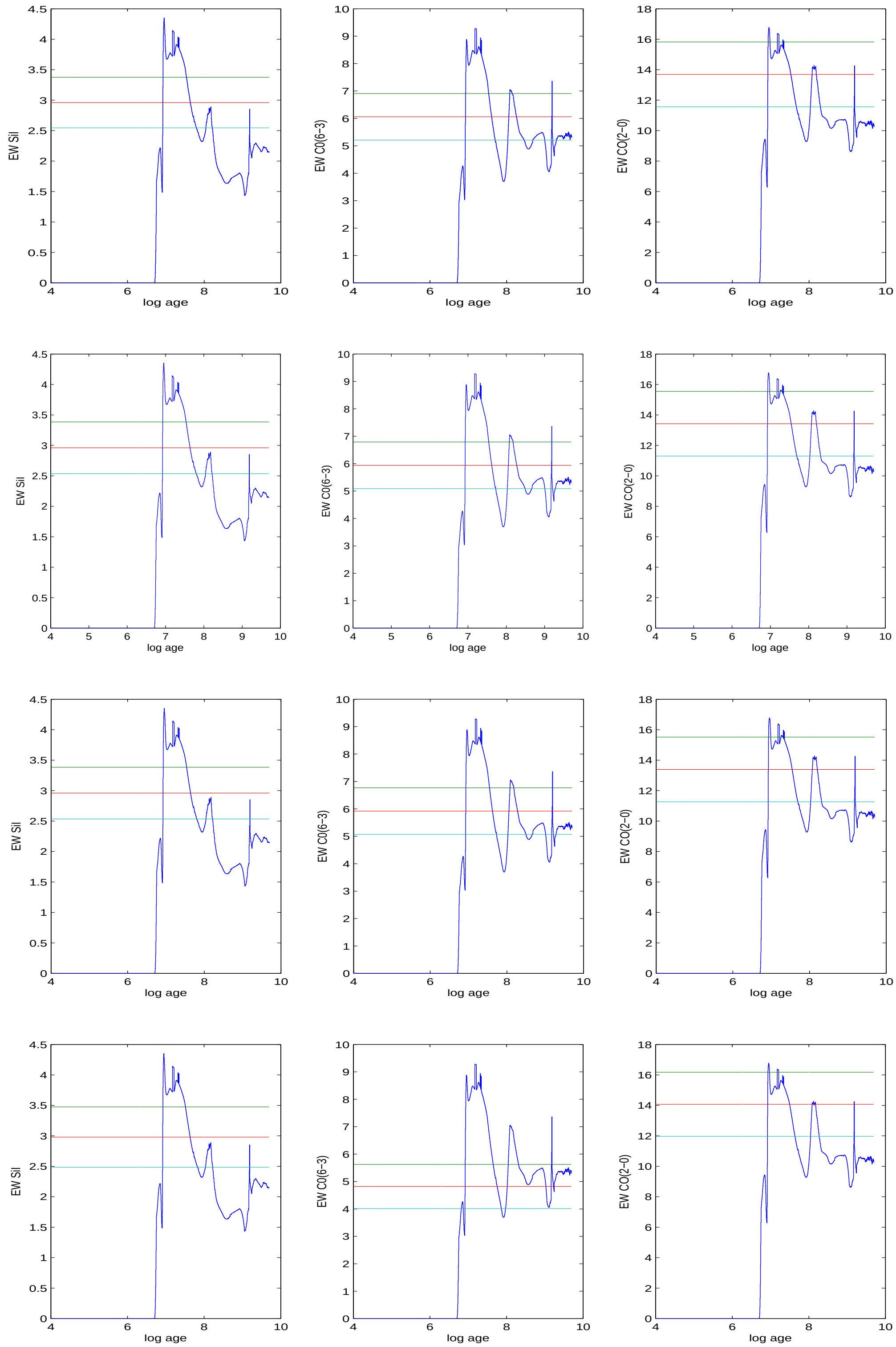

Figure 18: From top to bottom is shown the Starburst99 result for the 250pc spectrum, the 500pc spectrum, the 665-250pc circumnuclear ring ‘left’ and the 665-250pc circumnuclear ring ‘right’ of Mrk 1066. From left to right are given SiI, CO(6-3) and CO(2-0). Each plot shows the following: the blue line is the value of the equivalent width given by Starburst99, while the red line is the value we found as given in section 4.1. The green and light blue horizontal lines are the 0.5σ upper and lower boundaries for this value.

Mrk 1

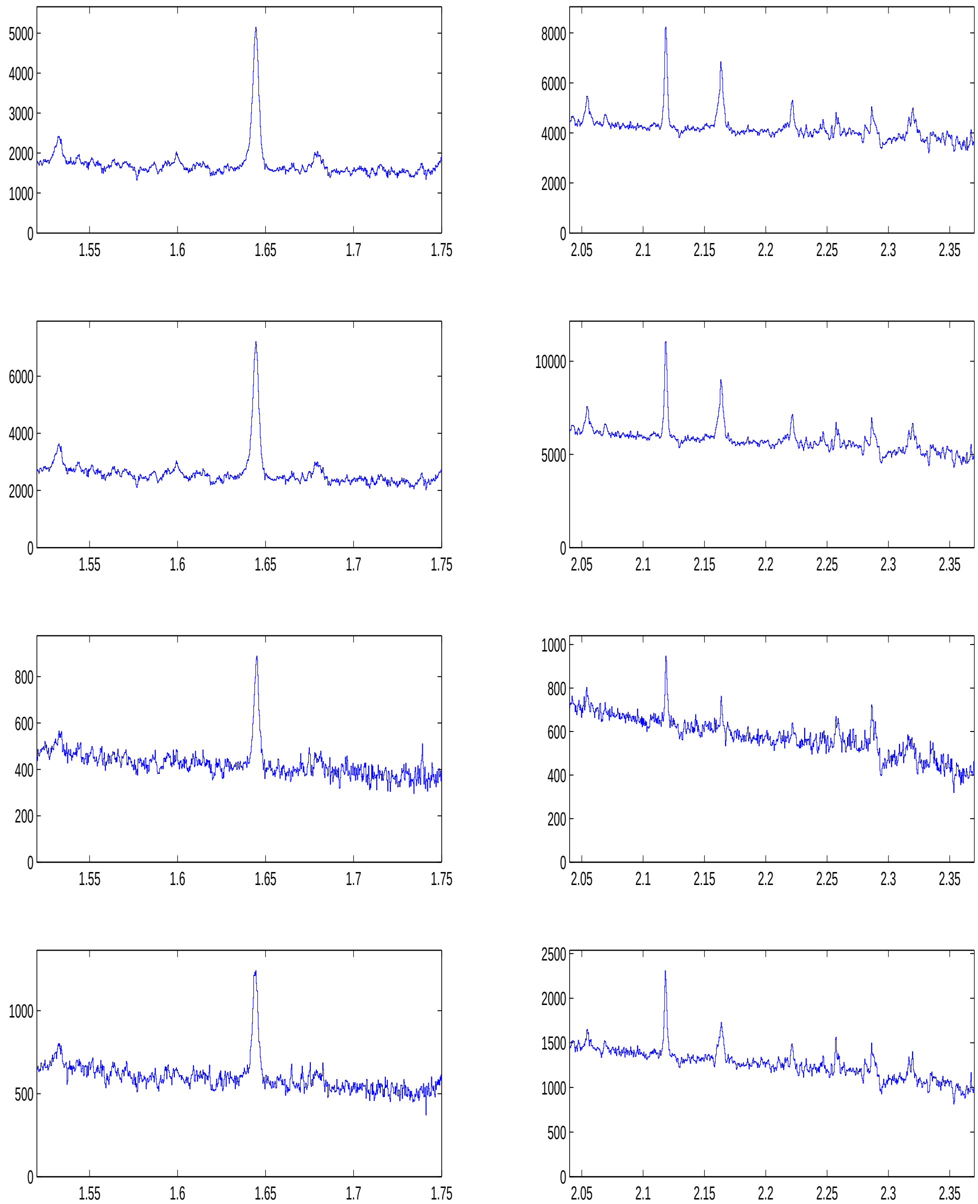

Figure 19: Shown here are the spectra of Mrk 1. The left column is the H band, the right column the K band spectra. From top to bottom are seen: 250pc nuclear, 500pc nuclear, 665-250pc circumnuclear 'left', 665-250pc circumnuclear 'right'.

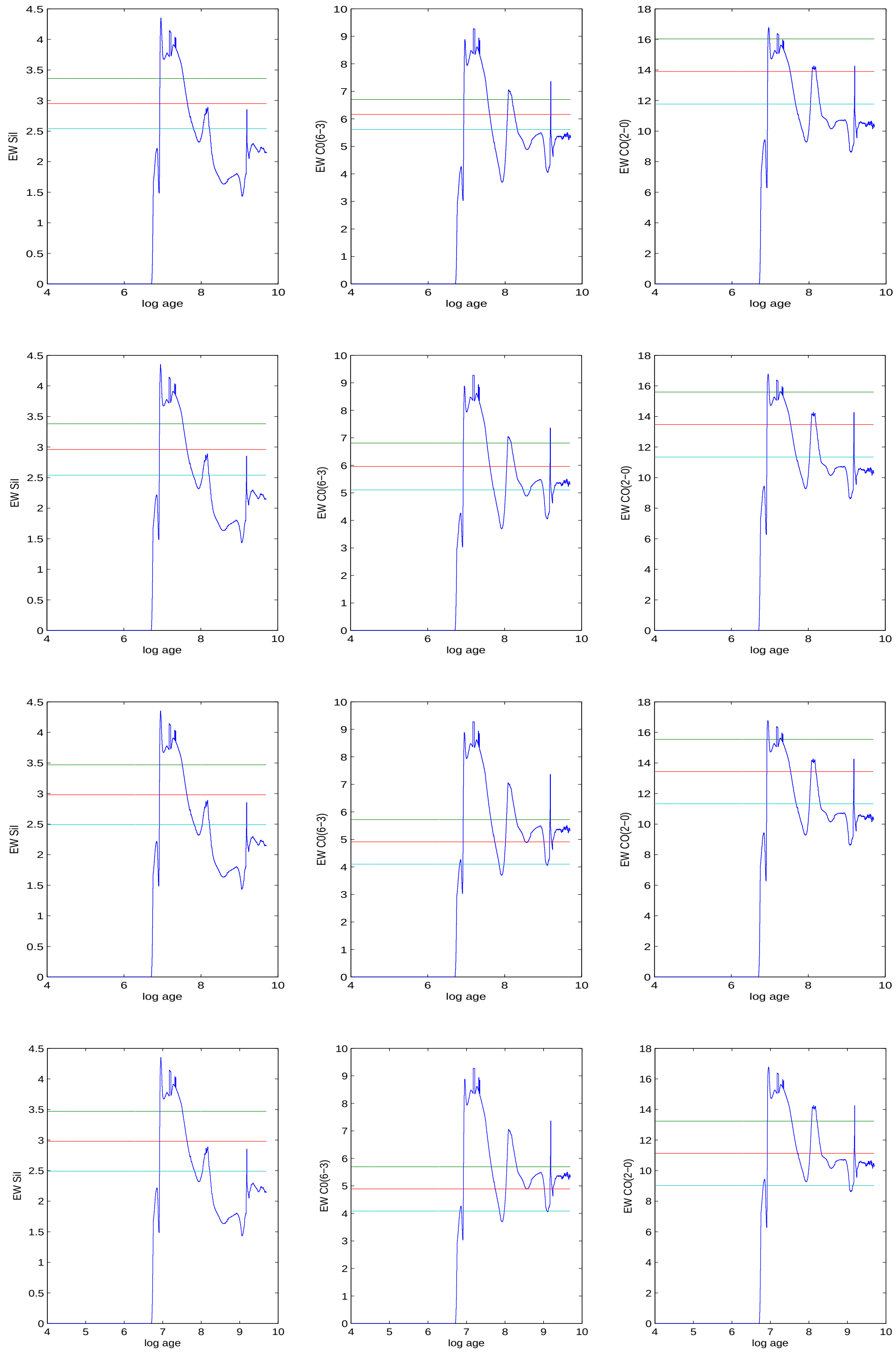

Figure 20: From top to bottom is shown the Starburst99 result for the 250pc spectrum, the 500pc spectrum, the 665-250pc circumnuclear ring 'left' and the 665-250pc circumnuclear ring 'right' of Mrk 1. From left to right are given SiI, CO(6-3) and CO(2-0). Each plot shows the following: the blue line is the value of the equivalent width given by Starburst99, while the red line is the value we found as given in section 4.1. The green and light blue horizontal lines are the 0.5σ upper and lower boundaries for this value.

Mrk 3

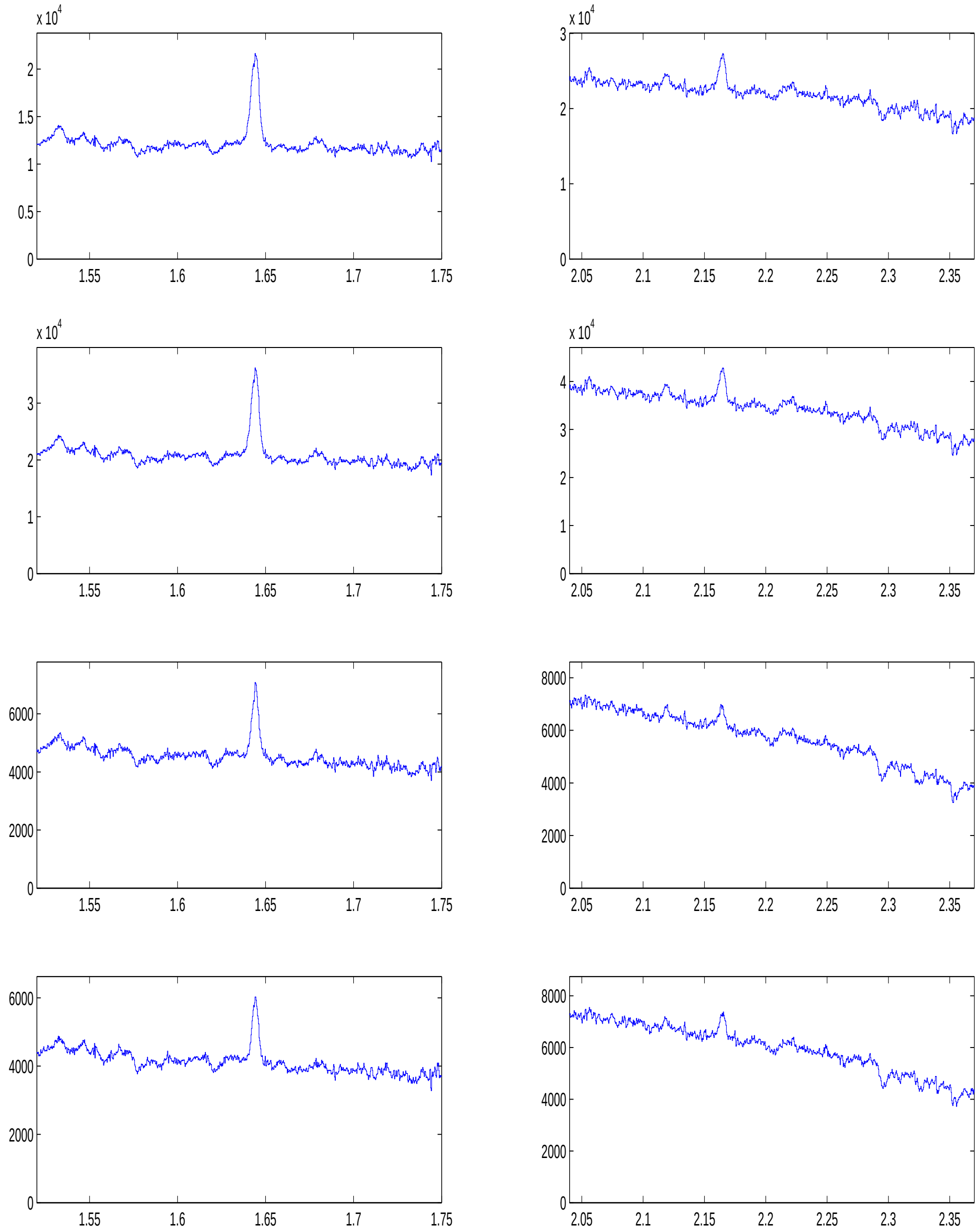

Figure 21: Shown here are the spectra of Mrk 3. The left column is the H band, the right column the K band spectra. From top to bottom are seen: 250pc nuclear, 500pc nuclear, 665-250pc circumnuclear 'left', 665-250pc circumnuclear 'right'.

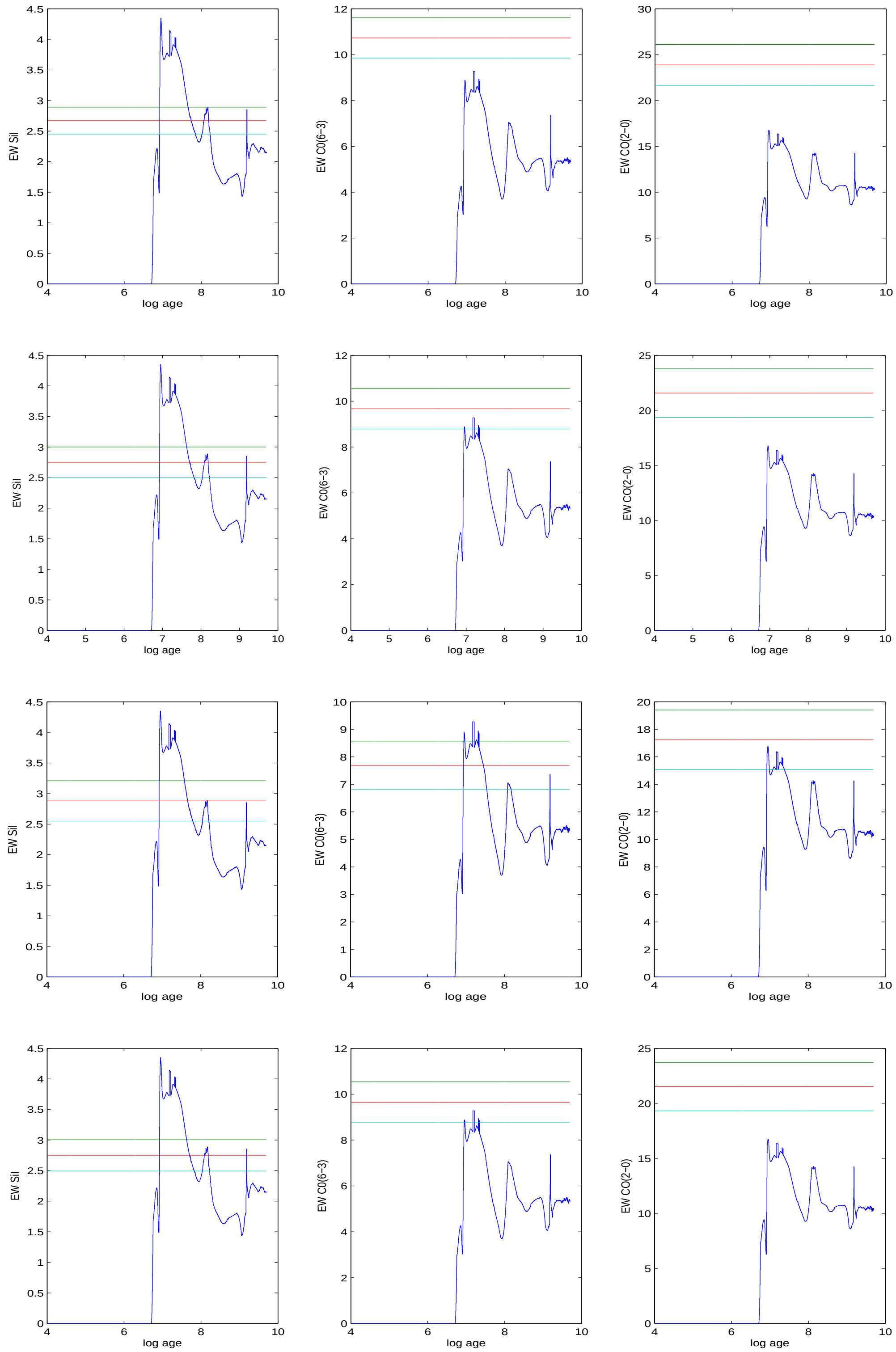

Figure 22: From top to bottom is shown the Starburst99 result for the 250pc spectrum, the 500pc spectrum, the 665-250pc circumnuclear ring 'left' and the 665-250pc circumnuclear ring 'right' of Mrk 3. From left to right are given SiI, CO(6-3) and CO(2-0). Each plot shows the following: the blue line is the value of the equivalent width given by Starburst99, while the red line is the value we found as given in section 4.1. The green and light blue horizontal lines are the 0.5σ upper and lower boundaries for this value.

NGC 1320

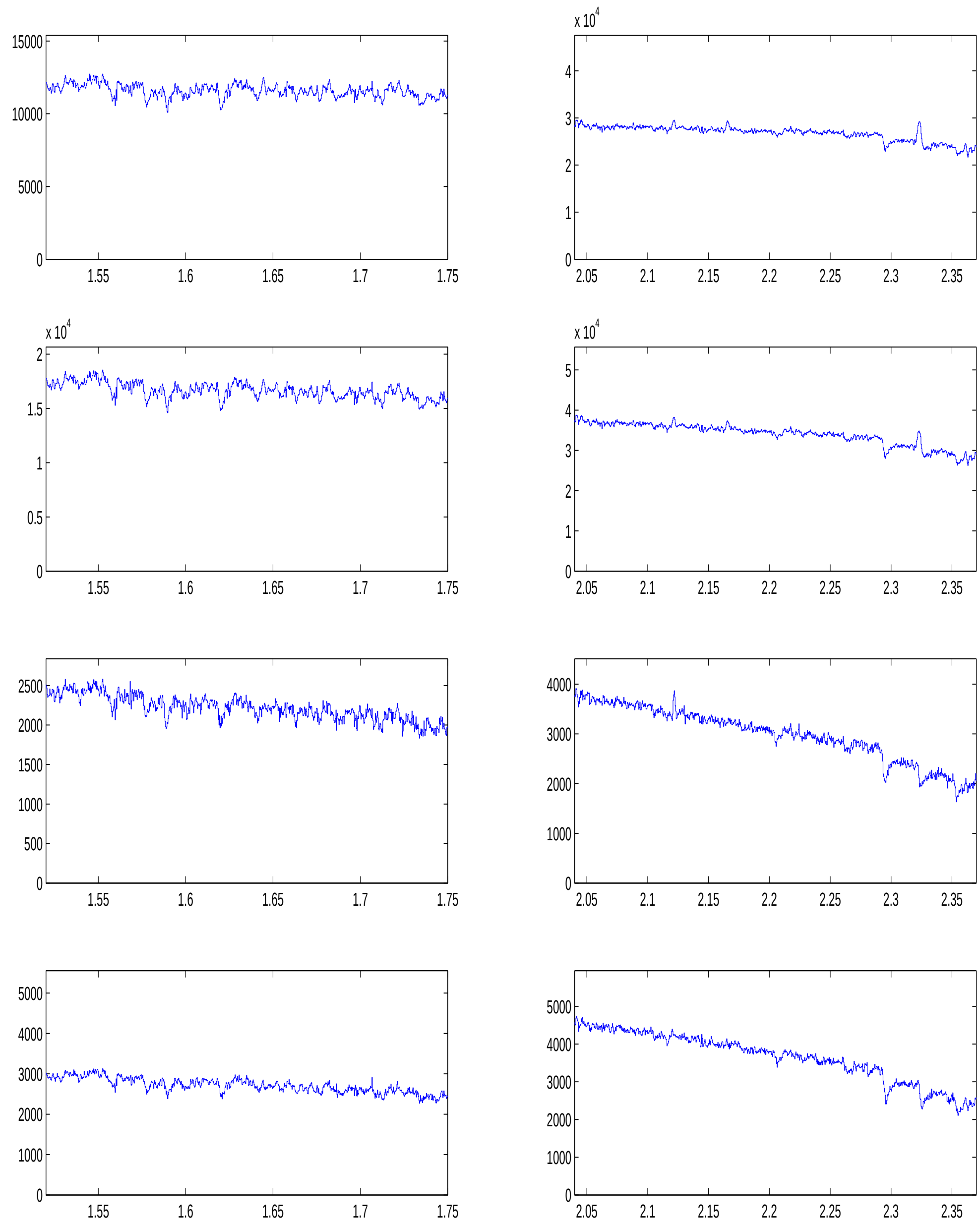

Figure 23: Shown here are the spectra of NGC 1320. The left column is the H band, the right column the K band spectra. From top to bottom are seen: 250pc nuclear, 500pc nuclear, 665-250pc circumnuclear ‘left’, 665-250pc circumnuclear ‘right’.

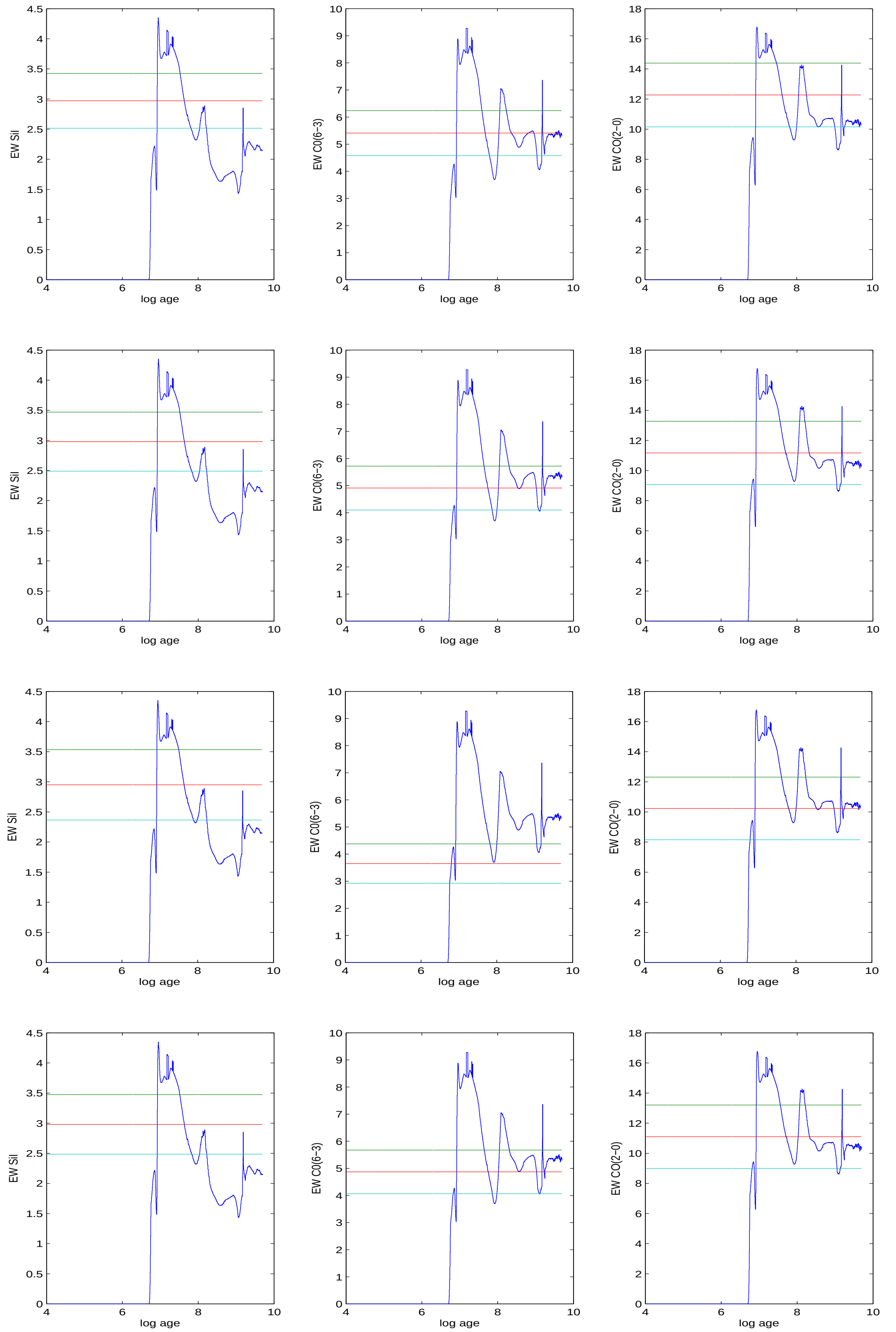

Figure 24: From top to bottom is shown the Starburst99 result for the 250pc spectrum, the 500pc spectrum, the 665-250pc circumnuclear ring ‘left’ and the 665-250pc circumnuclear ring ‘right’ of NGC 1320. From left to right are given SiI, CO(6-3) and CO(2-0). Each plot shows the following: the blue line is the value of the equivalent width given by Starburst99, while the red line is the value we found as given in section 4.1. The green and light blue horizontal lines are the 0.5σ upper and lower boundaries for this value.

NGC 1667

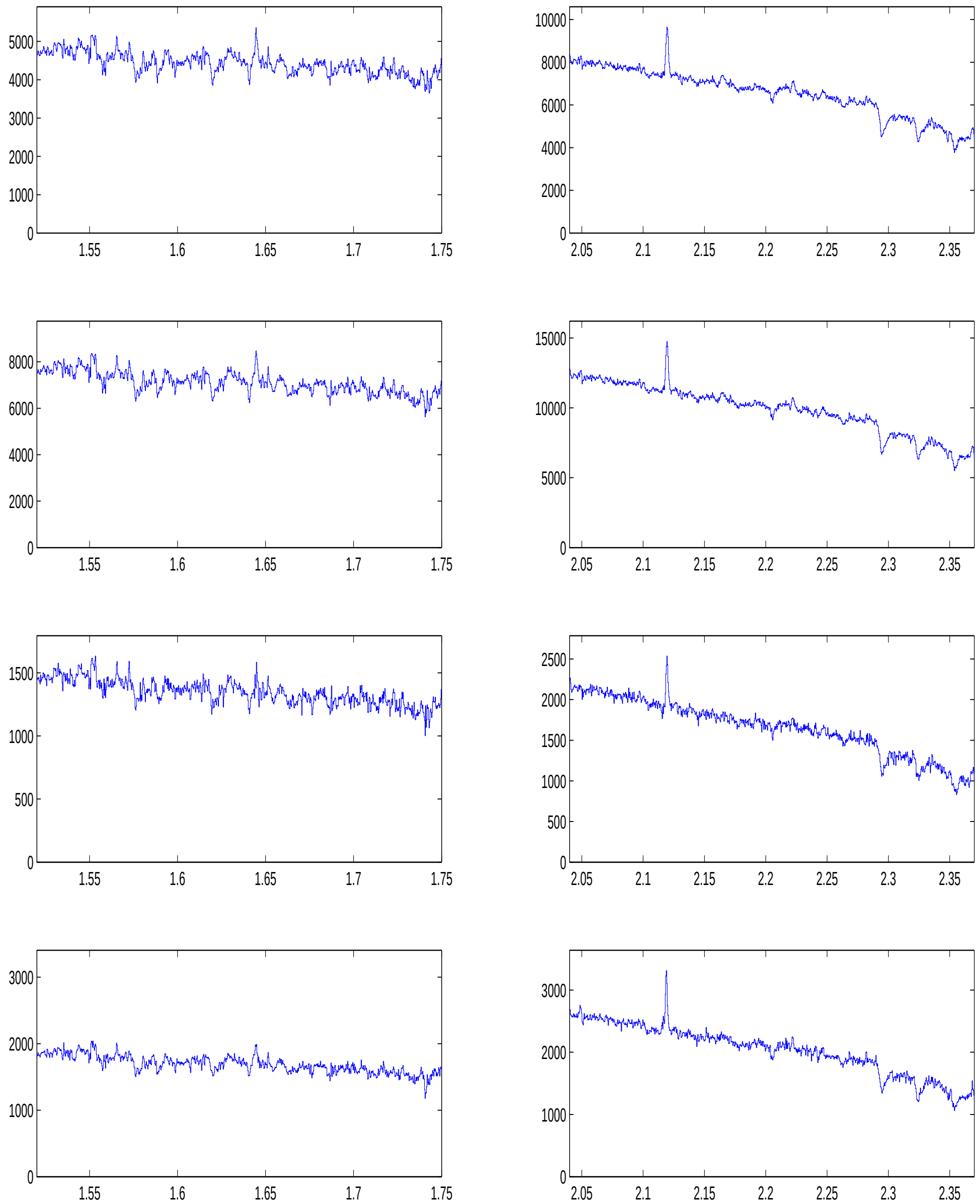

Figure 25: Shown here are the spectra of NGC 1667. The left column is the H band, the right column the K band spectra. From top to bottom are seen: 250pc nuclear, 500pc nuclear, 665-250pc circumnuclear ‘left’, 665-250pc circumnuclear ‘right’.

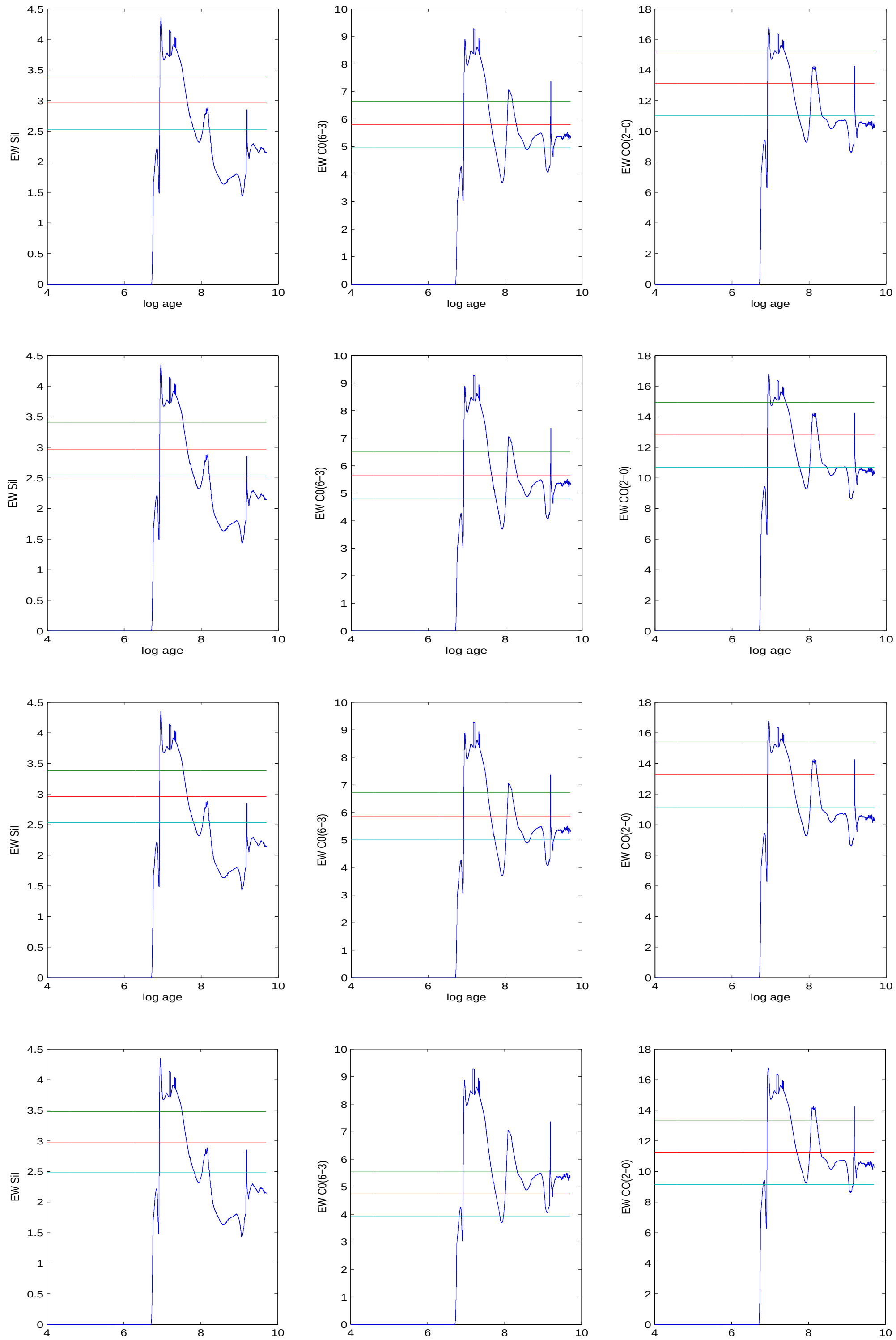

Figure 26: From top to bottom is shown the Starburst99 result for the 250pc spectrum, the 500pc spectrum, the 665-250pc circumnuclear ring 'left' and the 665-250pc circumnuclear ring 'right' of NGC 1667. From left to right are given SiI, CO(6-3) and CO(2-0). Each plot shows the following: the blue line is the value of the equivalent width given by Starburst99, while the red line is the value we found as given in section 4.1. The green and light blue horizontal lines are the 0.5σ upper and lower boundaries for this value.

NGC 2110

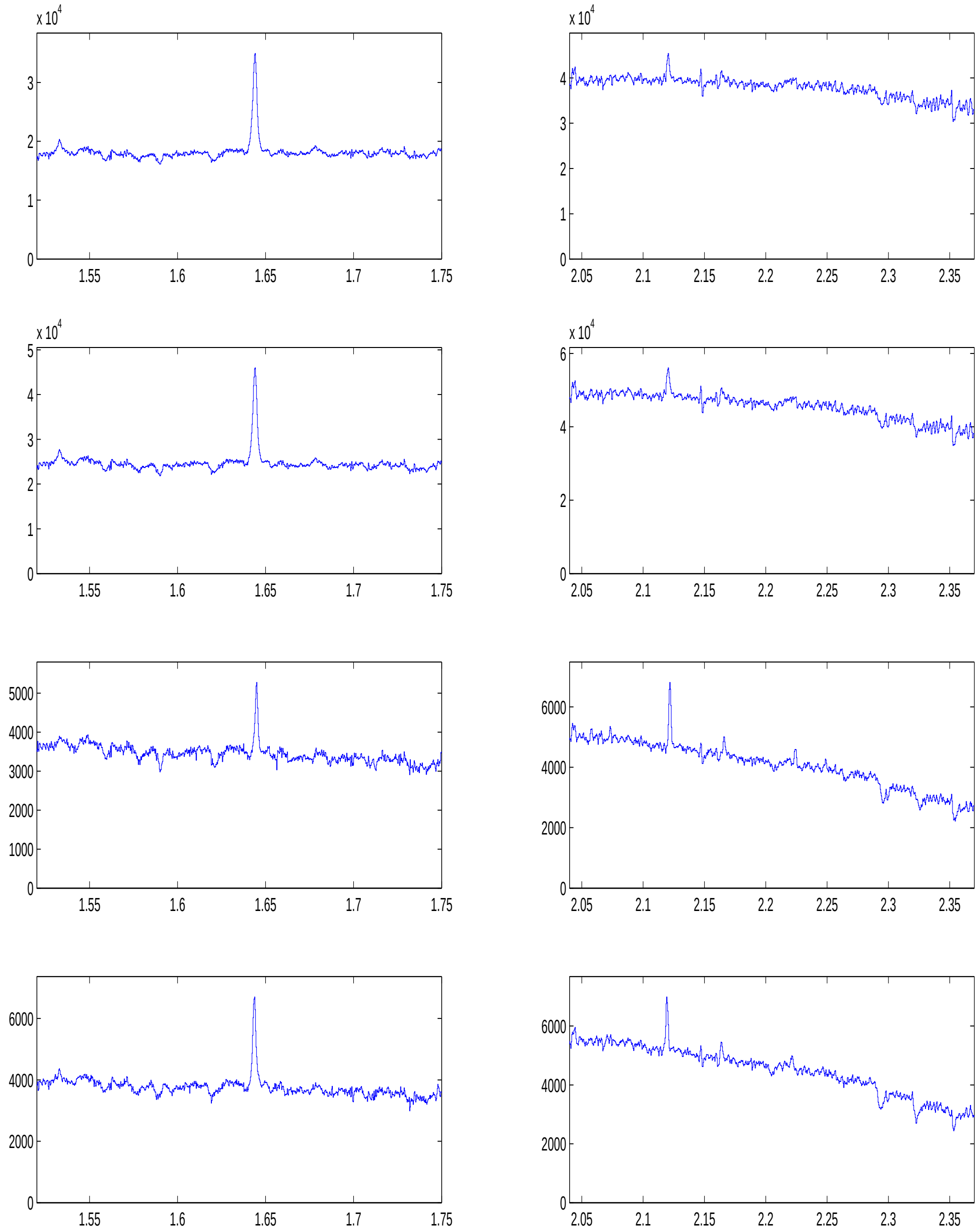

Figure 27: Shown here are the spectra of NGC 2110. The left column is the H band, the right column the K band spectra. From top to bottom are seen: 250pc nuclear, 500pc nuclear, 665-250pc circumnuclear ‘left’, 665-250pc circumnuclear ‘right’.

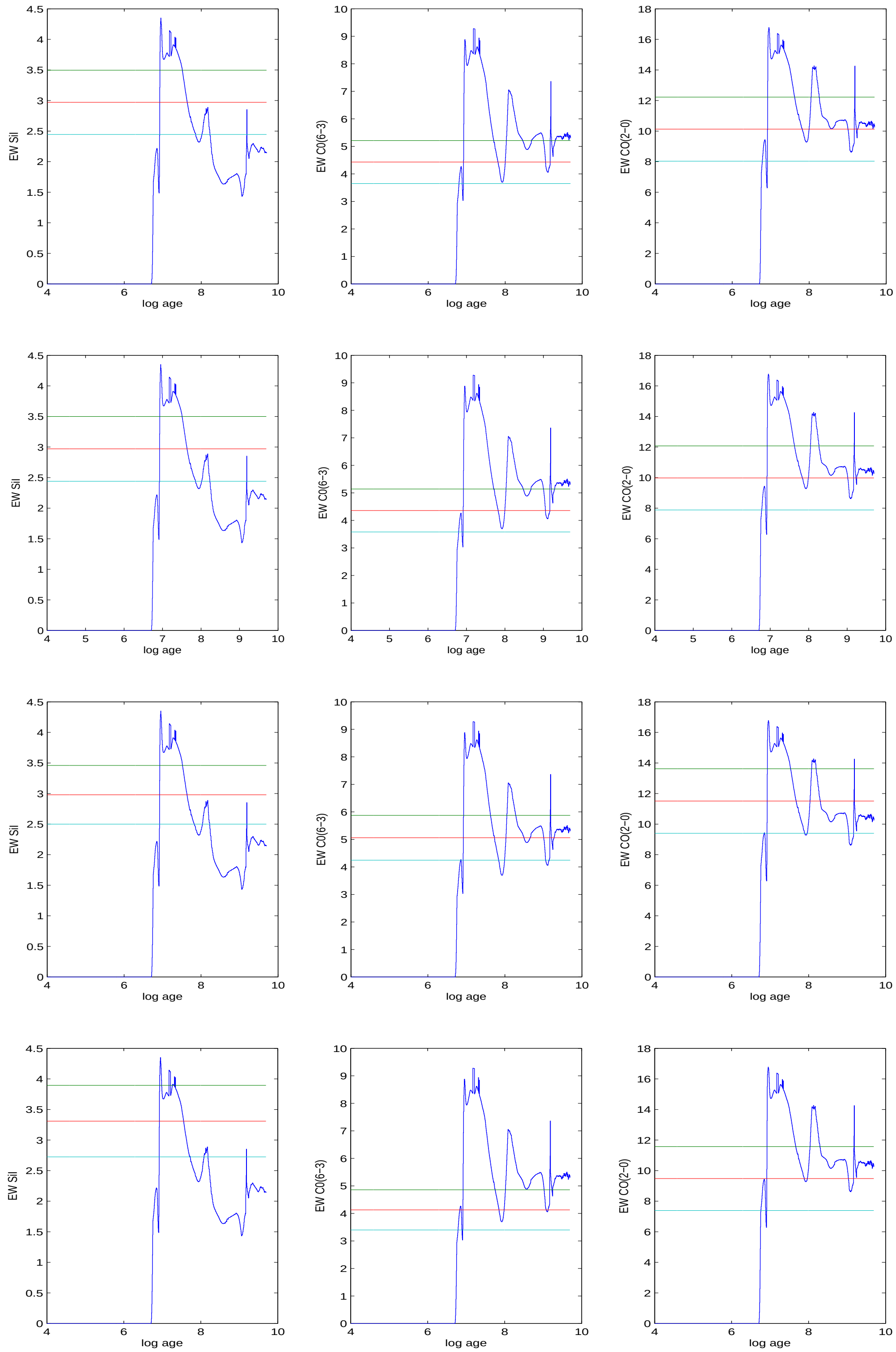

Figure 28: From top to bottom is shown the Starburst99 result for the 250pc spectrum, the 500pc spectrum, the 665-250pc circumnuclear ring 'left' and the 665-250pc circumnuclear ring 'right' of NGC 2110. From left to right are given SiI, CO(6-3) and CO(2-0). Each plot shows the following: the blue line is the value of the equivalent width given by Starburst99, while the red line is the value we found as given in section 4.1. The green and light blue horizontal lines are the 0.5σ upper and lower boundaries for this value.

NGC 2273

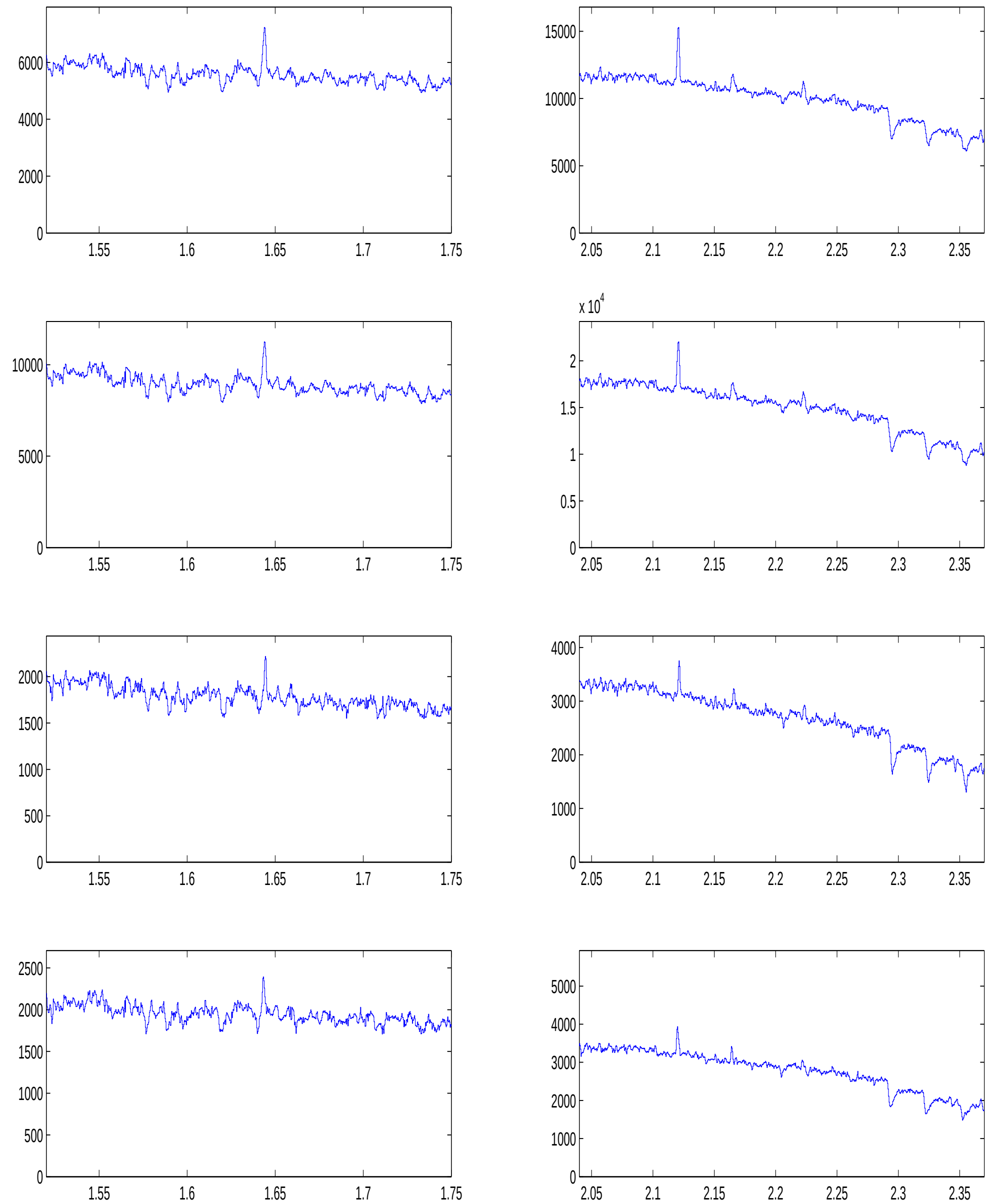

Figure 29: Shown here are the spectra of NGC 2273. The left column is the H band, the right column the K band spectra. From top to bottom are seen: 250pc nuclear, 500pc nuclear, 665-250pc circumnuclear 'left', 665-250pc circumnuclear 'right'.

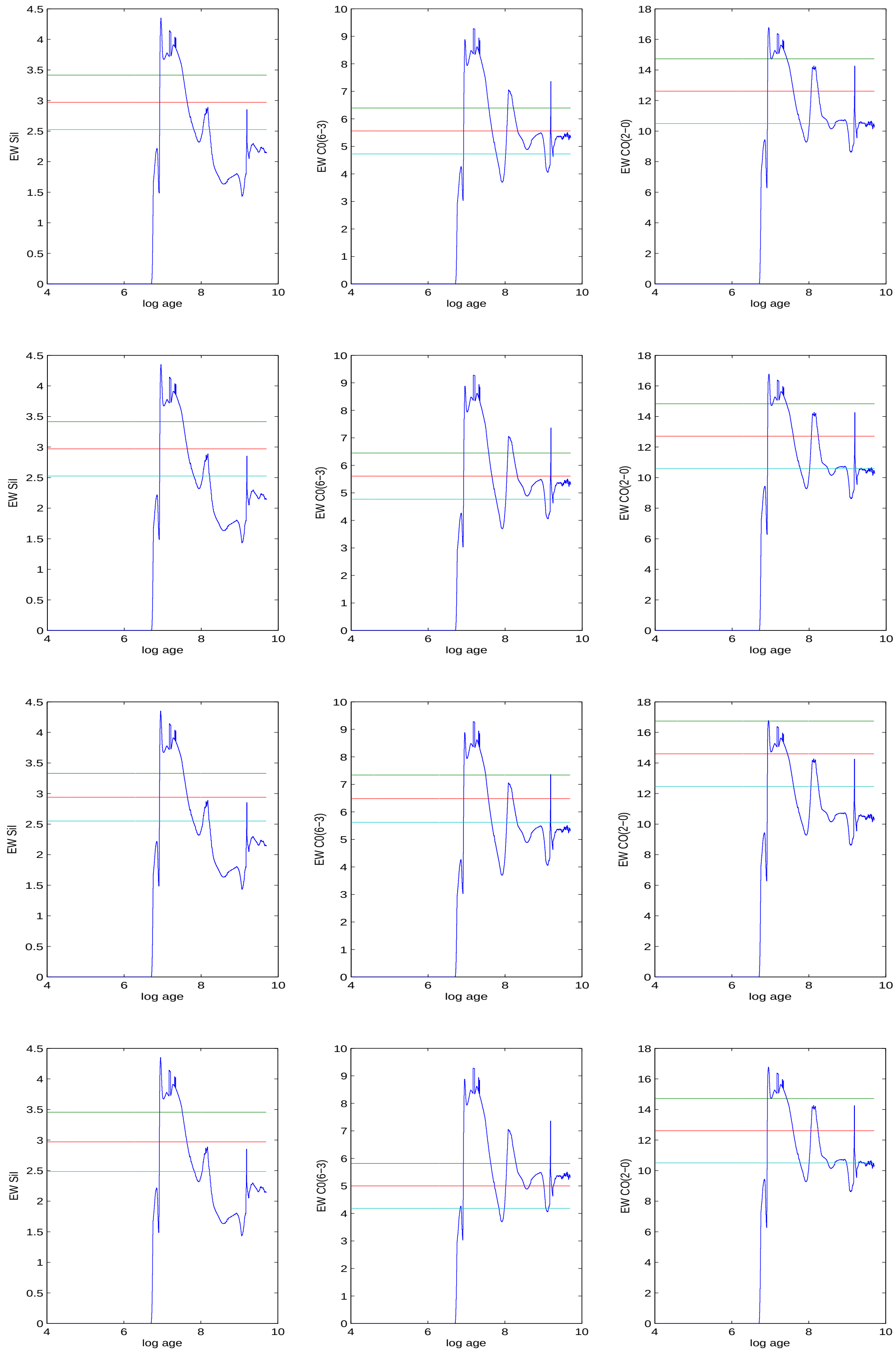

Figure 30: From top to bottom is shown the Starburst99 result for the 250pc spectrum, the 500pc spectrum, the 665-250pc circumnuclear ring ‘left’ and the 665-250pc circumnuclear ring ‘right’ of NGC 2273. From left to right are given SiI, CO(6-3) and CO(2-0). Each plot shows the following: the blue line is the value of the equivalent width given by Starburst99, while the red line is the value we found as given in section 4.1. The green and light blue horizontal lines are the 0.5σ upper and lower boundaries for this value.

NGC 262

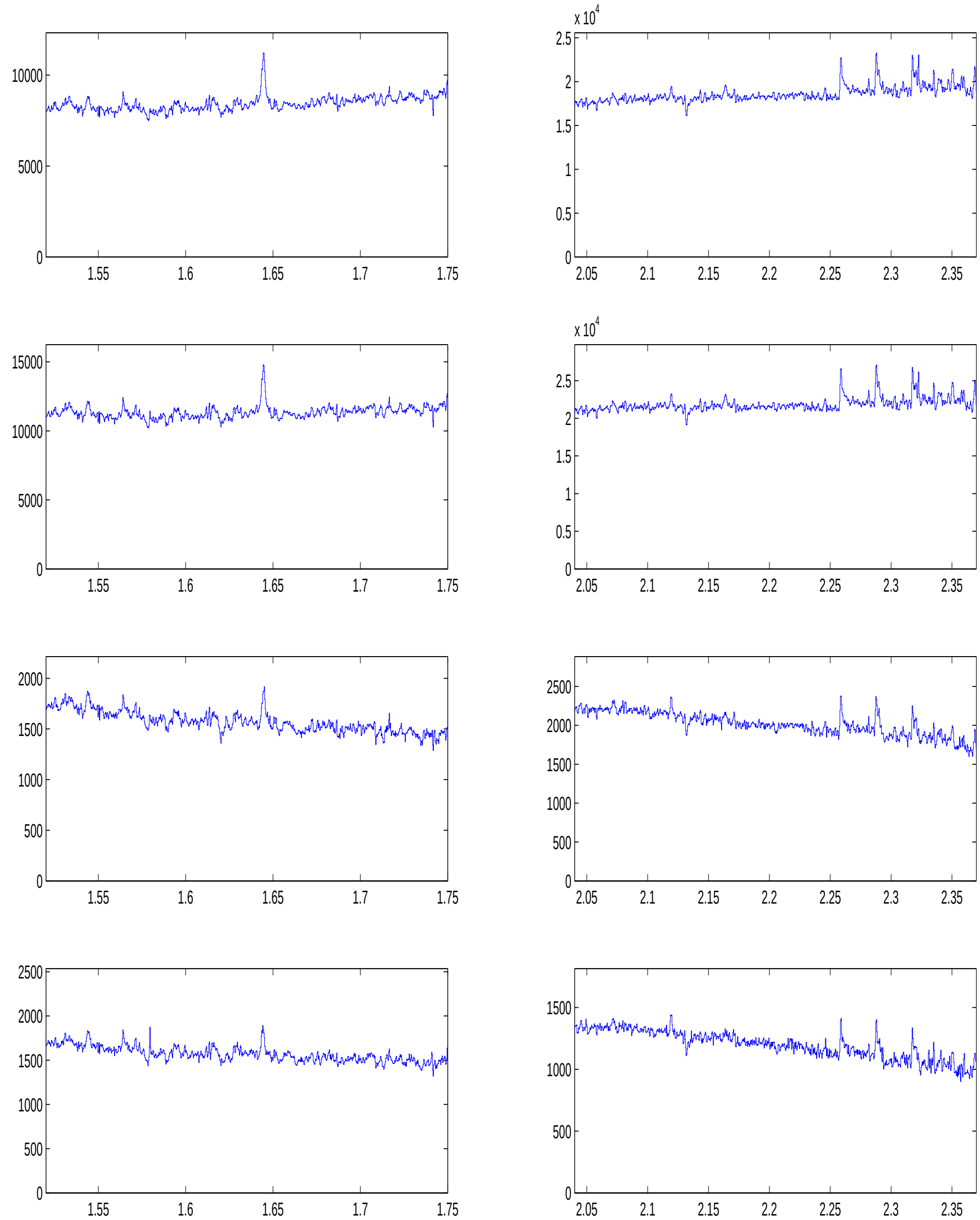

Figure 31: Shown here are the spectra of NGC 262. The left column is the H band, the right column the K band spectra. From top to bottom are seen: 250pc nuclear, 500pc nuclear, 665-250pc circumnuclear 'left', 665-250pc circumnuclear 'right'.

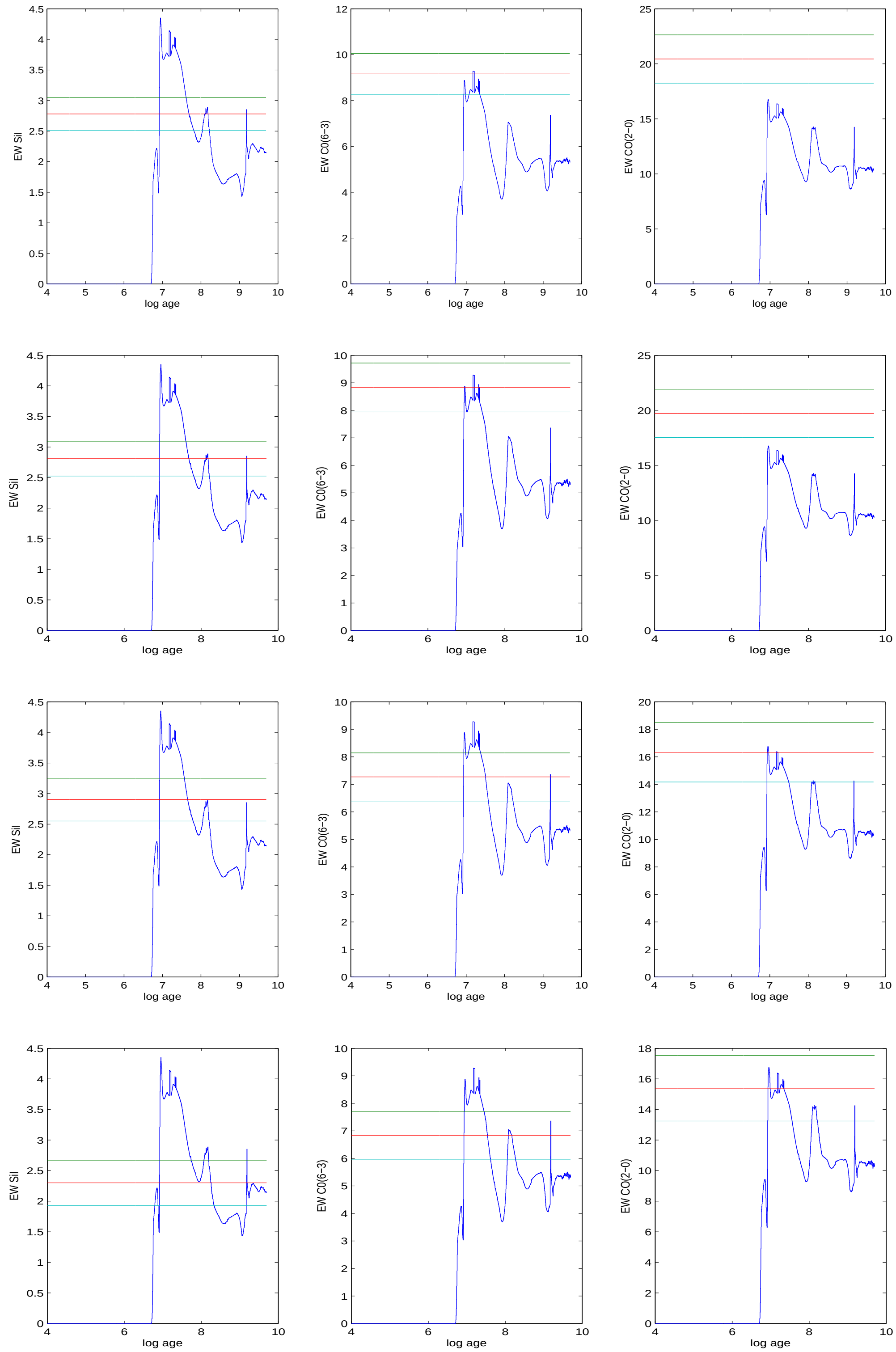

Figure 32: From top to bottom is shown the Starburst99 result for the 250pc spectrum, the 500pc spectrum, the 665-250pc circumnuclear ring 'left' and the 665-250pc circumnuclear ring 'right' of NGC 262. From left to right are given SiI, CO(6-3) and CO(2-0). Each plot shows the following: the blue line is the value of the equivalent width given by Starburst99, while the red line is the value we found as given in section 4.1. The green and light blue horizontal lines are the 0.5σ upper and lower boundaries for this value.

NGC 2685

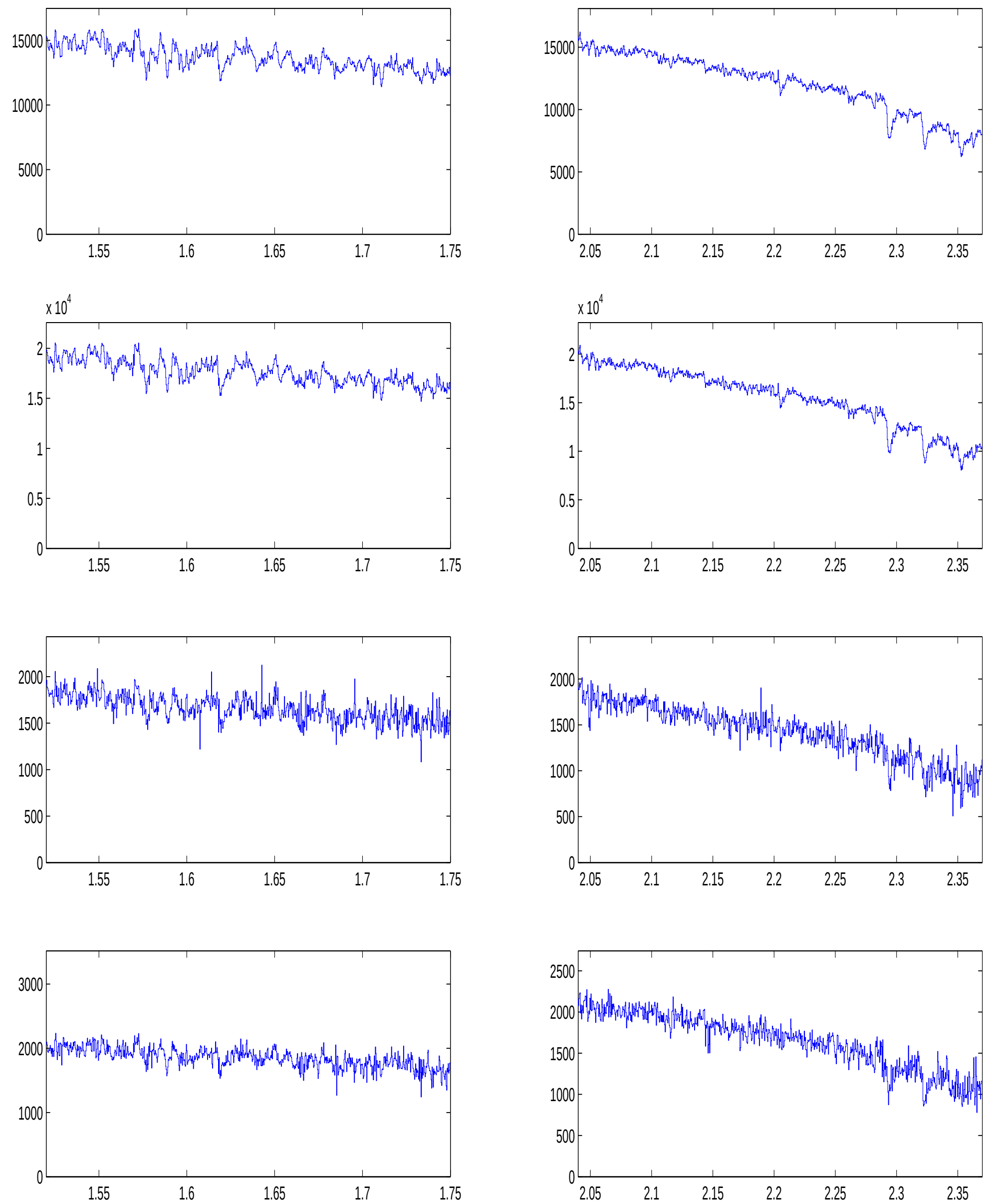

Figure 33: Shown here are the spectra of NGC 2685. The left column is the H band, the right column the K band spectra. From top to bottom are seen: 250pc nuclear, 500pc nuclear, 665-250pc circumnuclear ‘left’, 665-250pc circumnuclear ‘right’.

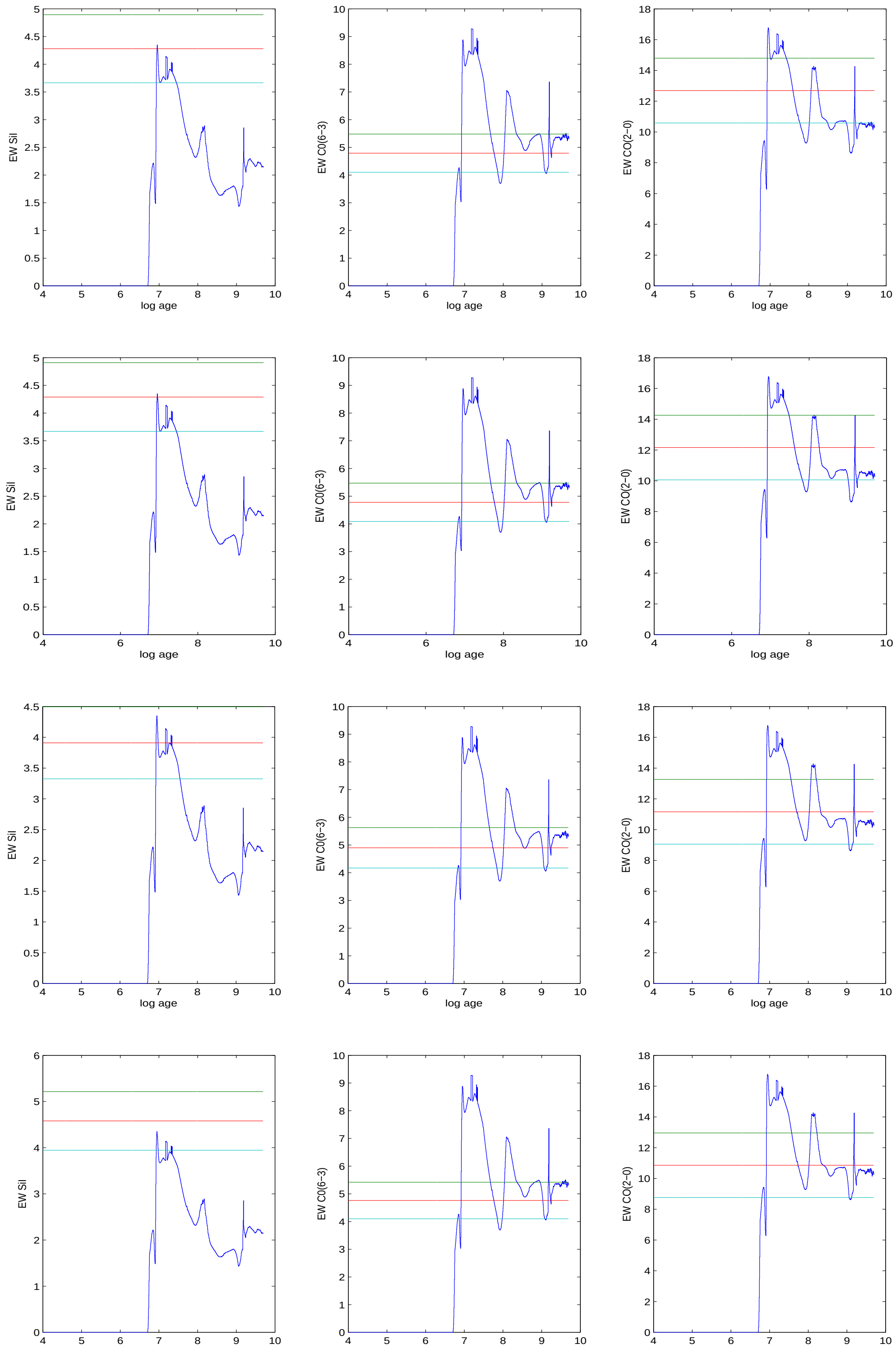

Figure 34: From top to bottom is shown the Starburst99 result for the 250pc spectrum, the 500pc spectrum, the 665-250pc circumnuclear ring 'left' and the 665-250pc circumnuclear ring 'right' of NGC 2685. From left to right are given SiI, CO(6-3) and CO(2-0). Each plot shows the following: the blue line is the value of the equivalent width given by Starburst99, while the red line is the value we found as given in section 4.1. The green and light blue horizontal lines are the 0.5σ upper and lower boundaries for this value.

NGC 2992

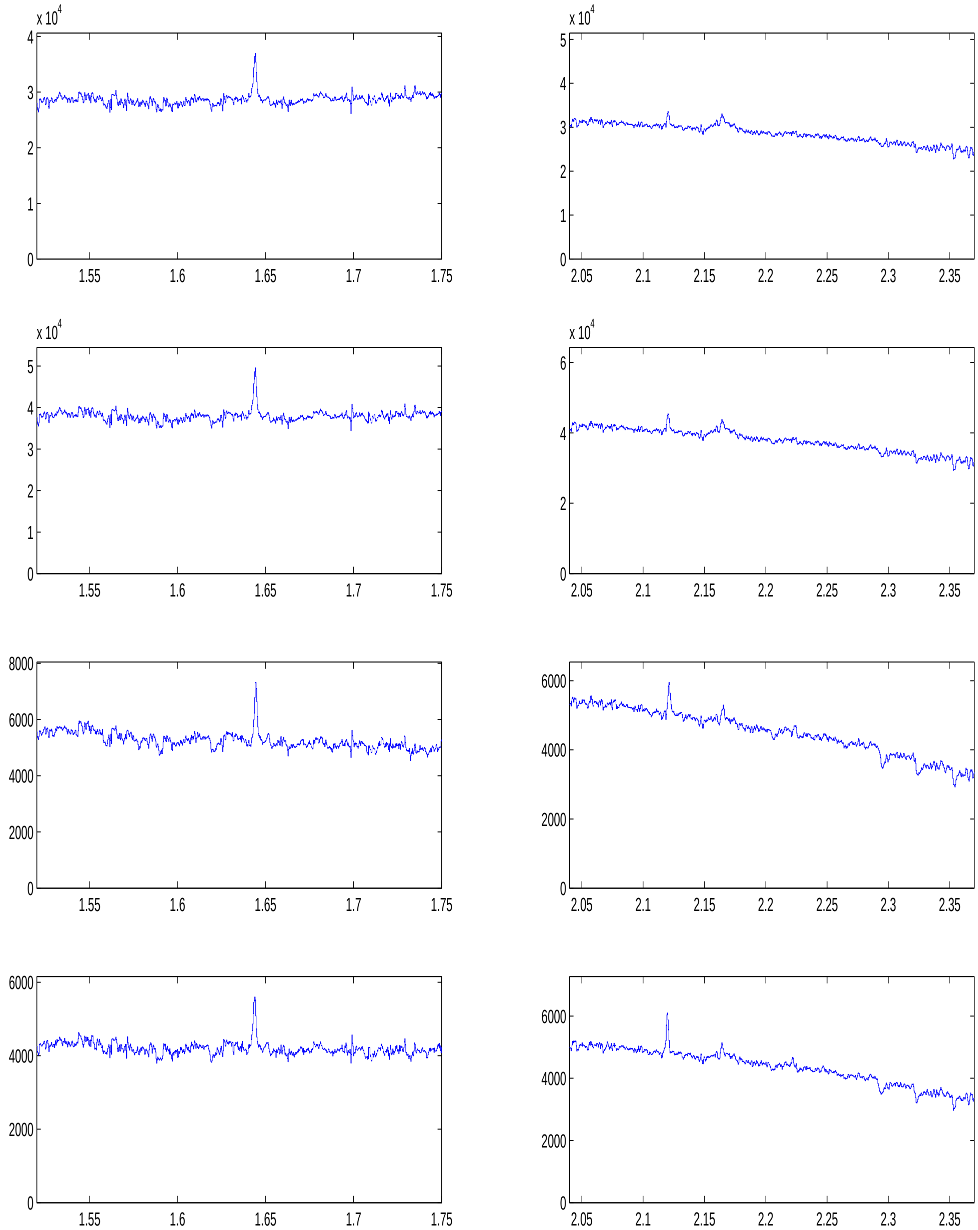

Figure 35: Shown here are the spectra of NGC 2992. The left column is the H band, the right column the K band spectra. From top to bottom are seen: 250pc nuclear, 500pc nuclear, 665-250pc circumnuclear 'left', 665-250pc circumnuclear 'right'.

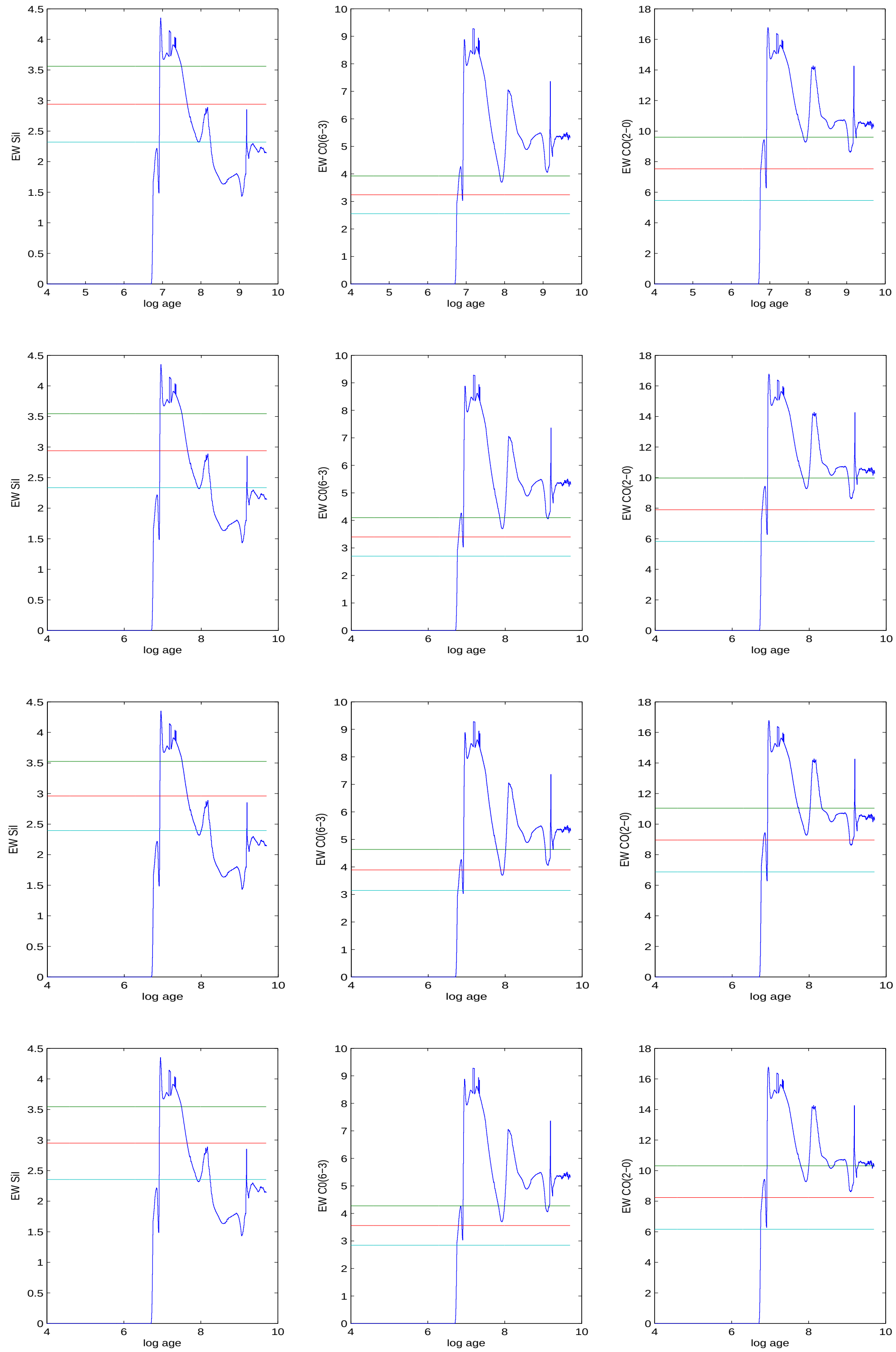

Figure 36: From top to bottom is shown the Starburst99 result for the 250pc spectrum, the 500pc spectrum, the 665-250pc circumnuclear ring ‘left’ and the 665-250pc circumnuclear ring ‘right’ of NGC 2992. From left to right are given SiI, CO(6-3) and CO(2-0). Each plot shows the following: the blue line is the value of the equivalent width given by Starburst99, while the red line is the value we found as given in section 4.1. The green and light blue horizontal lines are the 0.5σ upper and lower boundaries for this value.

NGC 3081

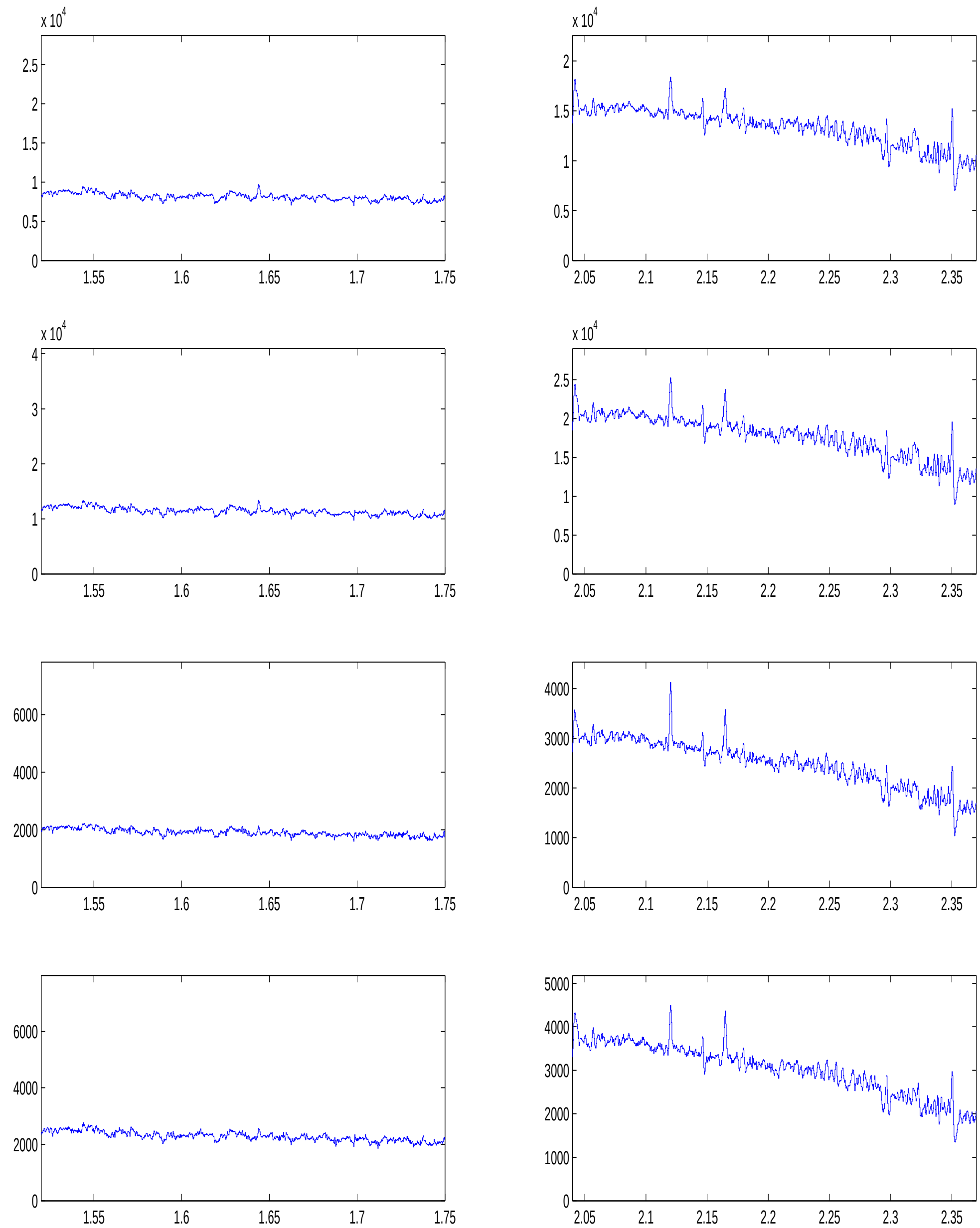

Figure 37: Shown here are the spectra of NGC 3081. The left column is the H band, the right column the K band spectra. From top to bottom are seen: 250pc nuclear, 500pc nuclear, 665-250pc circumnuclear ‘left’, 665-250pc circumnuclear ‘right’.

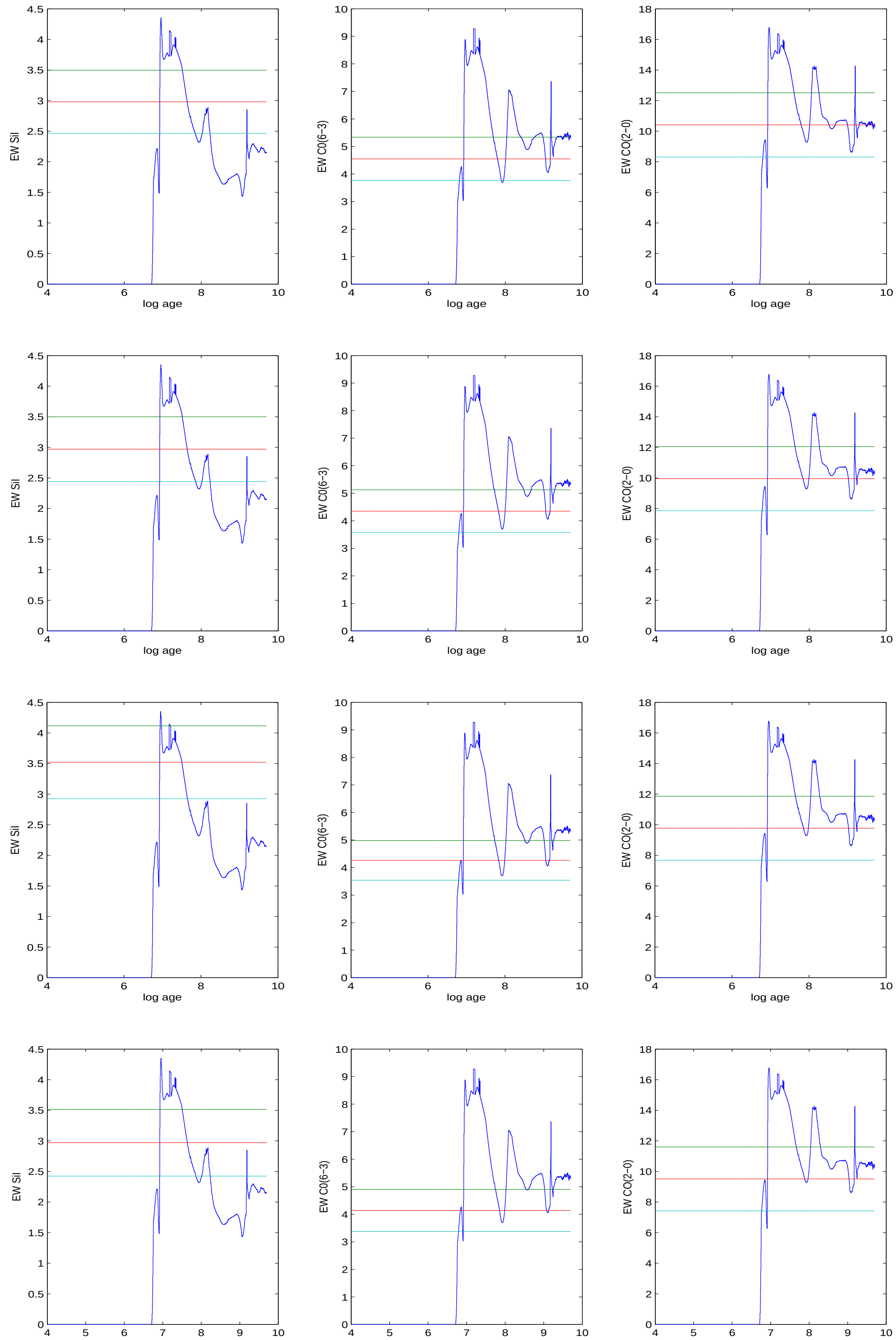

Figure 38: From top to bottom is shown the Starburst99 result for the 250pc spectrum, the 500pc spectrum, the 665-250pc circumnuclear ring 'left' and the 665-250pc circumnuclear ring 'right' of NGC 3081. From left to right are given SiI, CO(6-3) and CO(2-0). Each plot shows the following: the blue line is the value of the equivalent width given by Starburst99, while the red line is the value we found as given in section 4.1. The green and light blue horizontal lines are the 0.5σ upper and lower boundaries for this value.

NGC 3185

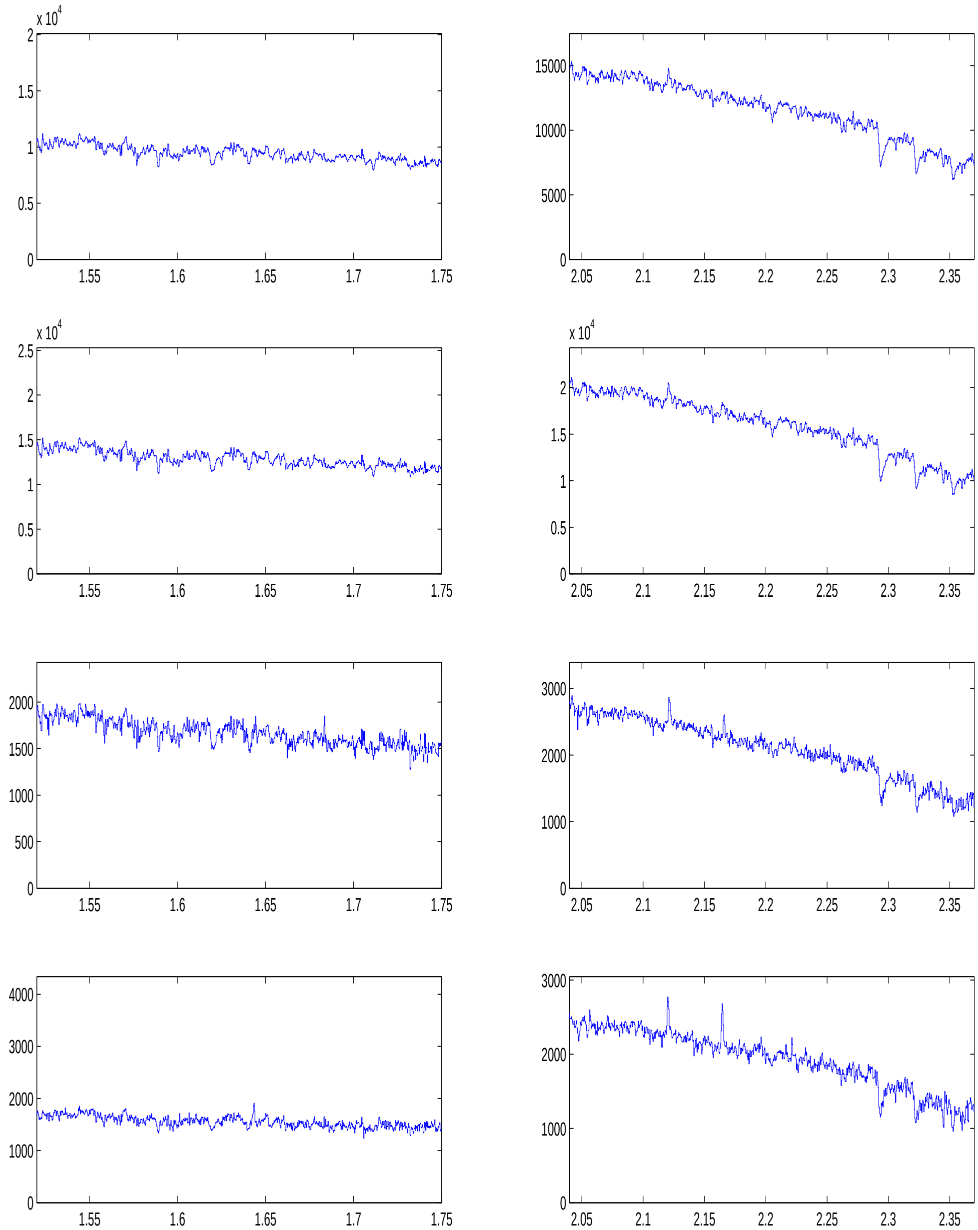

Figure 39: Shown here are the spectra of NGC 3185. The left column is the H band, the right column the K band spectra. From top to bottom are seen: 250pc nuclear, 500pc nuclear, 665-250pc circumnuclear ‘left’, 665-250pc circumnuclear ‘right’.

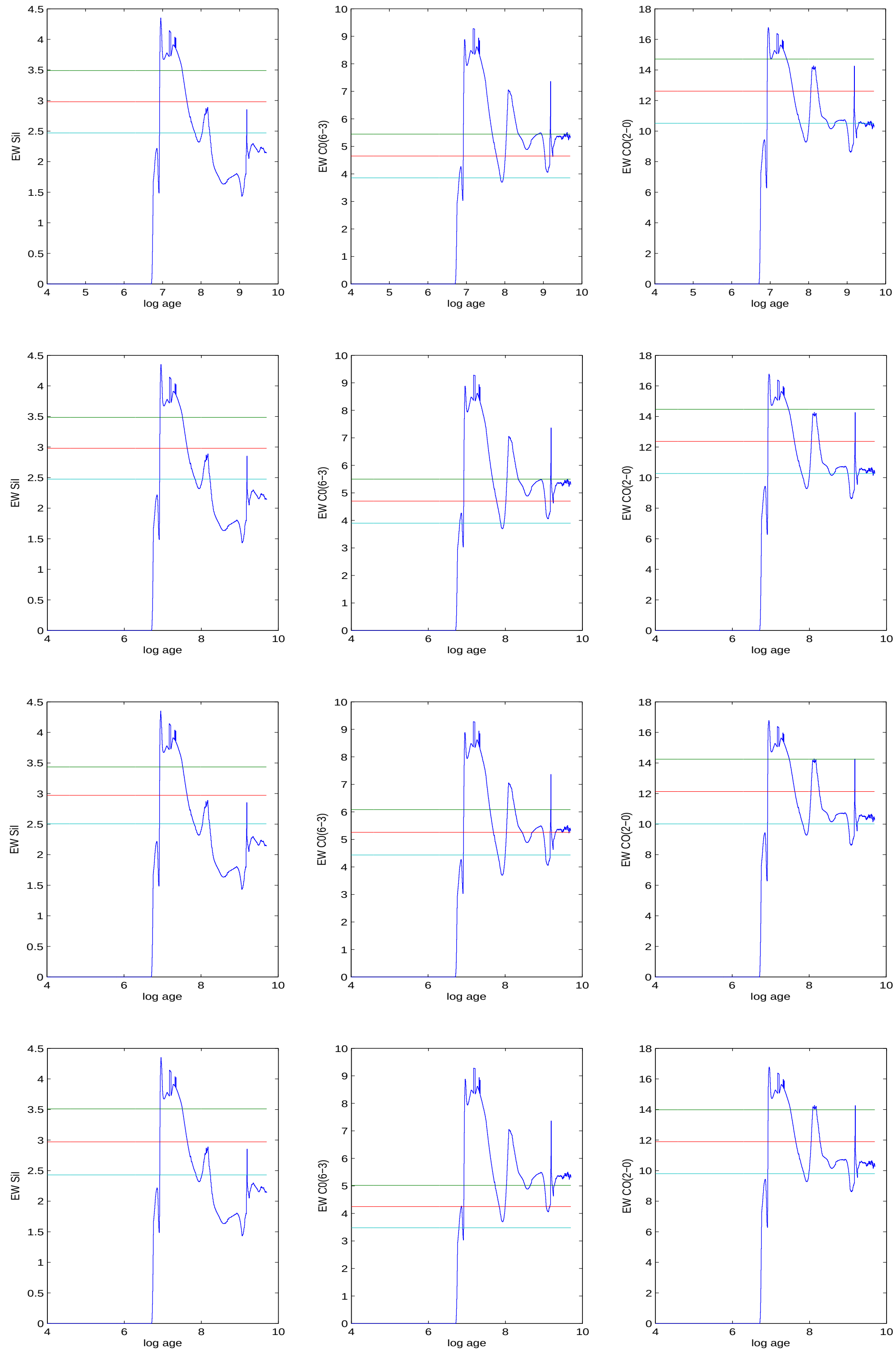

Figure 40: From top to bottom is shown the Starburst99 result for the 250pc spectrum, the 500pc spectrum, the 665-250pc circumnuclear ring 'left' and the 665-250pc circumnuclear ring 'right' of NGC 3185. From left to right are given SiI, CO(6-3) and CO(2-0). Each plot shows the following: the blue line is the value of the equivalent width given by Starburst99, while the red line is the value we found as given in section 4.1. The green and light blue horizontal lines are the 0.5σ upper and lower boundaries for this value.

NGC 3516

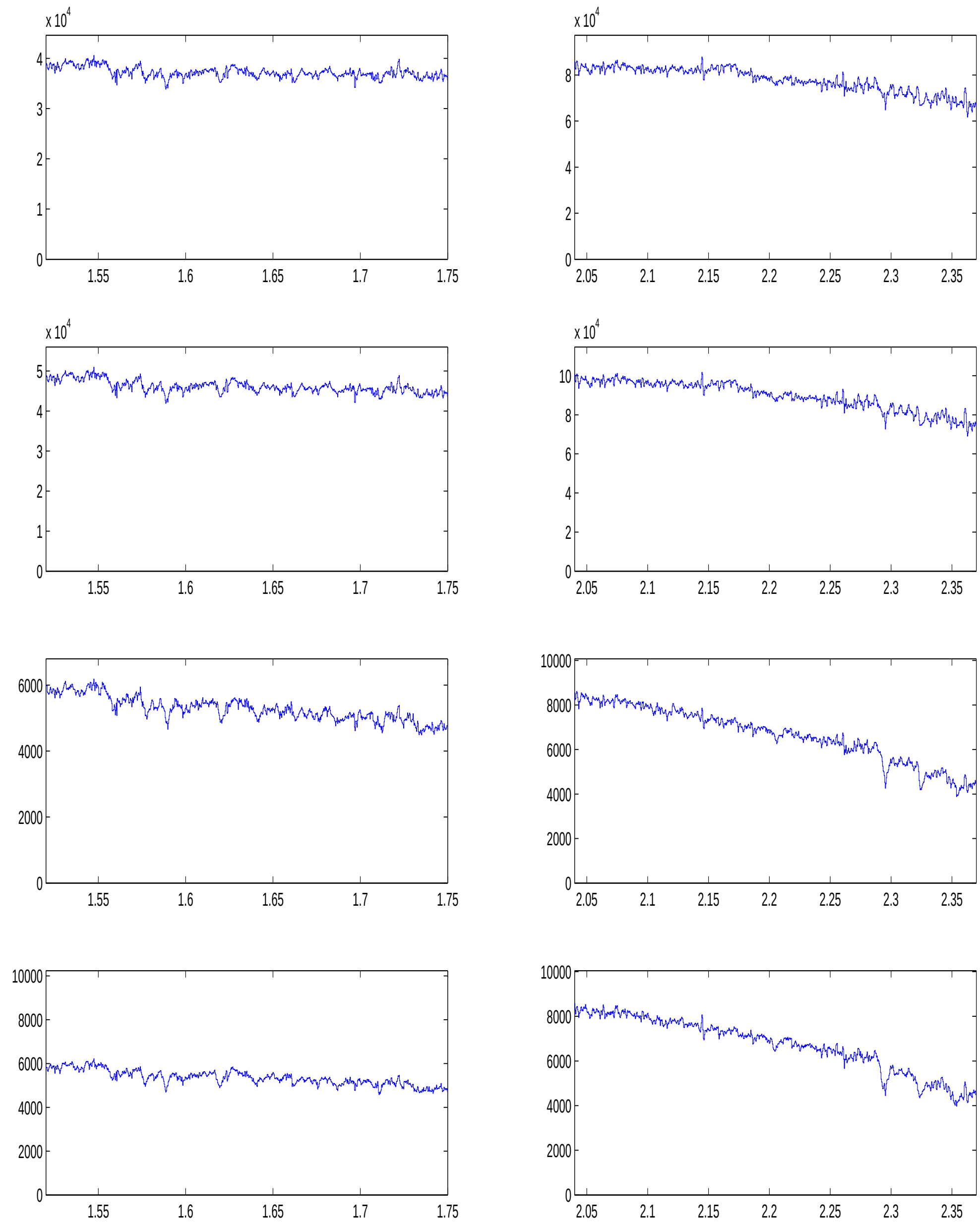

Figure 41: Shown here are the spectra of NGC 3516. The left column is the H band, the right column the K band spectra. From top to bottom are seen: 250pc nuclear, 500pc nuclear, 665-250pc circumnuclear 'left', 665-250pc circumnuclear 'right'.

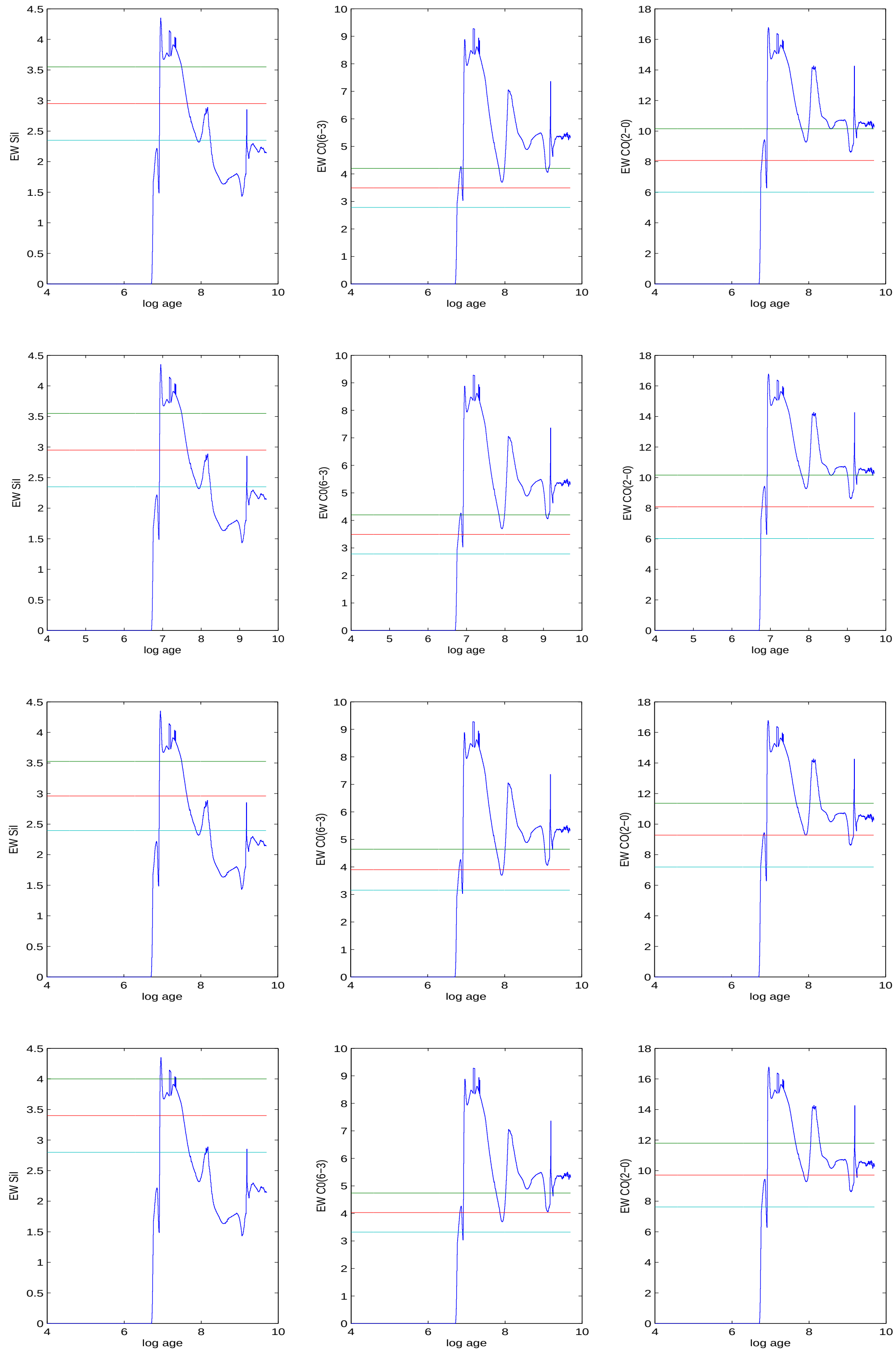

Figure 42: From top to bottom is shown the Starburst99 result for the 250pc spectrum, the 500pc spectrum, the 665-250pc circumnuclear ring ‘left’ and the 665-250pc circumnuclear ring ‘right’ of NGC 3516. From left to right are given SiI, CO(6-3) and CO(2-0). Each plot shows the following: the blue line is the value of the equivalent width given by Starburst99, while the red line is the value we found as given in section 4.1. The green and light blue horizontal lines are the 0.5σ upper and lower boundaries for this value.

NGC 4051

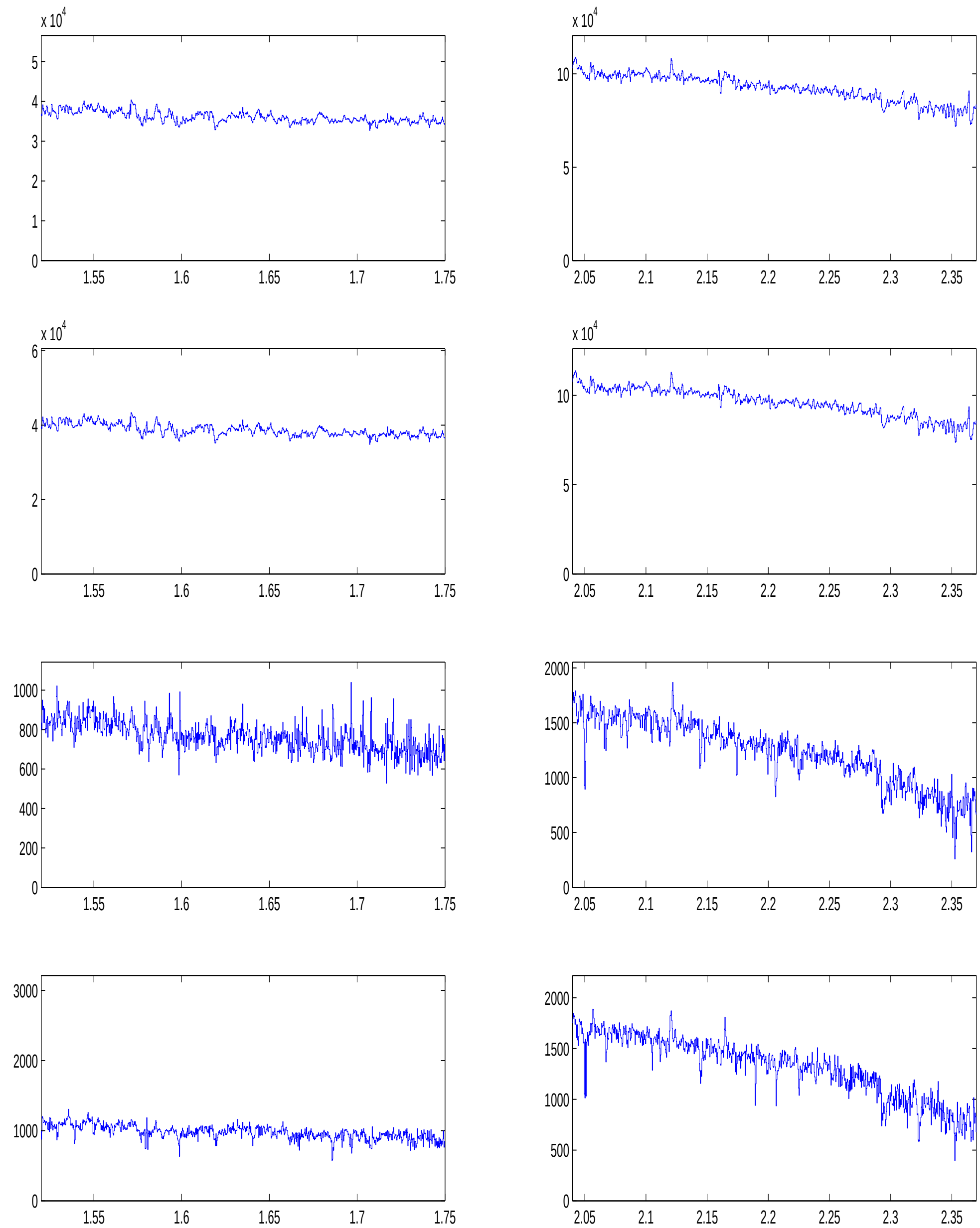

Figure 43: Shown here are the spectra of NGC 4051. The left column is the H band, the right column the K band spectra. From top to bottom are seen: 250pc nuclear, 500pc nuclear, 665-250pc circumnuclear 'left', 665-250pc circumnuclear 'right'.

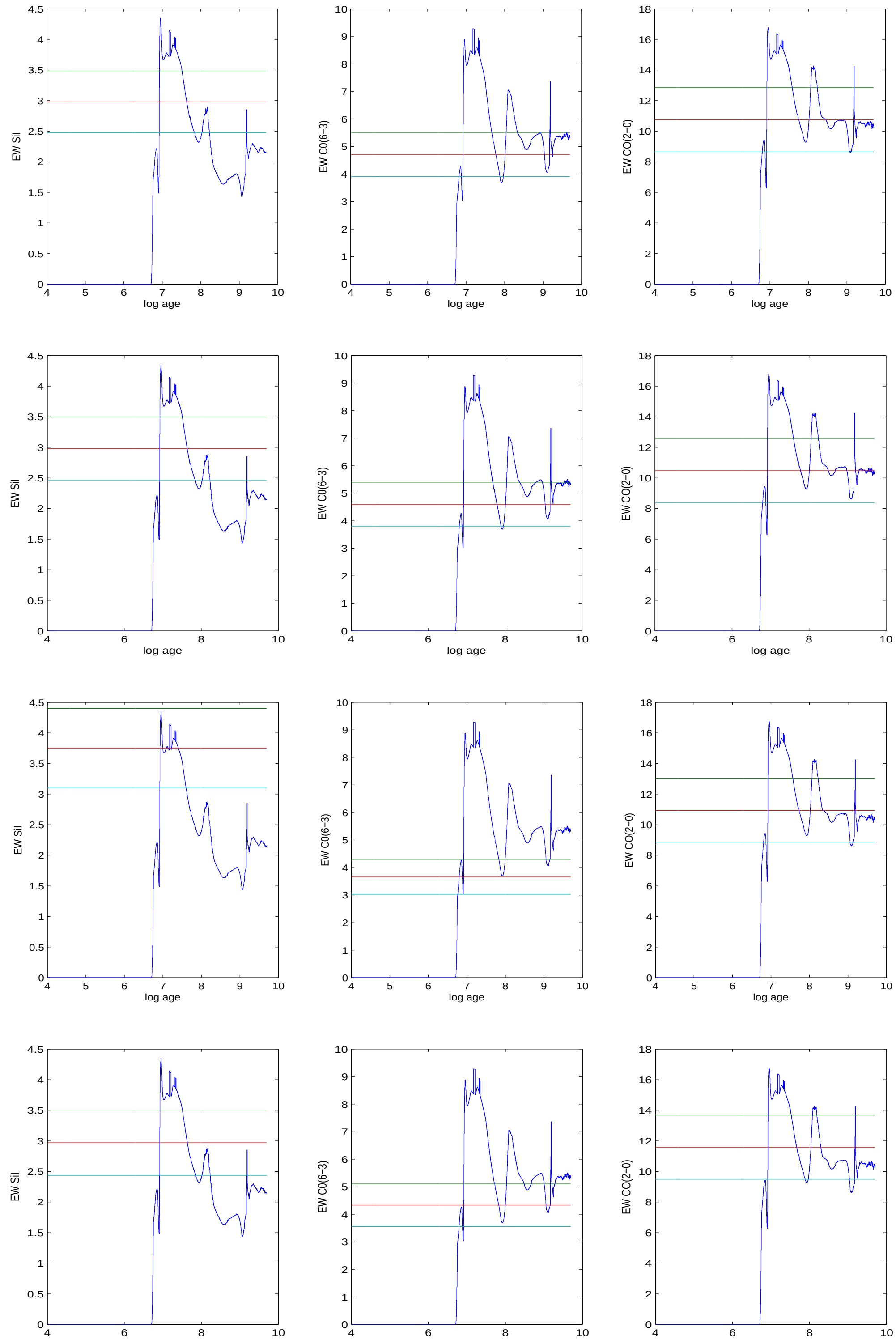

Figure 44: From top to bottom is shown the Starburst99 result for the 250pc spectrum, the 500pc spectrum, the 665-250pc circumnuclear ring 'left' and the 665-250pc circumnuclear ring 'right' of NGC 4051. From left to right are given SiI, CO(6-3) and CO(2-0). Each plot shows the following: the blue line is the value of the equivalent width given by Starburst99, while the red line is the value we found as given in section 4.1. The green and light blue horizontal lines are the 0.5σ upper and lower boundaries for this value.

NGC 4151

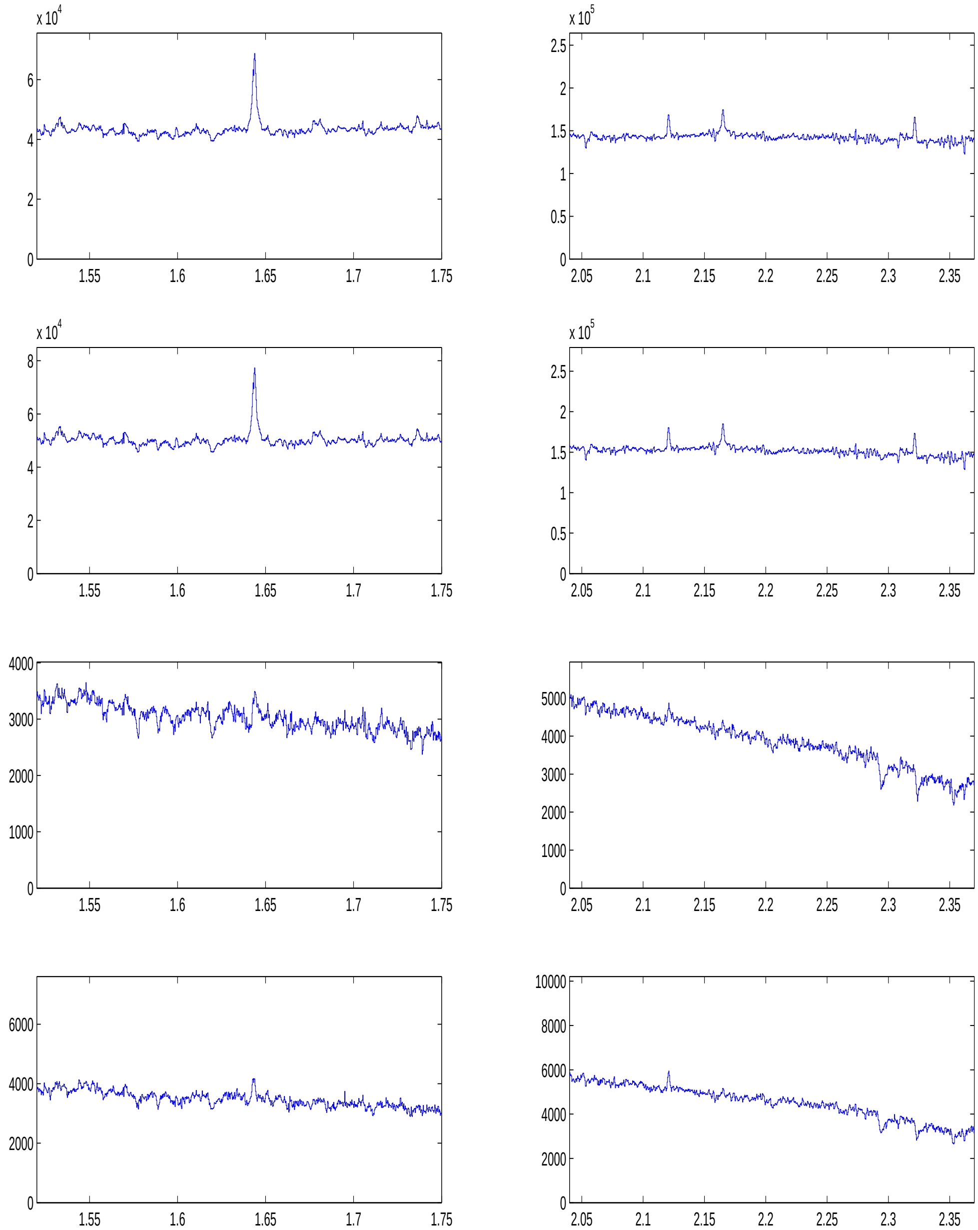

Figure 45: Shown here are the spectra of NGC 4151. The left column is the H band, the right column the K band spectra. From top to bottom are seen: 250pc nuclear, 500pc nuclear, 665-250pc circumnuclear ‘left’, 665-250pc circumnuclear ‘right’.

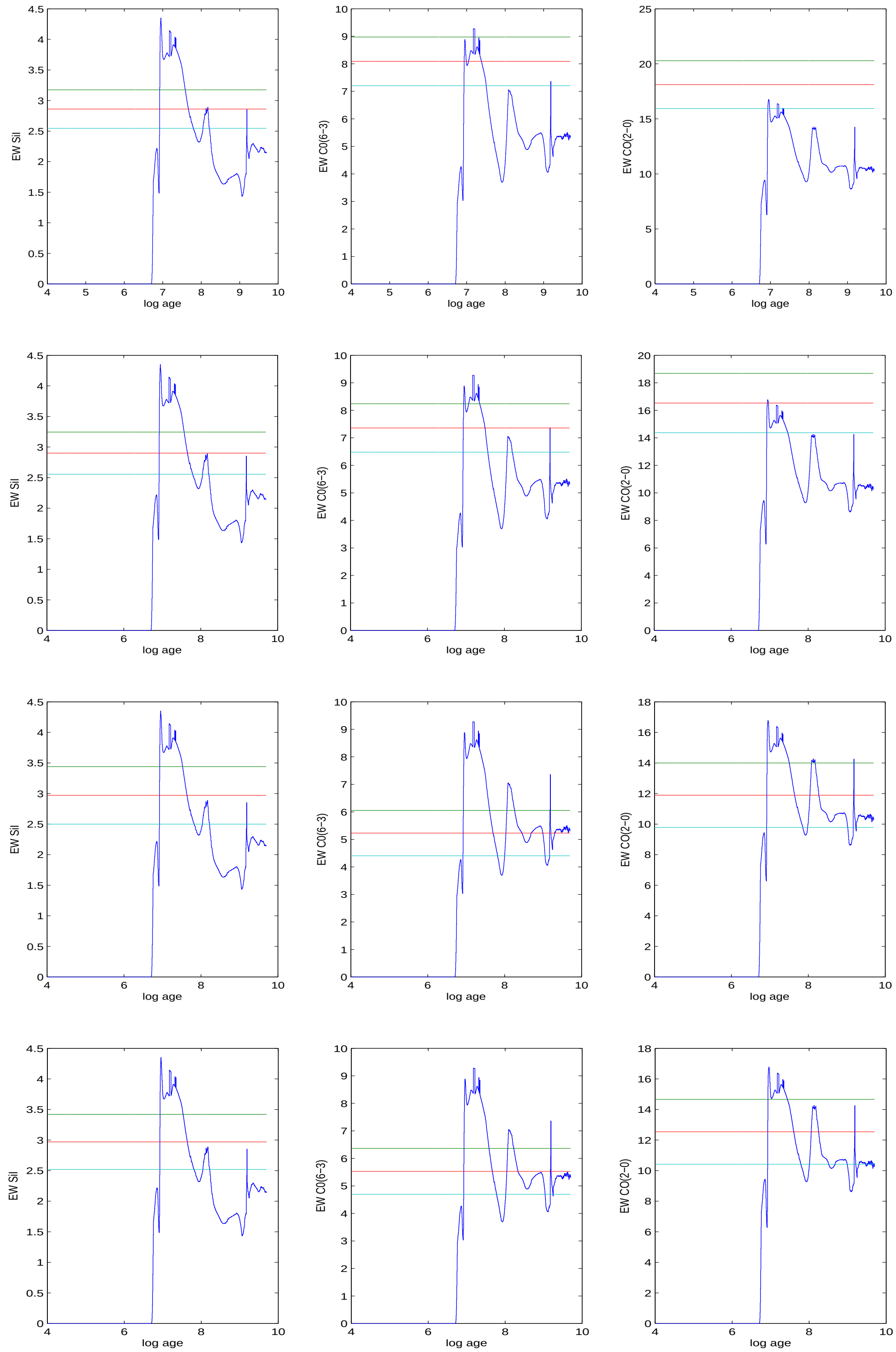

Figure 46: From top to bottom is shown the Starburst99 result for the 250pc spectrum, the 500pc spectrum, the 665-250pc circumnuclear ring ‘left’ and the 665-250pc circumnuclear ring ‘right’ of NGC 4151. From left to right are given SiI, CO(6-3) and CO(2-0). Each plot shows the following: the blue line is the value of the equivalent width given by Starburst99, while the red line is the value we found as given in section 4.1. The green and light blue horizontal lines are the 0.5σ upper and lower boundaries for this value.

NGC 4253

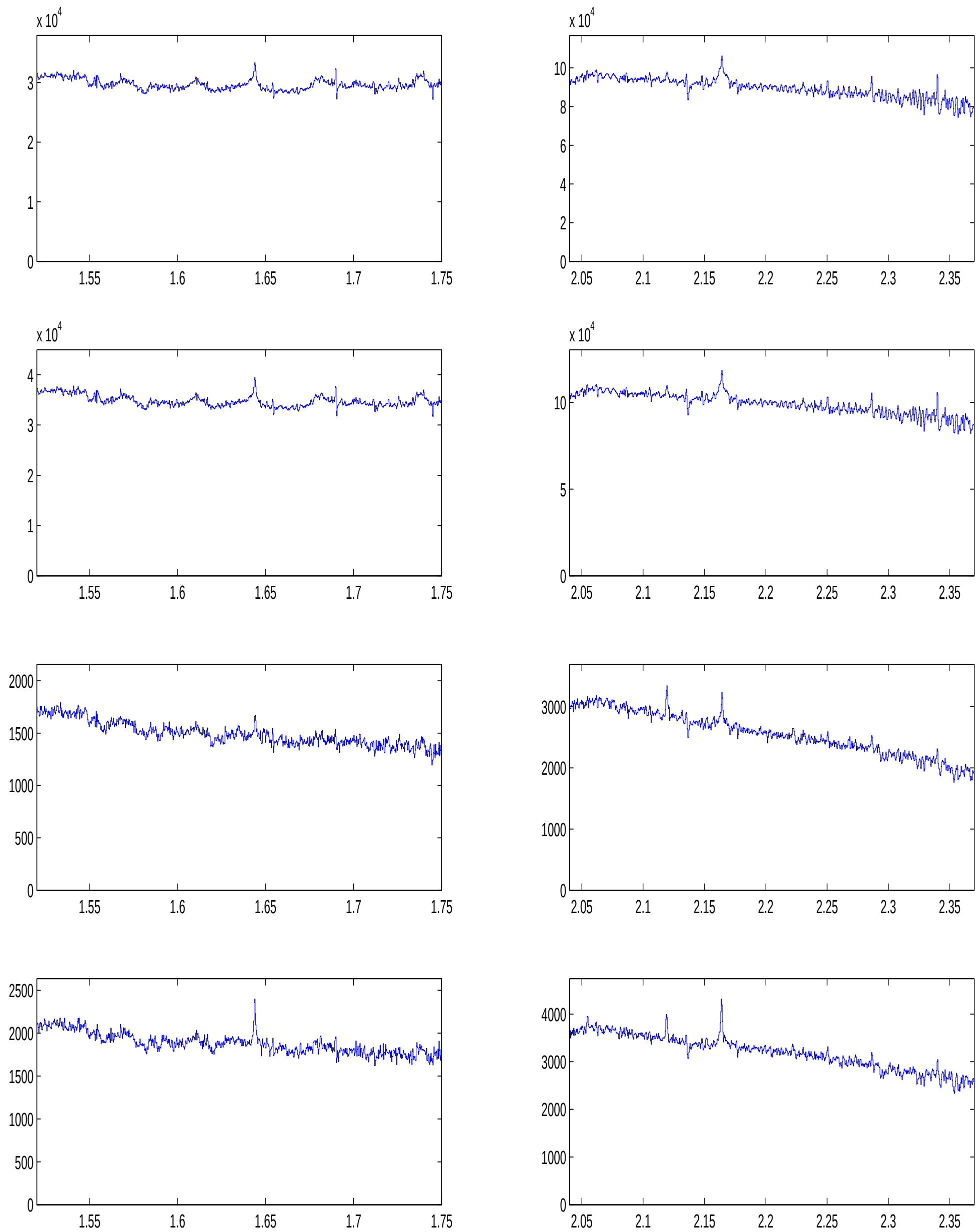

Figure 47: Shown here are the spectra of NGC 4253. The left column is the H band, the right column the K band spectra. From top to bottom are seen: 250pc nuclear, 500pc nuclear, 665-250pc circumnuclear ‘left’, 665-250pc circumnuclear ‘right’.

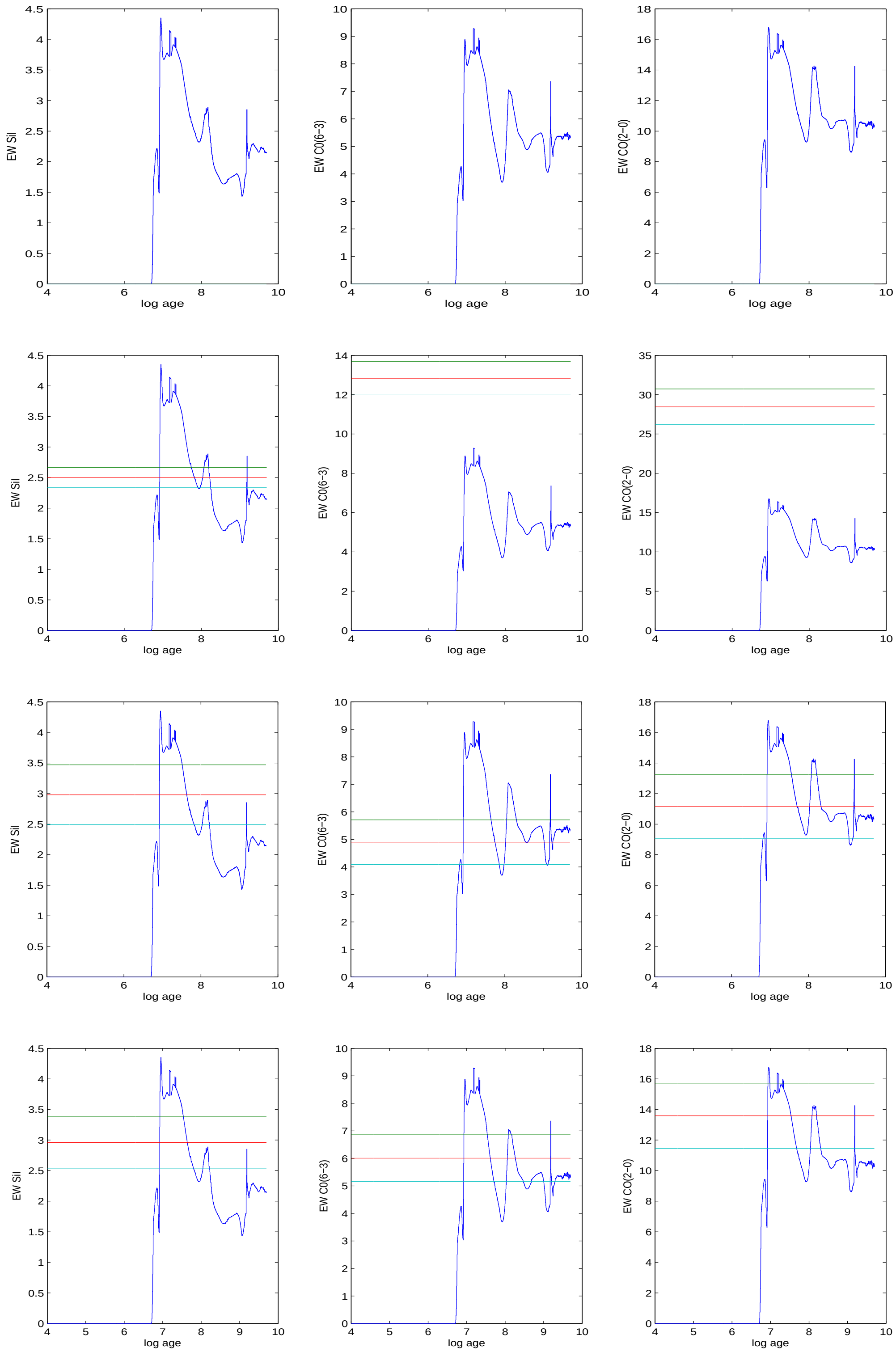

Figure 48: From top to bottom is shown the Starburst99 result for the 250pc spectrum, the 500pc spectrum, the 665-250pc circumnuclear ring 'left' and the 665-250pc circumnuclear ring 'right' of NGC 4253. From left to right are given SiI, CO(6-3) and CO(2-0). Each plot shows the following: the blue line is the value of the equivalent width given by Starburst99, while the red line is the value we found as given in section 4.1. The green and light blue horizontal lines are the 0.5σ upper and lower boundaries for this value.

NGC 4388

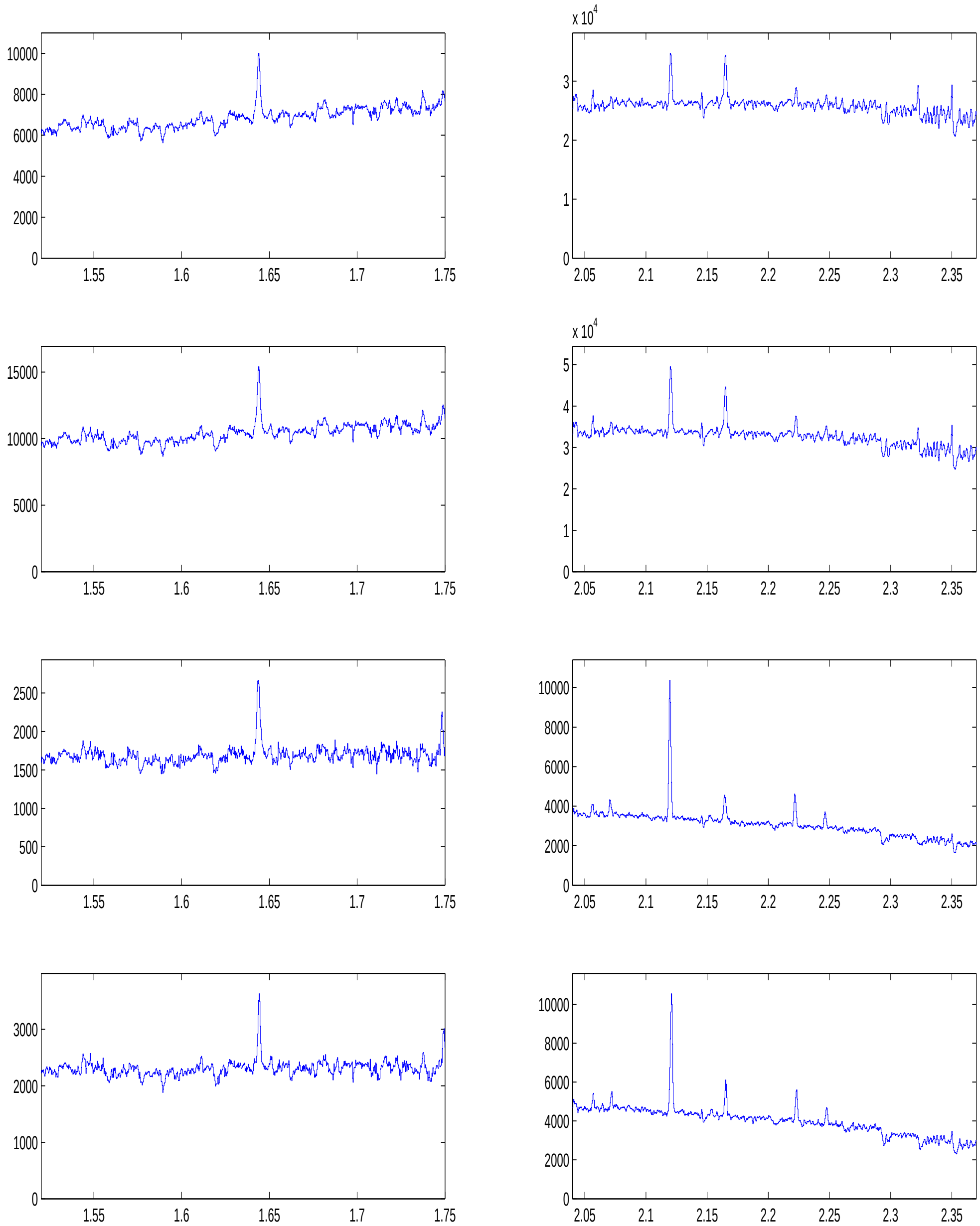

Figure 49: Shown here are the spectra of NGC 4388. The left column is the H band, the right column the K band spectra. From top to bottom are seen: 250pc nuclear, 500pc nuclear, 665-250pc circumnuclear ‘left’, 665-250pc circumnuclear ‘right’.

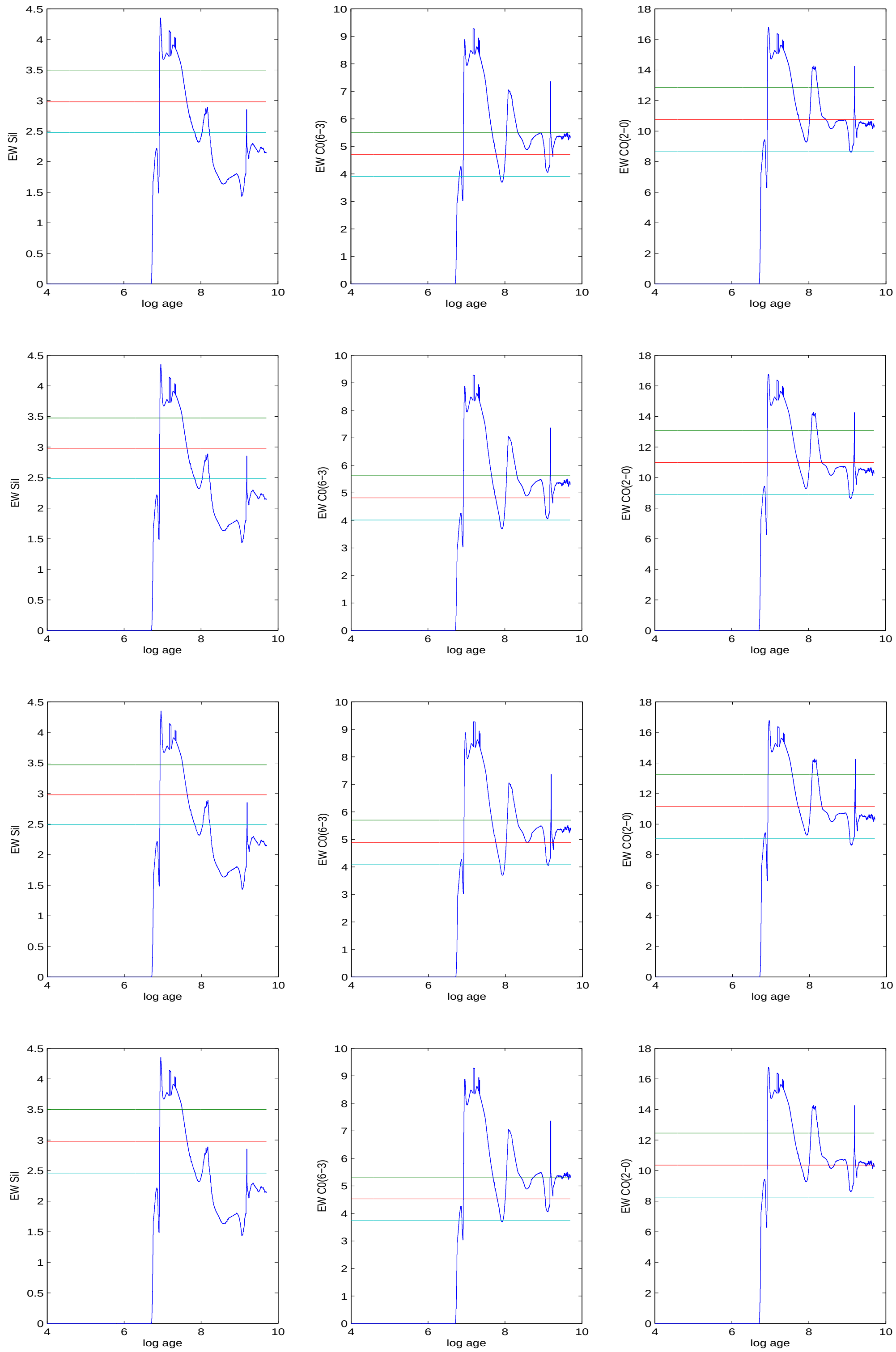

Figure 50: From top to bottom is shown the Starburst99 result for the 250pc spectrum, the 500pc spectrum, the 665-250pc circumnuclear ring ‘left’ and the 665-250pc circumnuclear ring ‘right’ of NGC 4388. From left to right are given SiI, CO(6-3) and CO(2-0). Each plot shows the following: the blue line is the value of the equivalent width given by Starburst99, while the red line is the value we found as given in section 4.1. The green and light blue horizontal lines are the 0.5σ upper and lower boundaries for this value.

NGC 5273

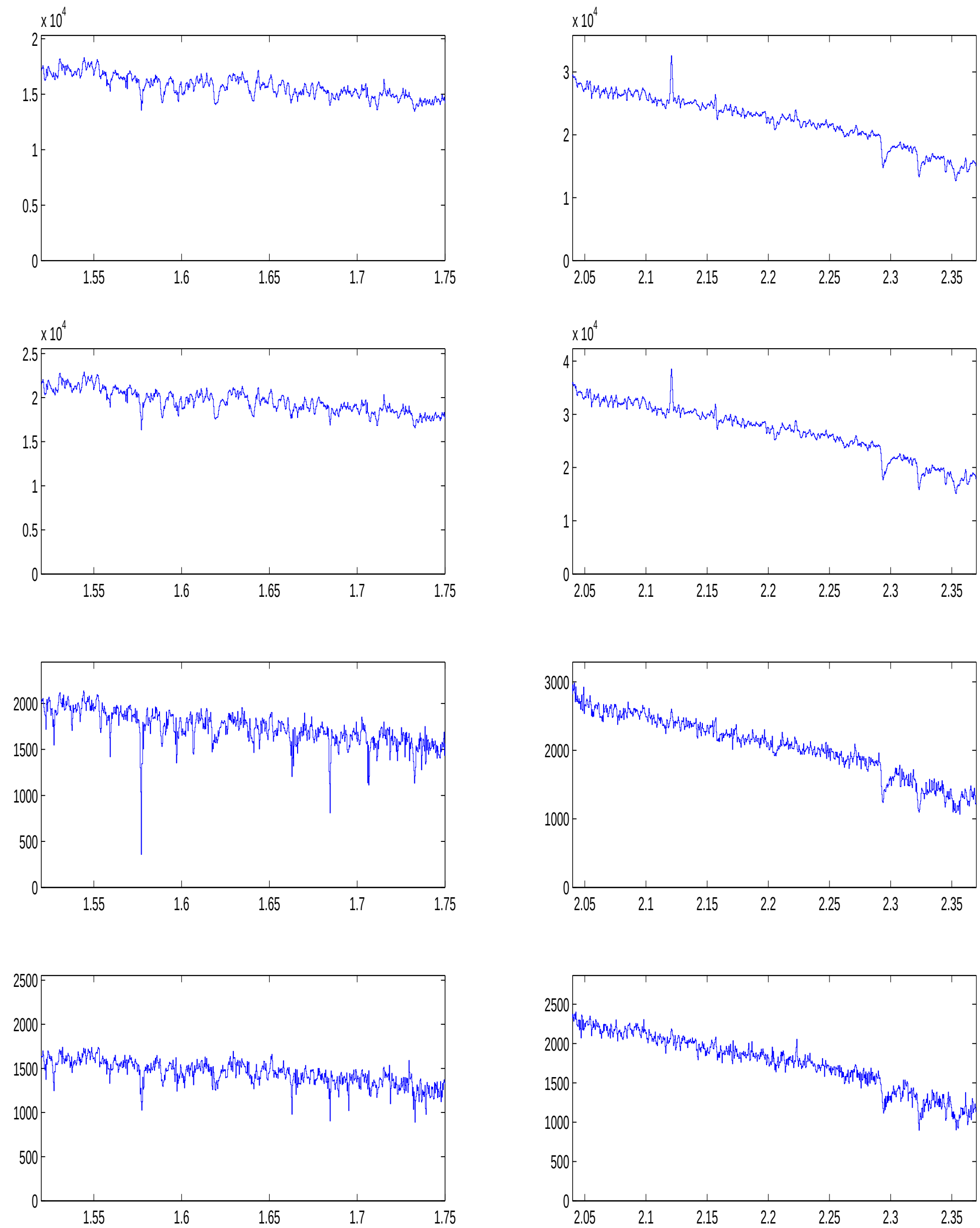

Figure 51: Shown here are the spectra of NGC 5273. The left column is the H band, the right column the K band spectra. From top to bottom are seen: 250pc nuclear, 500pc nuclear, 665-250pc circumnuclear 'left', 665-250pc circumnuclear 'right'.

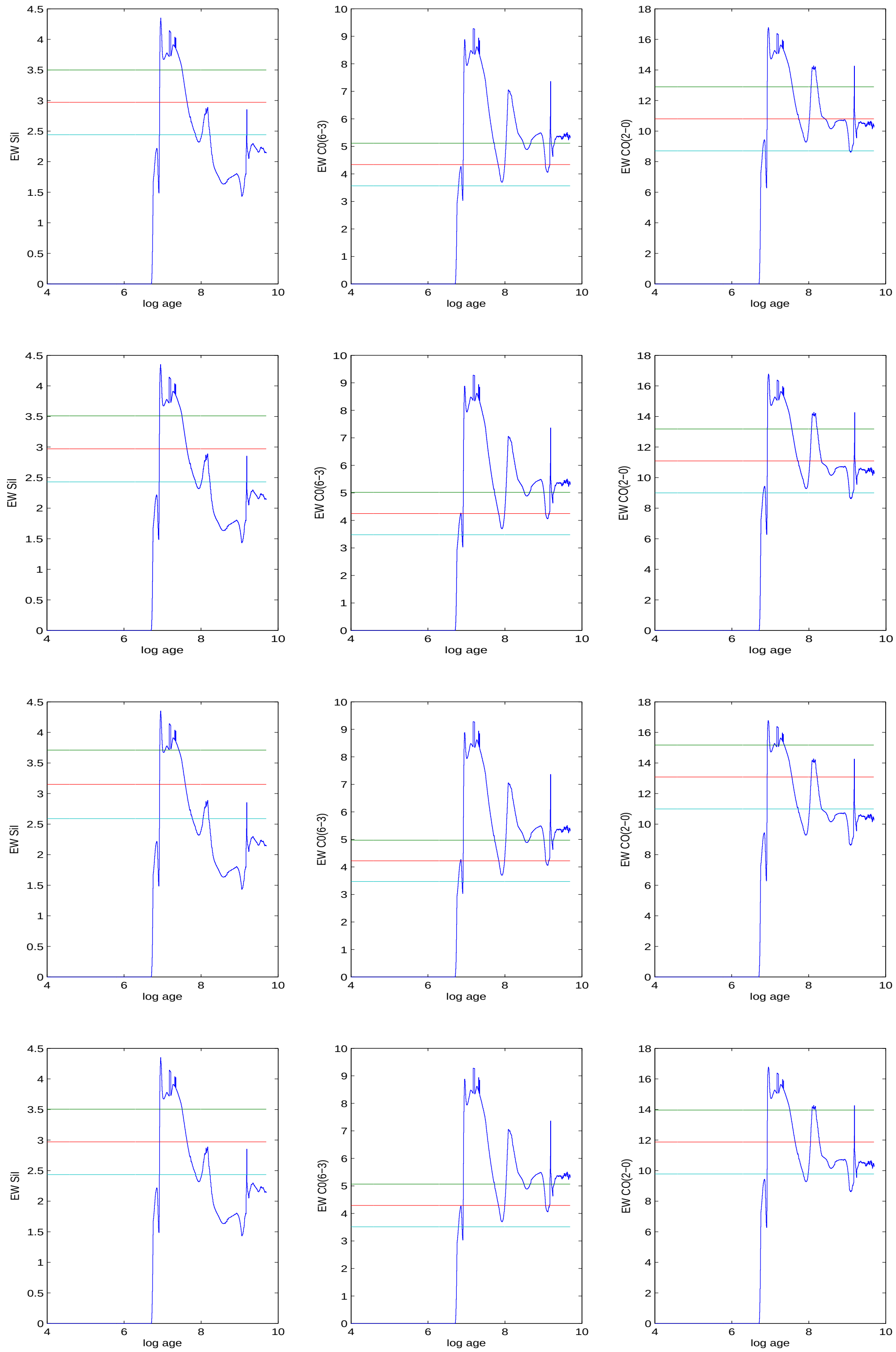

Figure 52: From top to bottom is shown the Starburst99 result for the 250pc spectrum, the 500pc spectrum, the 665-250pc circumnuclear ring 'left' and the 665-250pc circumnuclear ring 'right' of NGC 5273. From left to right are given SiI, CO(6-3) and CO(2-0). Each plot shows the following: the blue line is the value of the equivalent width given by Starburst99, while the red line is the value we found as given in section 4.1. The green and light blue horizontal lines are the 0.5σ upper and lower boundaries for this value.

NGC 5506

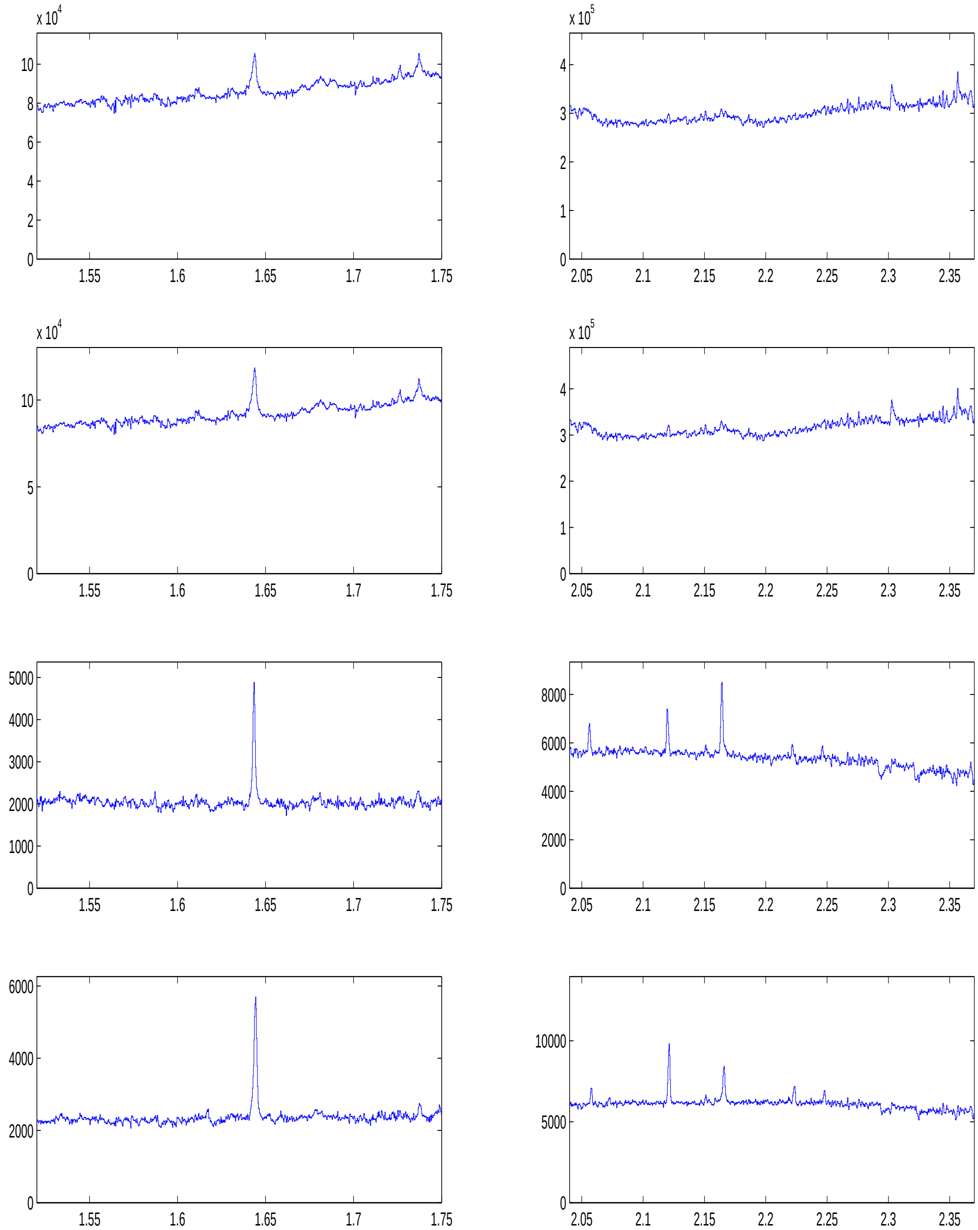

Figure 53: Shown here are the spectra of NGC 5506. The nucleus was overexposed. The left column is the H band, the right column the K band spectra. From top to bottom are seen: 250pc nuclear, 500pc nuclear, 665-250pc circumnuclear 'left', 665-250pc circumnuclear 'right'.

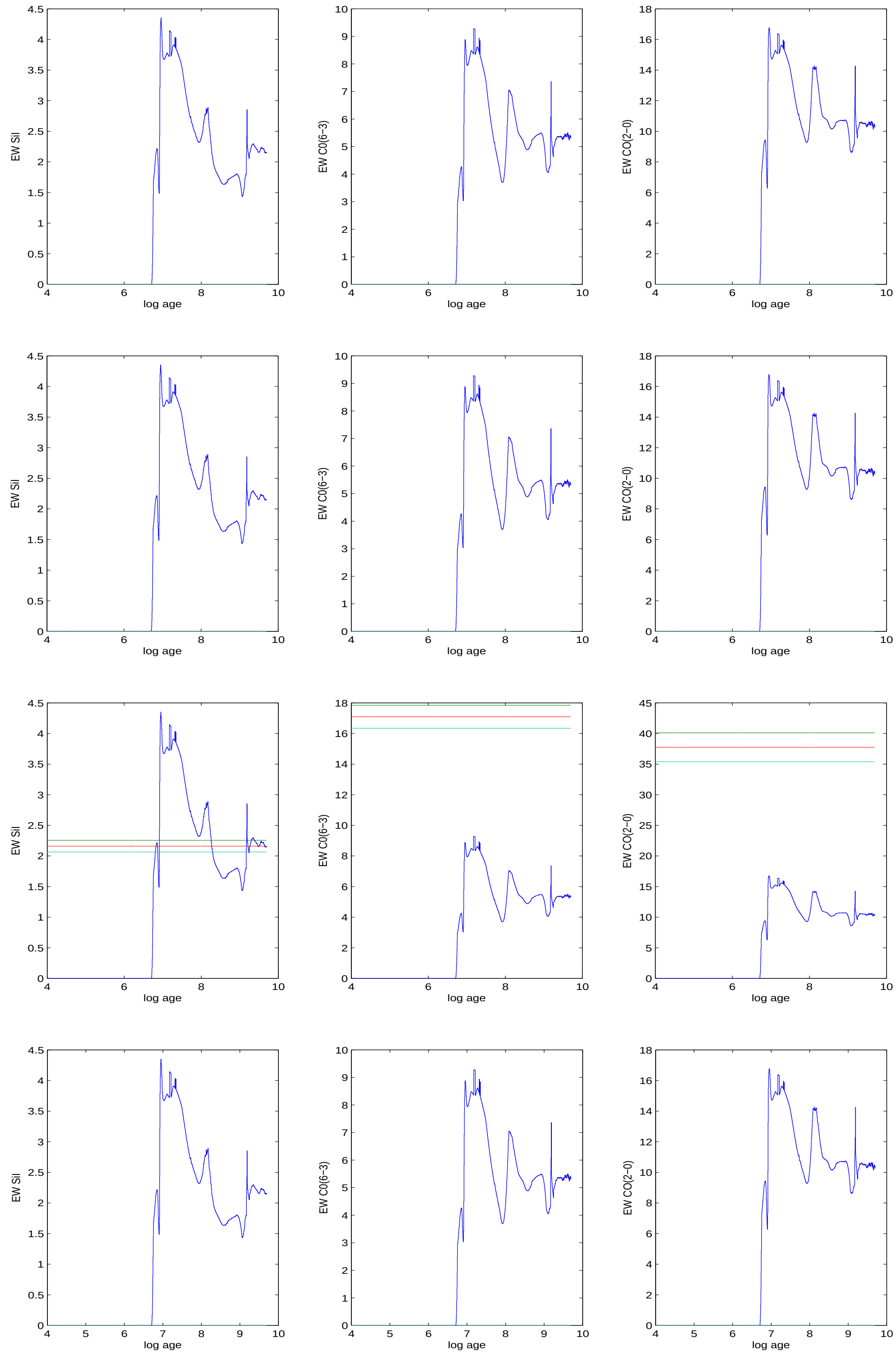

Figure 54: From top to bottom is shown the Starburst99 result for the 250pc spectrum, the 500pc spectrum, the 665-250pc circumnuclear ring 'left' and the 665-250pc circumnuclear ring 'right' of NGC 5506. From left to right are given SiI, CO(6-3) and CO(2-0). Each plot shows the following: the blue line is the value of the equivalent width given by Starburst99, while the red line is the value we found as given in section 4.1. The green and light blue horizontal lines are the 0.5σ upper and lower boundaries for this value.

NGC 7450

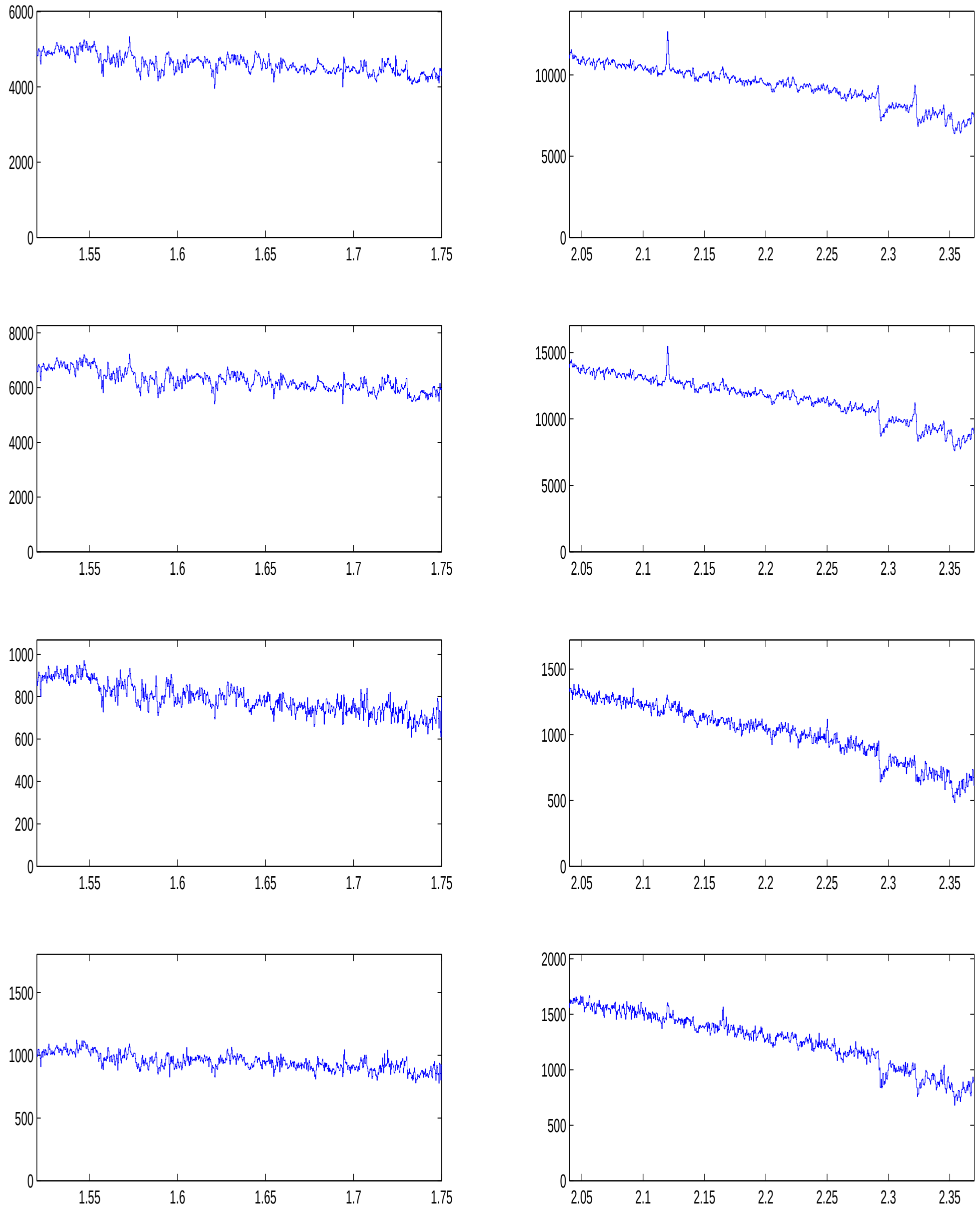

Figure 55: Shown here are the spectra of NGC 7450. The left column is the H band, the right column the K band spectra. From top to bottom are seen: 250pc nuclear, 500pc nuclear, 665-250pc circumnuclear ‘left’, 665-250pc circumnuclear ‘right’.

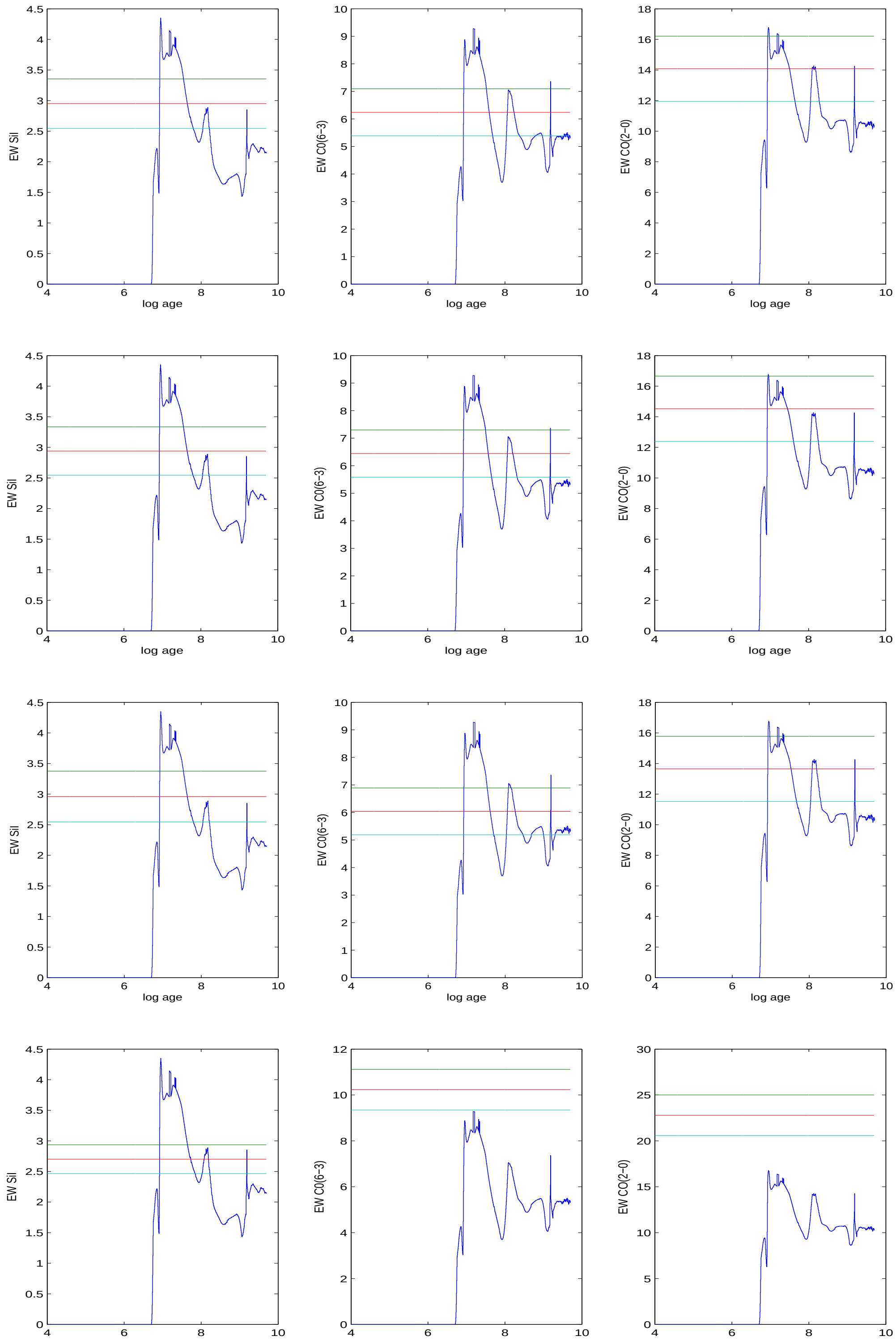

Figure 56: From top to bottom is shown the Starburst99 result for the 250pc spectrum, the 500pc spectrum, the 665-250pc circumnuclear ring ‘left’ and the 665-250pc circumnuclear ring ‘right’ of NGC 7450. From left to right are given SiI, CO(6-3) and CO(2-0). Each plot shows the following: the blue line is the value of the equivalent width given by Starburst99, while the red line is the value we found as given in section 4.1. The green and light blue horizontal lines are the 0.5σ upper and lower boundaries for this value.

NGC 931

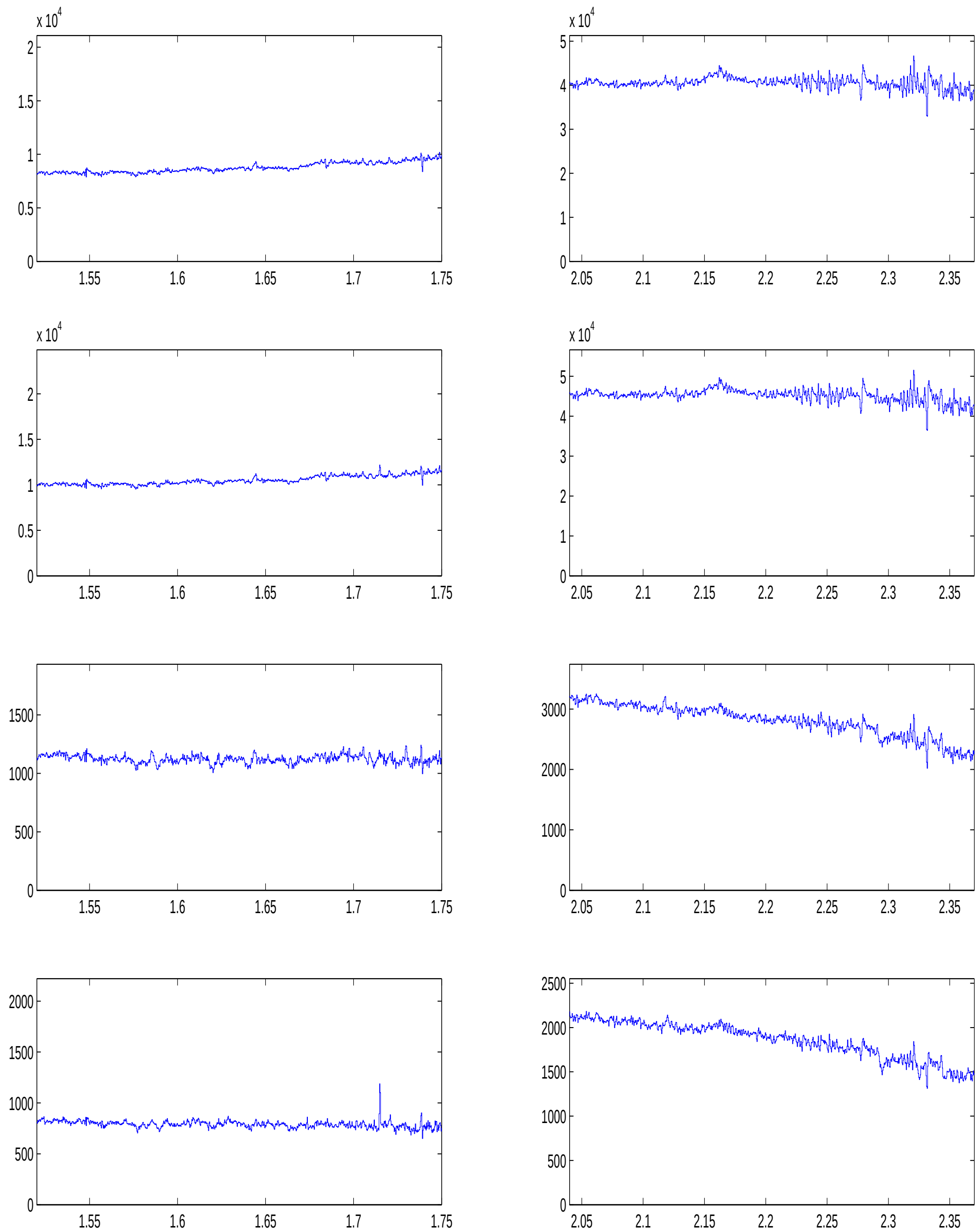

Figure 57: Shown here are the spectra of NGC 931. The left column is the H band, the right column the K band spectra. From top to bottom are seen: 250pc nuclear, 500pc nuclear, 665-250pc circumnuclear ‘left’, 665-250pc circumnuclear ‘right’.

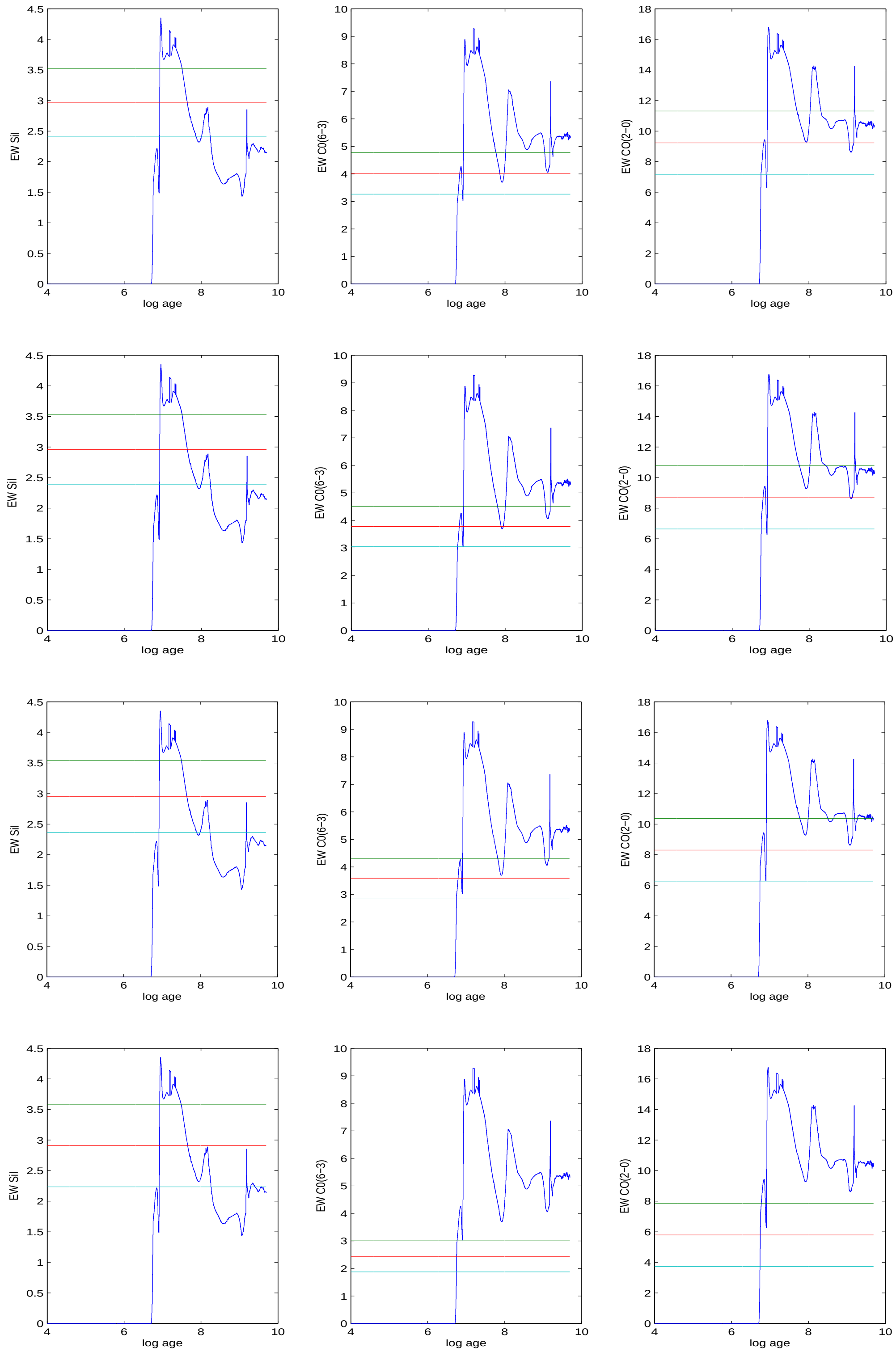

Figure 58: From top to bottom is shown the Starburst99 result for the 250pc spectrum, the 500pc spectrum, the 665-250pc circumnuclear ring 'left' and the 665-250pc circumnuclear ring 'right' of NGC 931. From left to right are given SiI, CO(6-3) and CO(2-0). Each plot shows the following: the blue line is the value of the equivalent width given by Starburst99, while the red line is the value we found as given in section 4.1. The green and light blue horizontal lines are the 0.5σ upper and lower boundaries for this value.